EFFECTS OF THE ADENOSINE A_{2A} RECEPTOR C-TERMINUS ON LIGAND BINDING, STABILITY, AND DOWNSTREAM SIGNALING

AN ABSTRACT

SUBMITTED ON THE TWENTY FOURTH DAY OF APRIL 2019

TO THE DEPARTMENT OF CHEMICAL AND BIOMOLECULAR ENGINEERING

IN PARTIAL FULFILLMENT OF THE REQUIREMENTS

OF THE SCHOOL OF SCIENCE AND ENGINEERING

OF TULANE UNIVERSITY

FOR THE DEGREE

OF

DOCTOR OF PHILOSOPHY

BY

Kirsten Swonger Koretz

APPROVED:
Anne S. Robinson, Ph.D.
Director

Noah Malmstadt, Ph.D.

Kim C. O'Connor, Ph.D.

Daniel F. Shantz, Ph.D.

ABSTRACT

G protein-coupled receptors (GPCRs) are the largest family of proteins in humans and are expressed widely throughout the body. GPCRs consist of seven-transmembrane helices that bind extracellular ligands to initiate intracellular downstream signaling via interaction with G proteins, and function in many short and long-term responses in the body, including taste, immune function, and sugar sensing. Extracellular binding and the coupled downstream signaling pathway means that GPCRs are ideal drug targets for many diseases, making them of great interest to the pharmaceutical industry. Some GPCRs have been crystallized in an effort to better elucidate the structure-function relationship to aid in the design of novel therapeutics.

The adenosine A_{2A} receptor ($A_{2A}R$) is a GPCR that has been crystallized bound to agonist, antagonist, and G protein. Although these crystal structures are informative in regards to $A_{2A}R$ structure when associated with binding partners, all current crystal structures truncate nearly 100 amino acids of the C-terminus. As a crystallization strategy, this truncation makes sense considering the C-terminus is long and unstructured. However, truncating roughly 25% of the protein, as well as making other point mutations calls into question the authenticity of the crystal structures in reflecting functional receptor and thus their potential value for therapeutic design.

Beyond structural studies, biophysical characterization of drug binding to receptors *in vitro* to predict efficacy *in vivo* has shifted away from measures of affinity and selectivity and towards determination of kinetic rates. Kinetic rate constants in combination with affinity and drug residence time are thought to be better predictors of

drug behavior *in vivo*. For these reasons, this thesis focuses on experiments to characterize $A_{2A}R$ kinetic rate constants.

Previously, our lab showed that truncating the $A_{2A}R$ C-terminus reduced downstream cAMP signaling in mammalian cells, although where the effect on the signaling pathway occurred was not determined. Here, we report that truncation of the C-terminus ablates receptor association to $G\alpha_s$, the first step in signaling. In this work, $A_{2A}R$ ligand binding kinetics, stability, and association to $G\alpha_s$ are characterized to better delineate the importance of interactions between receptor and stimuli in a way that is impactful to drug design.

EFFECTS OF THE ADENOSINE A_{2A} RECEPTOR C-TERMINUS ON LIGAND BINDING, STABILITY, AND DOWNSTREAM SIGNALING

A DISSERTATION

SUBMITTED ON THE TWENTY FOURTH DAY OF APRIL 2019

TO THE DEPARTMENT OF CHEMICAL AND BIOMOLECULAR ENGINEERING

IN PARTIAL FULFILLMENT OF THE REQUIREMENTS

OF THE SCHOOL OF SCIENCE AND ENGINEERING

OF TULANE UNIVERSITY

FOR THE DEGREE

OF

DOCTOR OF PHILOSOPHY

BY

Kirsten Swonger Koretz

APPROVED:

Anne S. Robinson, Ph.D.
Director

Noah Malmstadt, Ph.D.

Kim C. O'Connor, Ph.D.

Daniel F. Shantz, Ph.D.

ACKNOWLEDGEMENTS

I would like to start by thanking my family for their love and support through the years. Your encouragement in all aspects of my life, especially the effort you put in to trying to understand my graduate research is so greatly appreciated. My brother, Chris, and sister, Jenny, were always there to lend an ear or a shoulder when I needed someone to talk to. A special thank you to my parents for inspiring me to pursue my passion. I would not have made it this far without your love and encouragement.

I feel very fortunate to have had Professor Anne Skaja Robinson as my Ph.D. advisor. She has not only provided me with valuable guidance and suggestions about my research, but also life outside the lab. I cannot thank her enough for her patience when she understood that I needed to troubleshoot on my own, or giving me a nudge in another direction when an experiment was not going as planned. Anne has made me a better researcher, writer, and person in the time we have spent working together.

I would like to thank my thesis committee, Professor Noah Malmstadt, Professor Kim O'Connor, and Professor Dan Shantz, for their recommendations on data analysis and experimental direction throughout my graduate career. To my fellow Robinson labmates, Abhinav, Claire, Danny, and Evan, I have really enjoyed working alongside you all, and greatly appreciate the time we've shared together. Additional thank yous to the rest of the chemical and biomolecular engineering graduate students, especially Sean,

for being such inspiring friends and researchers. During my graduate studies, I was fortunate to have had the privilege of mentoring two great students, Annie Tir and Steven Stradley, during their undergraduate research. A special thank you to you both for your help with the endless protein purifications.

I would like to acknowledge that this work was funded in part by NIH grant P20 GM104316 and NSF CBET 1263768. The Biacore T200 was obtained through funding from NIH grant S10OD020117.

Finally, I’d like to thank my husband, Zak, for sharing this experience with me. I have so appreciated your willingness to be my sounding board on all subjects, and I could not have made it this far without your support during the most stressful moments. I’m sorry to see this chapter end, but I’m looking forward to all the chapters left to come.

TABLE OF CONTENTS

ACKNOWLEDGEMENTS ii
LIST OF TABLES viii
LIST OF FIGURES xii

1. INTRODUCTION 1

  1.1. G Protein-Coupled Receptors 1
  1.2. Adenosine Receptors 3
  1.3. Crystallization of the Adenosine A_{2A} Receptor 4
  1.4. Impact of the A_{2A}R C-terminus on Downstream Signaling 6
  1.5. Kinetics of Receptor Binding Interactions 7
  1.6. Thesis Objective 10

2. EFFECTS OF C-TERMINUS AND MUTATIONS ON A_{2A}R LIGAND BINDING CHARACTERISTICS AND STABILITY 12

  2.1. Introduction 12
  2.2. Materials and Methods 14

    2.2.1. Cell Growth and Expression 14
    2.2.2. Membrane Protein Purification 14
    2.2.3. Fluorescence Anisotropy Assay 15
    2.2.4. Equilibrium Ligand Binding 16
    2.2.5. Competitive Ligand Binding Anisotropy 17
    2.2.6. Kinetic Ligand Binding Anisotropy 18
    2.2.7. Thermostability Assay 19

2.3. Results 19

2.3.1. K_D values were not significantly different with mutations 19
2.3.2. IC_{50} values were affected by mutations to $A_{2A}R$ 22
2.3.3. Kinetic rates were affected by mutations to $A_{2A}R$ 24
2.3.4. Thermostability was affected by mutations 28

2.4. Discussion and Conclusions 30

3. EFFECTS OF THE $A_{2A}R$ C-TERMINUS ON G PROTEIN ASSOCIATION 32

3.1. Introduction 32
3.2. Materials and Methods 33

3.2.1. Cell Growth and Expression of G protein 33
3.2.2. Cell Growth and Expression of Membrane Protein 34
3.2.3. Purification of G protein 35
3.2.4. Purification of Membrane Protein 36
3.2.5. Mant-GTP assay 37
3.2.6. Fluorescent ligand binding 38
3.2.7. Surface Plasmon Resonance 38

3.3. Results 40

3.3.1. Expression and Purification of Active G protein 40
3.3.2. Fluorescent ligand binding is affected by addition of G protein 43
3.3.3. Attachment of G protein to NTA chip 45
3.3.4. Choice of appropriate negative control (denatured G protein) 46
3.3.5. Removal of C-terminus effects association with G protein 47

3.4. Discussion and Conclusions 49

4. EFFECTS OF PERTURBANCES ON G PROTEIN ASSOCIATION WITH $A_{2A}R$ AND $A_{2A}\Delta316R$ 52

4.1. Introduction 52
4.2. Materials and Methods 53

4.2.1. Cell Growth and Expression of G protein 53
4.2.2. Cell Growth and Expression of Membrane Protein 54
4.2.3. Purification of G protein 54
4.2.4. Purification of Membrane Protein 56
4.2.5. Surface Plasmon Resonance 57

4.3. Results 59

4.3.1. Effects of ligand added to $A_{2A}R$ may affect association with $G\alpha_s$ 59
4.3.2. Effects of ligand added to $A_{2A}\Delta316R$ may affect association with $G\alpha_s$ 63
4.3.3. GDP affects receptor association 66
4.3.4. GTPγs inhibits receptor association 71

4.4. Discussion and Conclusions 74

5. CONCLUSIONS AND FUTURE DIRECTIONS 79

APPENDICES

A. CHARACTERIZATION OF $A_{2B}R$ CHIMERA BY FLUORESCENCE ANISOTROPY AND RADIOLIGAND BINDING 84

A.1. Introduction 84
A.2. Materials and Methods 85

A.2.1. Cell Growth and Expression 85
A.2.2. Membrane Protein Purification 85
A.2.3 Fluorescence Anisotropy Assay 86

A.2.4 Equilibrium Ligand Binding 86
A.2.5 Kinetic Ligand Binding 87

A.3. Results 88

A.3.1 Overexpression of BA and B*A 88
A.3.2. Equilibrium binding of FITC-APEC to BA 89
A.3.3. Kinetic association of FITC-APEC to BA and B*A 91
A.3.4. Radioligand binding to BA and B*A 92

A.4. Discussion and Conclusions 94

B. CHARACTERIZATION OF A_1R CHIMERA BY FLUORESCENCE ANISOTROPY AND SURFACE PLASMON RESONANCE 95

B.1. Introduction 95
B.2. Materials and Methods 95

B.2.1. Cell Growth and Expression 95
B.2.2. Membrane Protein Purification 96
B.2.3. Fluorescence Anisotropy Assay 96
B.2.4. Equilibrium Ligand Binding 97
B.2.5. Surface Plasmon Resonance 97

B.3. Results 98

B.3.1. Equilibrium ligand binding anisotropy 98
B.3.2. SPR binding 99

B.4. Discussion and Conclusions 102

LIST OF REFERENCES 103

LIST OF TABLES

Table 2.1 Equilibrium dissociation constant, K_D, and maximum potential binding capacity, B_{max}, were determined from the Scatchard plot in **Figure 2.2**. 21

Table 2.2 IC_{50} values for unlabeled ligand to $A_{2A}R$ and Rag23. Agonist was found to have highly significantly different IC_{50} values between receptors (** indicates $p<0.0001$), while antagonist, ZM 241385, showed no significant difference. 24

Table 2.3 k_{on}, k_{off}, and B_{max} values, as well as calculated K_D, for FITC-APEC binding to receptor. (*) indicates values between receptors are statistically significant ($p=0.0277$), while (**) indicates values between receptors are highly significantly different ($p<0.0001$). Data were from two purifications collected in duplicate, n=4. Constants represent average ± standard error. 26

Table 2.4 Association and dissociation rates were fit in Prism to kinetics of competitive binding model using k_1 and k_2 values that were restricted to previously determined k_{on} and k_{off} values, respectively, for FITC-APEC. (*) represents values where receptors are significantly different, and (**) represents values were receptors are highly significantly different ($p<0.0001$). 28

Table 2.5 Unfolding temperature (T_{unf}) is determined for each receptor. No comparisons were statistically significant, although values for $A_{2A}\Delta316R$ and Rag23 were similar to those seen by the Tate lab (Magnani 2008). n=6. 30

Table 3.1 Dissociation constants and maximum potential binding capacities of $A_{2A}R$ and $A_{2A}\Delta316R$ in the absence or presence of $G\alpha_s$. (*) and (^) represent values that are statistically significantly different from one another. 44

Table 3.2 Association and dissociation rates of receptor and $G\alpha_s$ were determined by fitting kinetic SPR readings of 1333 and 2000 nM of receptor coupling to 300 nM $G_{\alpha s}$, n=6. The (*) indicates that upon comparison of the $A_{2A}R$ and $A_{2A}316R$ data, the values were found to be significantly different ($p>0.0001$). 49

Table 4.1 Association and dissociation rates of purified receptor ± ligand binding to $G\alpha_s$ were determined by fitting time-dependent SPR data of 1333 and 2000 nM receptor ± 25 nM ligand, n=6. Data were collected from three separate membrane protein purifications tested in duplicate. (*) and (^) indicates that values with the same symbol are significantly different, while ($^+$) and ($^\#$) indicates values are highly significantly different ($p<0.0001$).. 62

Table 4.2 Association and dissociation rate constants for of purified receptor ± ligand binding to $G_{\alpha s}$ were determined by fitting kinetic SPR data of 1333 and 2000 nM receptor ± 25 nM ligand, n=6. Data were collected from three separate membrane protein purifications tested in duplicate. (*) and (^) indicates that values with the same symbol are significantly different, while ($^+$) and ($^\#$) indicates values are highly significantly different ($p<0.0001$). 65

Table 4.3 Association and dissociation rates of purified receptor ± ligand coupling to 300 nM $G\alpha_s$ with 600 nM GDP were determined by fitting kinetic SPR data of 1333 and 2000 nM receptor ± 25 nM ligand, n=6. Data were collected from three separate membrane protein purifications tested in duplicate. (*) and (^) indicates that values with the same symbol and receptor type are significantly different, while ($^+$) and ($^\#$) indicates values are highly significantly different ($p<0.0001$). Underlined values indicate that they are significantly different from the values determined by SPR without added GDP. All comparisons between experiments with full-length vs truncated receptor are significantly different, except for k_{off} values, of which none are significantly different. This significance is therefore not indicated in this table for clarity. 71

Table 4.4 B_{max} values of 1333 and 2000 nM purified receptor associating with $G\alpha_s$ in the absence of or with 600 nM GDP or GTPγs, n=6. Data were collected from three separate membrane protein purifications tested in duplicate. All B_{max} values are highly significantly different ($p<0.0001$) except for comparison of $A_{2A}R$ to $A_{2A}\Delta 316R$ when $G\alpha_s$ is inactivated with GTPγs, which is not statistically significant. (*) represents values that are not statistically different.. 73

LIST OF FIGURES

Figure 1.1 Representative dose response curves of agonist, antagonist, and inverse agonist binding to GPCR 2

Figure 1.2 GPCR activation upon extracellular ligand binding. Inactive receptor is shown associated with stimulatory Gαβγ, which dissociates after exchanging GDP for GTP upon ligand binding. The Gα_s subunit goes on to activate adenylyl cyclase, which increases cyclic AMP production. 3

Figure 1.3 Full-length adenosine A_{2A} receptor with common truncation of amino acids 317-412 shown with light green shading. 5

Figure 1.4 Effect of C-terminus truncation on downstream signaling of adenosine A_{2A} receptor. Measured cAMP concentrations from cells transiently expressing A_{2A}R or $A_{2A}\Delta$316R following treatment with 1 μM CGS 21680 (a selective A_{2A}R agonist) (purple) compared to no ligand control (blue). Data are mean with error bars representing 95% confidence interval, from n=3 independent experiments done in triplicate.] Figure reproduced from Figure 6.3 of of Dr. Claire McGraw's dissertation (McGraw 2018). 7

Figure 2.1 Equilibrium Anisotropy: 800 nM purified receptor was incubated for 2 hours at room temperature with 0, 0.5, 1, 10, 30, 60, or 100 nM of FITC-APEC. Data points are from three or more distinct membrane protein purifications, and equilibrium binding from each purification was observed at least in duplicate, $n \geq 6$. Error indicates standard deviation from the average. 20

Figure 2.2 Conversion of the results shown in **Figure 2.1** to RL complexes (nM), graphed vs RL/Lf. Data points from FITC-APEC concentrations 0.5-30 nM (at or below the expected K_D) were linear and represented here. From this plot, the K_D can be determined from -1/slope, and the B_{max} is the x-axis intercept. $n \geq 6$. 21

Figure 2.3 Equilibrium ligand binding of unlabeled agonist and antagonist in competition with 30 nM FITC-APEC. RL complexes decrease as concentration of competitor increases. Competition of FITC-APEC with increasing concentrations of adenosine (A), CGS 21680 (B), NECA (C), and ZM 241385 (D). Curves represent a fit for IC50 binding model from Prism. n=6. 23

Figure 2.4 (A) 30 nM FITC-APEC associating to $A_{2A}R$ and Rag 23, and (B) addition of 1 μM CGS 21680 to cause dissociation of FITC-APEC. Data were fit to association kinetics and dissociation decay, respectively, in Prism. Data were collected from two purifications of receptor, collected in duplicate, n=4. 25

Figure 2.5 Association curves of 30 nM FITC-APEC and 1 or 50 nM competitor to 800 nM purified $A_{2A}R$ or Rag23. CGS 21680 was chosen as an unlabeled agonist and binding was observed to $A_{2A}R$ (A) and Rag23 (B). ZM 241385, an antagonist, was competitively bound to $A_{2A}R$ (C) and Rag23 (D). 50 nM concentrations are n=6, and 1 nM concentrations are n=2. 27

Figure 2.6 Incubation of receptor with a thiol reactive dye, CPM, which binds to exposed cysteines, allows for monitoring of protein unfolding due to increasing temperatures. 800 nM of receptors were incubated with CPM at increasing temperature and fluorescence was determined on the plate reader every 2-10 ºC. Points represent the average of 3 purifications with experiments performed in duplicate, n=6. Error bars are standard deviation from the mean. 29

Figure 3.1 Representative sensorgram of SPR injections. Here, nickel is used to regenerate NTA chip, then $G\alpha_s$ is attached by 6xHis tag to Ni-NTA chip. Once the baseline with $G\alpha_s$ stabilizes, $A_{2A}R$ is injected. Finally, anything bound to the chip is removed by EDTA injection before beginning the cycle again........ 40

Figure 3.2 Western blot of $G\alpha_s$ purification steps to examine whether $G\alpha_s$ was present. His-tag primary antibody was used to bind to $G\alpha_s$. (1) Western C ladder, (2) whole cell lysate, (3) soluble protein lysate (post centrifuge), (4) lysate from (3) after flowing over

Ni-NTA resin, (5) flow through after wash 1, (6) flow through after wash 2, (7-10) eluant of fractions 1-4, (11) eluant of fraction 6, (12) combined fractions 3, 4, and 5. 42

Figure 3.3 Fluorescence intensity of Mant-GTP in the absence or presence of 400 nM Gα_s. Addition of Gα_s increases the fluorescence intensity, indicating Mant-GTP is binding to G protein. Results are the average of 2 Gα_s purifications (n=3). 43

Figure 3.4 800 nM purified A_{2A}R or $A_{2A}\Delta316$R was incubated with 0, 1, 10, 30, or 100 nM FITC-APEC in the absence or presence of 800 nM Gα_s. Curves were fit to One site specific binding model in Prism, and K_D and B_{max} values are significantly decreased upon addition of Gα_s except the K_D for A_{2A}R. Error bars represent SD. Results are from 3 separate receptor purifications, n=3. 44

Figure 3.5 Injection of 300 nM purified Gα_s at time = 0 seconds. Injection lasts for 60 seconds, after which a new baseline is determined. Data are from one experiment as a representative indicator of Gα_s associating with Ni-NTA chip. 45

Figure 3.6 2000 nM purified A_{2A}R is injected at time = 60 seconds at 10 μL/second across denatured Gα_s (red) and active Gα_s (green). Nonspecific binding of A_{2A}R to denatured Gα_s is subtracted from that of A_{2A}R to the active Gα_s curve to give a specific binding curve shown in orange. Data are representative of typical results from a single experiment and expressed in RU. 46

Figure 3.7 Average specific binding of purified $A_{2A}R$ at 263, 395, 592, 889, 1333, and 2000 nM associating with 300 nM $G\alpha_s$. Upon further analysis, only $A_{2A}R$ concentrations of 1333 and 2000 nM were used to determine k_{on} (8235 ±45.2), k_{off} (0.0110 ±0.00008), B_{max} (1554 ±10.1), n=6. 47

Figure 3.8 Average specific binding of purified $A_{2A}\Delta316R$ at 263, 395, 592, 889, 1333, and 2000 nM associating with 300 nM $G\alpha_s$. Upon further analysis, only receptor concentrations of 1333 and 2000 nM were used to determine k_{on} (7869 ±60.0), k_{off} (0.0125 ±0.00011), B_{max} (1078 ±10.3), n=6. 48

Figure 4.1 State dependent cholesterol binding sites on $A_{2A}R$. Snapshots taken from all atom simulations show cholesterol binding at different sites on $A_{2A}R$ depending on ligation state (cholesterol in yellow). Active receptor (R*) shows cholesterol bound at the CCM, in the intracellular leaflet between helices 2 and 4. Inactive receptor (I) shows cholesterol bound to helix 6 in the extracellular leaflet. $A_{2A}R$ is rotated to show the location of interaction. Figure reproduced with permission from Lyman, McGraw, and Robinson, unpublished work. 59

Figure 4.2 2000 nM $A_{2A}R$ without ligand (green) or preincubated with 25 nM agonist (CGS 21680) (blue) or antagonist (ZM 241385) (yellow) was injected at time zero onto $G\alpha_s$-bound SPR chips as described in section 3.2.7. In parallel, $A_{2A}R$ with and without ligand was injected onto denatured $G\alpha_s$-bound SPR chips to correct for non-specific binding (not shown). Kinetic fits were performed for specific binding of both 1333 and 2000 nM concentrations of $A_{2A}R$, but for clarity only 2000 nM is shown in this figure. Dashed lines represent SEM, n=6. 60

Figure 4.3 Schematic of kinetic rate constants for $A_{2A}R$ associating with $G\alpha_s$ in the presence or absence of ligand. Rate of association was significantly faster when $A_{2A}R$ was bound to ZM 241385 (green) than bound to CGS 21680 (red). Additionally, when $A_{2A}R$ was bound to ZM 241385 the rate of dissociation was significantly slower (purple). 62

Figure 4.4 2000 nM $A_{2A}\Delta316R$ without ligand (purple) or preincubated with 25 nM agonist (CGS 21680) (blue) or antagonist (ZM 241385) (pink) was injected at time zero onto $G\alpha_s$-bound SPR chips as described in section 3.2.7. In parallel, $A_{2A}\Delta316R$ with and without ligand was injected onto denatured $G\alpha_s$-bound SPR chips to correct for non-specific binding (not shown). Kinetic fits were performed for specific binding of both 1333 and 2000 nM concentrations of $A_{2A}\Delta316R$, but for clarity only 2000 nM is shown in this figure. Dashed lines represent SEM, n=6. 63

Figure 4.5 Schematic of kinetic rate constants for $A_{2A}\Delta316R$ associating with $G\alpha_s$ in the presence or absence of ligand (blue). All k_{on} rates are significantly different. $A_{2A}\Delta316R$ with CGS 21680 has the fastest association to $G\alpha_s$ (green solid), while $A_{2A}\Delta316R$ with ZM 241385 has the slowest (purple solid). Dissociation rate constants were significantly different, with $A_{2A}\Delta316R$ bound to ZM 241385 having the fastest dissociation (green dashed) and $A_{2A}\Delta316R$ bound to CGS 21680 having the slowest dissociation (purple dashed). 65

Figure 4.6 SPR data of 2000 nM $A_{2A}R$ with or without ligand injected at time=0 onto 300 nM $G\alpha_s$ activated with 600 nM GDP. Data were fit using data from $A_{2A}R$ at 1333 and 2000 nM, but for clarity only 2000 nM is shown. Dashed lines represent SEM. Experiments were performed using three separate receptor purifications collected in duplicate, n=6. 66

Figure 4.7 SPR data of 2000 nM $A_{2A}\Delta316R$ with or without ligand injected at time=0 onto 300 nM $G\alpha_s$ activated with 600 nM GDP. Data were fit using data from $A_{2A}\Delta316R$ at 1333 and 2000 nM, but for clarity only 2000 nM is shown. Dashed lines represent SEM. Experiments were performed using three separate receptor purifications collected in duplicate, n=6. 67

Figure 4.8 Schematic of kinetic rate constants for $A_{2A}R$ associating with $G\alpha_s$-GDP in the presence or absence of ligand. Kinetic rate constants are not significantly different, except for $A_{2A}R$ bound to CGS 21680, which has a significantly slower on rate (red). .. 69

Figure 4.9 Schematic of kinetic rate constants for $A_{2A}\Delta316R$ associating with $G\alpha_s$-GDP in the presence or absence of ligand (blue). All k_{on} rates are significantly different. $A_{2A}\Delta316R$ bound to CGS 21680 has the fastest association to $G\alpha_s$ (green), while $A_{2A}\Delta316R$ bound to ZM 241385 has the slowest (purple). 70

Figure 4.10 SPR of 2000 nM $A_{2A}R$ injected at time=0 over 300 nM $G\alpha_s$ in the absence of (green) or presence of either 600 nM GDP (blue) or 600 nM GTPγs (black). Data were fit using data from $A_{2A}R$ at 1333 and 2000 nM, but for clarity only 2000 nM is shown. Dashed lines represent SEM. Experiments were performed using three separate receptor purifications collected in duplicate, n=6. 72

Figure 4.11 SPR of 2000 nM $A_{2A}\Delta316R$ injected at time=0 over 300 nM $G\alpha_s$ in the absence of (purple) or presence of either 600 nM GDP (blue) or 600 nM GTPγs (black). Data were fit using data from $A_{2A}\Delta316R$ at 1333 and 2000 nM, but for clarity only 2000 nM is shown. Dashed lines represent SEM. Experiments were performed using three separate receptor purifications collected in duplicate, n=6. 72

Figure A.1 Western blot of lysed cells expressing BA and B*A induced by galactose for 12-24 hours. The lower band at 40 kDa represents the expressed receptor. 88

Figure A.2 Raw anisotropy data (scatter subtracted) of 1 μM BA and empty detergent micelles incubated with 0-10 nM FITC-APEC. Data suggests that BA is active and binding to FITC-APEC, as the anisotropy curve is greater than the micelle anisotropy. All points have at least 4 replicates, but most have n≥6. Error bars represent standard deviation from the mean. 90

Figure A.3 RL complexes of FITC-APEC and BA. Anisotropy from Figure A.1. was converted into RL complexes as described in Chapter 2. Curve was fit to a One site-Specific binding model in Prism. Data represent n≥4. Error bars represent standard deviation from the mean. 90

Figure A.4 RL complexes of 0.5 nM FITC-APEC associating to BA and B*A over 80 minutes. Raw anisotropy data (not shown) was converted to RL complexes to obtain ligand association curve. Data represent n=3. 91

Figure A.5 Incubation of purified BA with 80 nM [^{3}H] NECA ± 5000 nM BAY60-6583. Addition of competitor appears to decrease radioligand binding by 15%, although perhaps with a hot ligand that binds more BA, the addition of BAY60-6583 would further improve the signal to noise ratio. Results were from one purification with experiment performed in duplicate. 93

Figure A.6 CPM of purified BA and B*A at room temperature or 4°C incubated with 5 nM [^{3}H] MRE 2029-F20. Results were read after 2 hours of incubation with ligand (2 hrs shown in blue) and again after 24 hours without ligand (shown in orange). An increase in CPM was observed by reading the samples at 24 hours, although the amount of radioligand in each sample was the same at the 2 and 24 hour time points. Data are from one purification with each experiment performed in duplicate. 93

Figure B.1 Equilibrium ligand binding of 1-100 nM FITC-APEC to purified A_{2A}R and A_{1-2A}R. Points represent FITC-APEC concentrations of 1, 10, 30, 60, and 100 nM, and each point represents 2 separate purifications tested to check for receptor activity......... 98

Figure B.2 Conversion of the data points from Figure B.1 to RL complexes (nM) as described in Section 2.2.4 Equilibrium Ligand Binding. Points represent FITC-APEC concentrations of 1, 10, 20, 60, and 100 nM binding to 800 nM of purified A_{2A}R or A_{1-2A}R. Each point represents two separate purifications.. 99

Figure B.3 Affinity curve of 1, 5, 10, and 20 nM NECA with 1 μM purified $A_{1\text{-}2A}R$ and $A_{2A}R$. $A_{2A}R$ appears to have a greater affinity for NECA. Data are from 2 separate receptor purifications. N=1, 2, or 3 depending on the NECA concentration................. 100

Figure B.4 Representative kinetic binding of 1, 5, or 10 nM NECA to 1 μM purified $A_{1\text{-}2A}R$. Data suggest a concentration dependent affinity of NECA for receptor. 100

Figure B.5 Representative kinetic binding of 1, 5, 10, or 20 nM NECA to 1 μM purified $A_{2A}R$. Data suggest a concentration dependent affinity of NECA for receptor. 101

Figure B.6 Representative kinetic binding of 0.05, 0.1, 0.5, or 1 nM DPCPX to 1 μM purified $A_{1\text{-}2A}R$. Data suggest a concentration dependent affinity of antagonist for receptor. 101

Chapter 1

INTRODUCTION

1.1. G Protein-Coupled Receptors

G protein-coupled receptors (GPCRs) are the largest family of receptor proteins in humans. These receptors have seven transmembrane alpha-helices that interact with extracellular ligands to promote intracellular downstream signaling via interaction with G proteins. This positioning in the cell membrane makes GPCRs ideal drug targets, as they respond to a variety of extracellular stimuli (e.g. light, hormones, small molecules) that may activate or inhibit a downstream signaling response. More than 30% of all drugs on the market target GPCRs for conditions such as pain, hypertension, and schizophrenia, making GPCRs of great interest to the pharmaceutical industry (Hill 2006). However, these drugs target only 10% of known GPCRs, indicating an opportunity for further drug development potential in this area (Rask-Andersen 2011; Sriram 2018).

GPCRs all interact with G proteins to communicate signals from extracellular stimuli such as light, hormones, and neurotransmitters (Devree 2016). Types of stimuli are agonists, antagonists, or inverse agonists. The type of stimuli is determined by how the binding affects the receptor behavior (**Figure 1.1**). An antagonist binding to receptor maintains the receptor signaling at constitutive signaling levels, but prevents agonist binding, thereby keeping the receptor in a neutral state. Binding of an agonist to receptor increases downstream signaling levels, while binding of inverse agonist decreases signaling levels below that of constitutive activity (Duc 2015; Bokoch 2010).

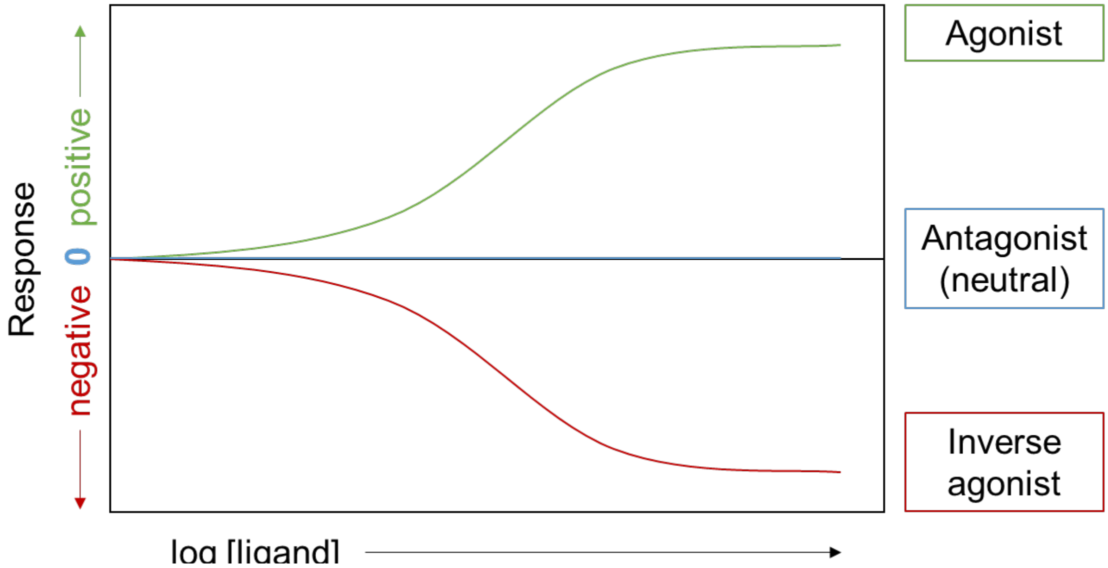

Figure 1.1 Representative dose response curves of agonist, antagonist, and inverse agonist binding to GPCR

Addition of agonist, antagonist, or inverse agonist all effect the downstream signaling cascade, and therefore G protein activation. There are many types of G proteins, all of which begin different intracellular signaling cascades by coupling to and dissociating from different GPCRs upon activation. These G proteins are comprised of three subunits, α, β, and γ, that couple and signal in different ways, although the β and γ subunits often signal as a complex (Neves 2002). In this work, stimulatory G protein α subunit, $G\alpha_s$, will be the most relevant. Briefly, $G\alpha_s\beta\gamma$ bound to GDP is associated with a GPCR not yet activated by ligand. Agonist binding to the receptor activates the downstream signaling cascade by way of a conformational change in the GPCR. Upon ligand binding, the GPCR undergoes a conformational change, causing interactions within the G protein, which releases GDP in exchange for GTP (**Figure 1.2**) (Latorraca 2016). This exchange causes Gα_s to dissociate from the G$\beta\gamma$ subunit. Gα_s goes on to activate adenylyl cyclase (AC), which in turn increases second messenger cyclic AMP (cAMP) production that, further downstream, increases gene expression (Tuteja 2009; Adamson 2014).

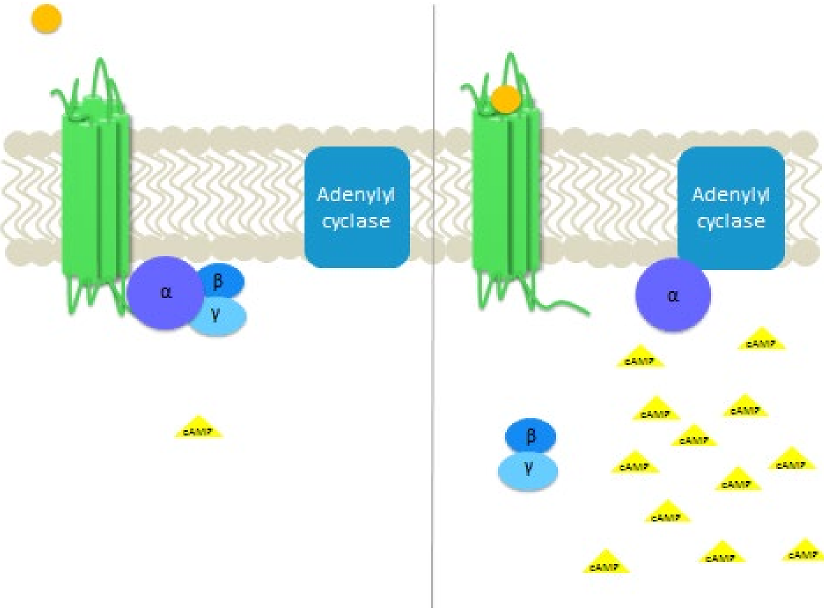

Figure 1.2 GPCR activation upon extracellular ligand binding. Inactive receptor is shown associated with stimulatory G$\alpha\beta\gamma$, which dissociates after exchanging GDP for GTP upon ligand binding. The Gα_s subunit goes on to activate adenylyl cyclase, which increases cyclic AMP production.

1.2. Adenosine Receptors

Adenosine receptors are GPCRs that are expressed widely throughout the body, and are therefore often a therapeutic target for many diseases including neurodegenerative, inflammatory, and heart diseases (Fried 2017; Rivera-Oliver 2014; de Lera Ruiz 2014). Within the adenosine receptor family, there are four types, A_1R, $A_{2A}R$,

$A_{2B}R$, and A_3R, that all bind to adenosine, albeit with different affinities, as well as a variety of other agonists and antagonists (Jacobson 2006). Many agonists and antagonists that are selective for just one of the adenosine receptors have been discovered and characterized; however, only a handful of these have gone through clinical trials and been approved for market (Muller 2011).

1.3. Crystallization of the Adenosine A_{2A} Receptor

The adenosine A_{2A} receptor, $A_{2A}R$, is the most well characterized of the four adenosine receptors, in part due to its higher level of expression. Greater concentrations of $A_{2A}R$ mean a better signal to noise ratio when observing binding with labeled ligand. However, ligand binding characterization does not always fully elucidate the structure-function relationship of the receptor. Therefore, there has been interest in crystallizing $A_{2A}R$ so that the ligand binding pocket may be better characterized for drug discovery efforts. To date, $A_{2A}R$ has been crystallized in a few different conformations, namely, bound to agonist (Xu 2011), bound to antagonist (Jaakola 2008; Dore 2011; Hino 2012), and associated with a mini-G_s (Carpenter 2016).

Although these crystal structures are detailed and informative in regards to $A_{2A}R$ structure when associated with different ligands and G protein, all current crystal structures truncate the $A_{2A}R$ C-terminus from 412 amino acids down to 316 or 310 (Lebon 2011; Dore 2011). As a crystallization strategy, this truncation makes sense considering that the C-terminus of the $A_{2A}R$ receptor is long and unstructured (**Figure 1.3**). Additionally, other mutations such as thermostabilizing point mutations and/or stabilization by T4 lysozyme fusion, have been performed to further stabilize the receptor in a given conformation for crystallization (Jaakola 2008; Dore 2011). These point mutations are often designed to enhance receptor affinity for either agonist or antagonist, so that the presence of the given ligand will further stabilize the receptor to enhance crystallization (Tate 2012). However, the addition of so many mutations calls into question the authenticity of the crystal structure and its potential value for therapeutic design. Point mutations and truncation of the C-terminus make it difficult to know if the mutant receptor that has been crystallized truly behaves in the same manner as wild-type $A_{2A}R$.

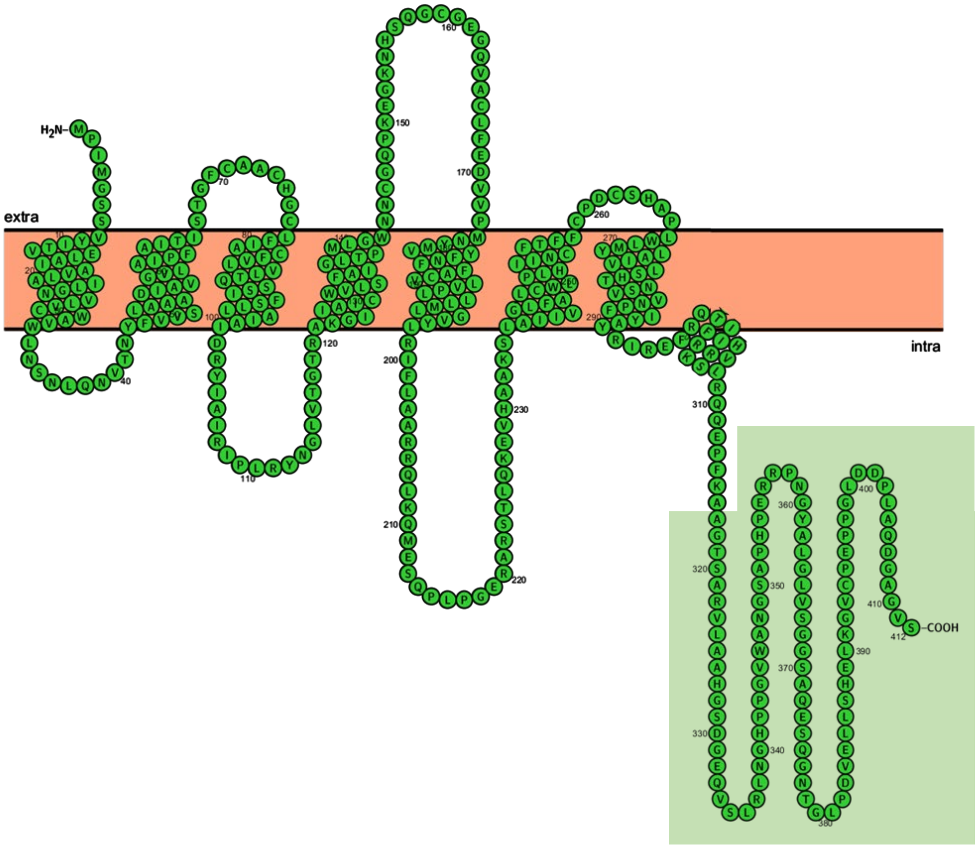
H_2N-
extra
intra
-COOH
20
40
70
100
110
120
150
160
170
200
210
220
230
260
270
290
310
320
330
340
350
360
370
380
390
400
410
412

Figure 1.3 Full-length adenosine A_{2A} receptor with common truncation of amino acids 317-412 shown with light green shading.

1.4. Impact of the $A_{2A}R$ C-terminus on Downstream Signaling

Despite the common use of a truncated $A_{2A}R$ for all of the crystal structures, previous work in our lab showed that truncation of the $A_{2A}R$ C-terminus reduced downstream signaling. Dr. Claire McGraw measured cAMP activity in HEK cells transiently expressing empty vector, $A_{2A}R$, and receptor truncated at amino acid 316, $A_{2A}\Delta316R$ (**Figure 1.4**). In the absence of ligand (blue bars), $A_{2A}R$ showed constitutive cAMP activity, and upon addition of 1 μM CGS 21680, a potent $A_{2A}R$ agonist expected to increase cAMP production, Dr. McGraw observed an increase in cAMP. Empty vector (pCEP4) showed little constitutive activity with little change upon addition of CGS 21680, and $A_{2A}\Delta316R$ behaved in the same manner as pCEP4. These results suggest that the presence of the $A_{2A}R$ C-terminus is critical for initiation of the downstream signaling cascade, although the point where signaling is affected is unknown. Due to the observed effect on cAMP, we can expect that the signaling pathway is disrupted somewhere between the receptor and cAMP production, and we hypothesize that the absence of the C-terminus has an effect on G protein coupling to the receptor.

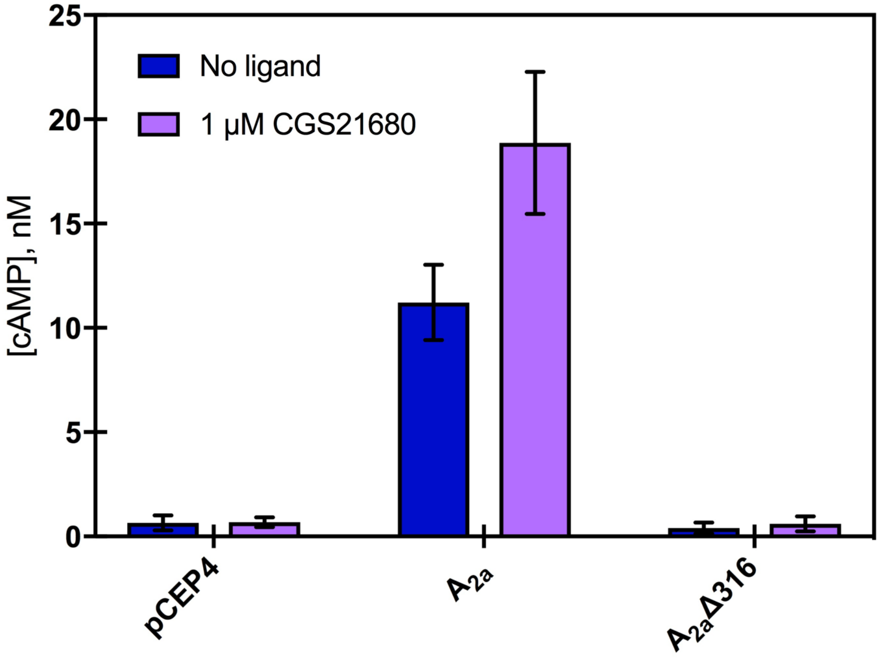

Figure 1.4 Effect of C-terminus truncation on downstream signaling of adenosine A_{2A} receptor. Measured cAMP concentrations from cells transiently expressing A_{2A}R or $A_{2A}\Delta316$R following treatment with 1 µM CGS 21680 (a selective A_{2A}R agonist) (purple) compared to no ligand control (blue). Data are mean with error bars representing 95% confidence interval, from n=3 independent experiments done in triplicate.] Figure reproduced from Figure 6.3 of of Dr. Claire McGraw's dissertation (McGraw 2018).

1.5. Kinetics of Receptor Binding Interactions

Ligand binding is often used to characterize GPCRs in a way that is meaningful when considering pharmaceutical development. Typically, drugs are characterized by their affinity for receptor, their binding duration, and their ability to alter behavior (e.g. initiate a downstream signaling response) (Kenakin 2012). Observation of agonists, antagonists, and inverse-agonists binding to receptors is one important way to determine if a ligand has a great enough affinity or is selective for the target receptor. However, recent reports suggest that determination of affinity and selectivity of a drug for receptor *in vitro* is not enough to predict the characteristics of the drug *in vivo*, instead indicating that kinetic association and dissociation rates are more predictive of drug efficacy (Strasser 2017; Nederpelt 2017; Guo 2014). Initially, the concept of drug residence time in the receptor, simplified to $1/k_{off}$, was determined to be an important characteristic in predictability of drug success (Copeland 2006). Today, it is believed that full characterization of kinetic events (e.g. association and dissociation rate constants) in combination with affinity and drug residence time can provide a more complete picture of drug behavior *in vivo* (Strasser 2017; Nederpelt 2017).

Traditionally, ligand binding experiments are performed with a labeled ligand so that binding events can be readily observed. Historically, ligand binding was often characterized via radiolabeled ligand binding. However, determination of fast association and dissociation rates can be difficult, as unbound radiolabeled ligand must be washed away before measurement. For this reason, fluorescent ligand binding has become a more common, less expensive, safer, method of determining kinetic binding rates (Swonger 2018). This technique uses a fluorescently labeled ligand to observe polarized light scatter, which can be converted into anisotropy to determine the amount of bound and free fluorescent ligand. This technique is versatile as binding events can be read in near-real time to give rate constants, or unlabeled competitor ligand can be added to determine competition binding constants.

A newer technique for characterization of ligand binding is surface plasmon resonance, SPR. This method is unique in that it does not require the use of labeled ligand or receptor, other than a method of attaching one to a gold chip. In this dissertation, a 6 or

10xHis tag with affinity for Ni-NTA was used to attach proteins of interest to an SPR chip, as the presence of this His tag shows little indication that it affects receptor activity (Stenlund 2011). SPR works by measuring the angle at which polarized light resonates off an electrically conducting surface (e.g. gold chip). As the mass on the chip surface changes (e.g. ligand binding to receptor), the resonance angle changes, and the equipment reports a change in resonance units (GE Healthcare 2019). SPR has been shown to be sensitive enough to capture fast kinetic rate constants that may be useful in characterizing drug efficacy.

1.6. Thesis Objective

The primary objective of this work was to determine how mutations to the adenosine A_{2A} receptor ($A_{2A}R$), especially truncation of the C-terminus, affect ligand binding characteristics, thermostability, and downstream signaling events. This was observed in several ways:

- Fluorescent ligand binding to characterize equilibrium binding, competitive binding, and kinetic rate constants of $A_{2A}R$ and mutants (Chapter 2)
- Determination of thermostability of $A_{2A}R$ and mutants (Chapter 2)
- Observation and kinetic characterization of coupling of $A_{2A}R$ and $A_{2A}\Delta316R$ to $G\alpha_s$ via SPR (Chapter 3)
- Effects of ligand on receptor association to $G\alpha_s$ via SPR (Chapter 4)

Fluorescence anisotropy was used to observe ligand binding to purified $A_{2A}R$ and mutants to characterize any changes in a number of ligand binding constants with a range of ligands. This is explored in Chapter 2, which additionally discusses whether the mutations alter thermostability of the receptor. Then, effects on downstream signaling due to truncation of the C-terminus were expanded upon by observing $A_{2A}R$ and $A_{2A}\Delta316R$ coupling to $G\alpha_s$. In Chapter 3, receptors in the absence of ligand were injected across purified G protein at a range of concentrations to observe kinetic rates of association and dissociation of receptors to $G\alpha_s$. In Chapter 4, associations between receptors incubated with ligand and/or $G\alpha_s$ incubated with GDP or GTP were observed via SPR. This dissertation explores a variety of methods for observing the effects of mutations on ligand binding and downstream signaling, and thus informs on the effects of C-terminal truncation on ligand binding, stability, and association to Gα_s.

Chapter 2

EFFECTS OF C-TERMINUS AND MUTATIONS ON $A_{2A}R$ LIGAND BINDING CHARACTERISTICS AND STABILITY

2.1. Introduction

High-resolution structures (e.g. crystal structures) or biophysical characterization of a GPCR can provide a better understanding of the structure-function relationship and aid in drug discovery (Piirainen 2011). However, crystallization of membrane proteins can be difficult due to challenges that arise when removing the protein from its native membrane, as well as difficulties crystallizing unstable proteins. For these reasons, most membrane proteins undergo stabilizing mutations to aid in crystallization and are extracted in a membrane-mimetic environment to maintain proper folding. Common stabilizing mutations include point mutations to increase the unfolding temperature or enhance affinity for ligand, as well as removing or replacing unstable segments of the receptor (Heydenreich 2015). These mutations, while useful for crystallization, may alter the GPCR structure and/or function, although it is unknown to what degree.

Despite the challenges involved in crystallizing GPCRs, a number of receptors have already been crystallized, including rhodopsin, β_2AR, and $A_{2A}R$ (Palczewski 2000; Rasmussen 2011; Xu 2011). The adenosine A_{2A} receptor ($A_{2A}R$) is the most well characterized adenosine receptor and has been crystallized in a number of conformations, including receptor bound to agonist and antagonist, as well as interacting with a mini G_s (Carpenter 2016; Jaakola 2008; Xu 2011). However, each of the $A_{2A}R$ crystal structures has been discovered using an altered version of $A_{2A}R$. That is, all of the crystal structures truncate nearly 100 amino acids from the $A_{2A}R$ C-terminus. One variant, Rag23, is truncated at amino acid 316, and has five thermostabilizing point mutations designed to have an increased affinity for agonist binding (Magnani 2008). Since thermostability was engineered relative to $A_{2A}\Delta 316R$, the impact of the point mutations relative to the wild type protein has not been previously described. These crystal structures provide insight into the ligand binding pocket for therapeutic development, but may not elucidate dynamic binding features, especially protein-protein interactions (Bertheleme 2013). In fact, recent results from our lab implicate the C-terminus in G protein specificity for the adenosine receptor family (Jain, in review).

In this chapter, fluorescent ligand binding was used to characterize the impact of mutations on $A_{2A}R$. Polarized light determined from rotation of bound and unbound fluorescent ligand can be read almost instantaneously and converted to anisotropy. This allows for characterization of fast kinetic on and off rates, which are difficult to obtain via radioligand binding, since radioligand binding requires time to remove any unbound ligand. Here, anisotropy is also used in determining equilibrium binding as well as competition with unlabeled ligand (Swonger 2018). Additionally, the thermostability of the Rag23 variant was quantified alongside wild-type receptor. The effects of the $A_{2A}R$ C-terminus and point mutations on ligand binding and thermostability for $A_{2A}R$, $A_{2A}\Delta 316R$, and Rag23 can be characterized by fluorescence.

2.2. Materials and Methods

2.2.1. Cell Growth and Expression

Receptors were expressed in yeast strain BJ5464 (*MATa ura3-52 trp1 leu2Δ1 hisΔ200 pep4::HIS3 prb1Δ1.6R can1* GAL) using a multi-integrating vector, pITy. pITy contains a Gal1-10 promoter, allowing for galactose induction, and a C-terminal His10 tag, allowing for efficient purification of the receptors. $A_{2A}R$, $A_{2A}\Delta 316R$, and Rag23 were grown overnight in glucose media (YPD consisting of 1% yeast extract, 2% peptone, and 2% glucose) to an optical density (O.D.) of 13 or more. Cells were induced by transfer into galactose-containing media (YPG consisting of 1% yeast extract, 2% peptone, and 2% galactose) to an O.D. of 1 and grown for 30 hours before pelleting. Cell pellets contained 1250 ODs of yeast cells and were stored at -80°C.

2.2.2. Membrane Protein Purification

Receptors were purified as previously described (Naranjo 2016). Briefly, cell pellets were resuspended with 22 mL lysis buffer, 220 μL 100 mM phenylmethane sulfonyl fluoride (PMSF), and one cOmplete™, EDTA-free Protease Inhibitor tablet (Sigma Aldrich) before lysis with 0.5 mm zirconia silica beads (BioSpec). Lysed cells were then sonicated at 50% pulses for 20 seconds, placed on ice for 20 seconds, and sonicated a second time. The sonicated samples were centrifuged at 3200 g for 30 minutes to pellet any remaining cell debris. The supernatant was then centrifuged at 100,000 g for 1 hour to pellet the cell membranes. Membranes were resuspended in 0.1% n-Dodecyl-β-D-Maltopyranoside (DDM)/0.1% 3-[(3-Cholamidopropyl)-Dimethylammonio]-1-Propane Sulfonate (CHAPS)/0.02% cholesterol hemisuccinate

(CHS) (Anatrace) and left to equilibrate overnight at 4°C. The next day, the solution was centrifuged at 70,000 g for 1 hour to remove any insoluble material. Supernatant was incubated overnight at 4ºC with 0.5 mL Ni-NTA resin (Qiagen) previously equilibrated with lysis buffer and detergents. The next day, the resin was washed with increasing concentrations of imidazole (20-50 mM), and, finally, incubated with 50 mM imidazole and 10 mM EDTA for 2 hours to elute the receptor. The final solution was run through PD-10 desalting columns (GE Healthcare) (previously equilibrated with lysis buffer and 0.1% DDM/0.1% CHAPS/0.02% CHS) to remove any remaining imidazole, and receptor concentrations were determined by A_{280} measurements. Purified receptors were stored at 4°C and used within one week of purification.

2.2.3. Fluorescence Anisotropy Assay

FITC-APEC (NIMH synthesis program, nimh-repository.rti.org, NIMH code: D-906), an adenosine receptor agonist, was used to determine ligand binding affinity and kinetics. Samples were read in 96 well half-area black Corning plates (catalog #3875, Corning Incorporated) on a Synergy H1 plate reader (BioTek, Winooski, VT) using a polarized filter cube with an excitation wavelength of 480-485 nm and an emission wavelength of 520-528 nm. All measurements were taken at a constant gain of 75, and scatter measurements were taken for each sample at each experiment. Parallel and perpendicular values were recorded and anisotropy was calculated as previously described (Swonger 2018). Briefly, the fluorescence due to scatter was subtracted from respective parallel and perpendicular FITC-APEC containing samples. Further calculations are described below. All unlabeled ligands were purchased from Tocris.

2.2.4. Equilibrium Ligand Binding

Purified receptor (in 0.1% DDM/0.1% CHAPS/0.02% CHS) was incubated with increasing amounts of fluorescent adenosine receptor agonist FITC-APEC for 2 hours at room temperature. Protein and control (detergent micelles lacking receptor) were incubated in 96 well half-area black Corning at a final concentration of 800 nM and a working volume of 100 µL. FITC-APEC was previously aliquoted into DMSO such that 1 µL could be added to each well, ensuring that each sample consisted of the same amount of DMSO. Previous work has indicated that DMSO concentrations below 5% have little effect on observed anisotropy signal (Allen 2000), so these experiments were designed to contain up to 2% DMSO. Samples were incubated at room temperature in darkness for 2 hours, then samples were read on a Synergy H1 plate reader using a polarized filter cube with an excitation wavelength of 480-485 nm and an emission wavelength of 520-528 nm. Parallel and perpendicular values were recorded and anisotropy was calculated as previously described (Swonger 2018). Fluorescence emission from samples without labeled ligand was subtracted from parallel and perpendicular emission, respectively, of samples with labeled ligand to account for light scattering. Next, anisotropy was calculated for each sample using

$$A = \frac{(F_{||} - F_{+})}{(F_{||} + 2 * F_{+})} * 1000$$

where A is anisotropy in milli-anisotropy, $F_{||}$ is parallel emission intensity, corrected for scatter, and F_{+} is perpendicular emission intensity, corrected for scatter. From these values, maximum anisotropy, A_{max}, was determined for each protein, and A_{min} was defined as the minimum anisotropy given by micelles with no receptor. Using these values, the receptor-ligand complex, RL, is calculated by

$$A = A_{max} \frac{RL}{L_T} + A_{min} \frac{L_T - RL}{L_T}$$

where L_T is the total labeled ligand added, here 0.5, 1, 10, 30, 60, and 100 nM. Next, the number of RL complexes were determined for each receptor at each labeled ligand concentration. Finally, the results were graphed in a Scatchard plot (RL vs RL/L_f where $L_f = L_T - RL$) and fit to determine K_D and B_{max} values. K_D is equal to -1/slope and B_{max} is the x-axis intercept.

2.2.5. Competitive Ligand Binding Anisotropy

Purified receptor (in 0.1% DDM/0.1% CHAPS/0.02%CHS) was incubated with 30 nM FITC-APEC and increasing amounts of competitor (adenosine, CGS 21680, NECA, or ZM 241385) for 2 hours in darkness at room temperature. Protein and control (detergent micelles lacking receptor) were incubated in 96 well half-area black Corning plates at a final concentration of 800 nM and a working volume of 100 µL. All ligands were previously aliquoted into DMSO so that 1 µL could be added to each well, ensuring that each sample consisted of the same amount of DMSO. After incubating for 2 hours, the samples were read on a Synergy H1 plate reader using a polarized filter cube with an excitation wavelength of 480-485 nm and an emission wavelength of 520-528 nm. Parallel and perpendicular values were recorded and anisotropy and RL were determined as described in Section 2.2.4. Ligand binding curves were fit to one site—IC50 binding model using Prism (GraphPad) to determine IC_{50} values.

2.2.6. Kinetic Ligand Binding Anisotropy

To determine FITC-APEC kinetic association and dissociation rates, 800 nM of purified receptor (in 0.1% DDM/0.1% CHAPS/0.02% CHS) was added to a half area 96 well plate. 30 nM FITC-APEC was added to each well, and the plate reader began taking measurements immediately, using the same conditions as in Equilibrium Ligand Binding. Measurements were taken every 7 seconds for 2 hours. After 2 hours, 1 μM of competitor (CGS 21680) was added and measurements began immediately. Measurements were taken every 7 seconds for 2 hours following addition of competitor. Anisotropy and RL were determined as described in Equilibrium Ligand Binding. Ligand dissociation curves were fit to a dissociation--one phase decay model using Prism (GraphPad) to determine the k_{off} for FITC-APEC. Next, the k_{on} for FITC-APEC was determined by constraining the k_{off} to the previously determined value, and fit to the association kinetics—one concentration of hot ligand model using Prism (GraphPad).

After characterizing the kinetic rates of FITC-APEC, kinetic rates of competitor can be determined. 1 or 50 nM of competitor (CGS 21680 or ZM 241385) premixed with 30 nM FITC-APEC was added to 800 nM of purified receptor (in 0.1% DDM/0.1% CHAPS/0.02% CHS) in a half area 96 well plate. The plate reader began taking measurements immediately, reading each well every 7 seconds for 2 hours. Simultaneous association of 30 nM FITC-APEC and 1 nM or 50 nM of competitor were fit to kinetics of competitive binding model using Prism (GraphPad). This model requires at least two concentrations of unlabeled competitor to be added simultaneously with one concentration of labeled ligand with predetermined k_{on} and k_{off} values. The model was restricted using the kinetic rate constants determined above for FITC-APEC, and k_{on} and k_{off} rates were fit for unlabeled competitors.

2.2.7. Thermostability Assay

Purified receptor (in 0.1% DDM/0.1% CHAPS/0.02%CHS) and control (detergent micelles lacking receptor) were incubated with 10 µg/mL 7-diethylamino-3-(4′-maleimidylphenyl)-4-methylcoumarin (CPM) (Invitrogen) for 1 hour at 4°C in a half area 96 well plate. Samples were incubated at increasing temperatures for 1 minute and read on a Synergy H1 plate reader at an excitation/emission of 387/463 nm. Results were graphed as temperature (°C) vs fluorescence intensity. Unfolding temperature curves were fit to an [agonist] vs response variable slope binding model using Prism, and T_{unf} was determined.

2.3. Results

2.3.1. K_D values were not significantly different with mutations

To explore the effects of the C-terminus and stabilizing point mutations on $A_{2A}R$ we began by comparing equilibrium ligand binding characteristics of $A_{2A}R$, $A_{2A}\Delta316R$, and Rag23 ($A_{2A}\Delta316R$ plus 5 thermostabilizing point mutations designed to increase affinity for agonist binding) (Magnani 2008). The equilibrium dissociation constant (K_D) was determined in the depleted ligand regime by incubating 800 nM of purified receptors with increasing amounts of fluorescent ligand (FITC-APEC). Using fluorescence polarization measurements, anisotropy of bound complexes was calculated (**Figure 2.1**). Anisotropy was transformed into receptor ligand complexes (RL) to enhance visualization of binding differences (**Figure 2.2**), and the K_D and maximum available binding sites (B_{max}) were determined (**Table 2.1**). These results indicate that Rag23 has increased affinity for FITC-APEC, an agonist, and $A_{2A}\Delta316R$ has decreased affinity for FITC-APEC as compared to $A_{2A}R$. This suggests that removal of the $A_{2A}R$ C-terminus leads to decreased agonist affinity that can be compensated for with the addition of agonist affinity enhancing point mutations.

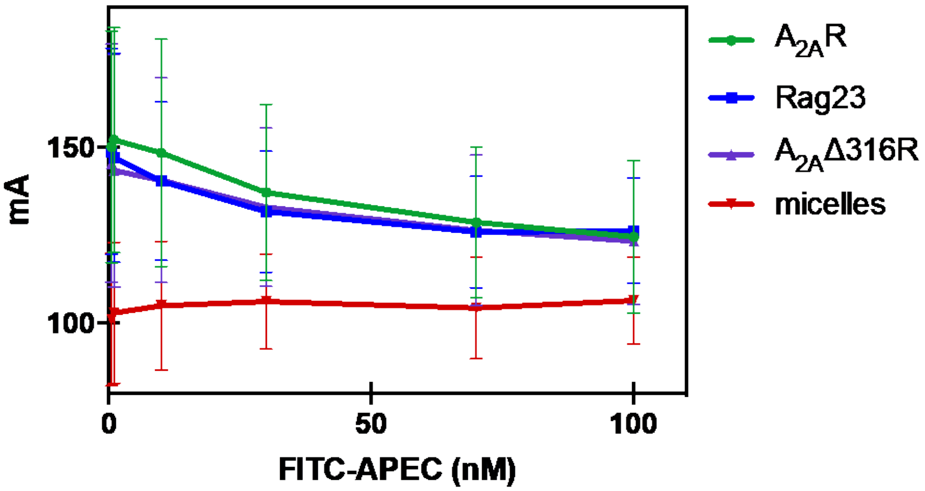

Figure 2.1 Equilibrium Anisotropy: 800 nM purified receptor was incubated for 2 hours at room temperature with 0, 0.5, 1, 10, 30, 60, or 100 nM of FITC-APEC. Data points are from three or more distinct membrane protein purifications, and equilibrium binding from each purification was observed at least in duplicate, n≥6. Error indicates standard deviation from the average.

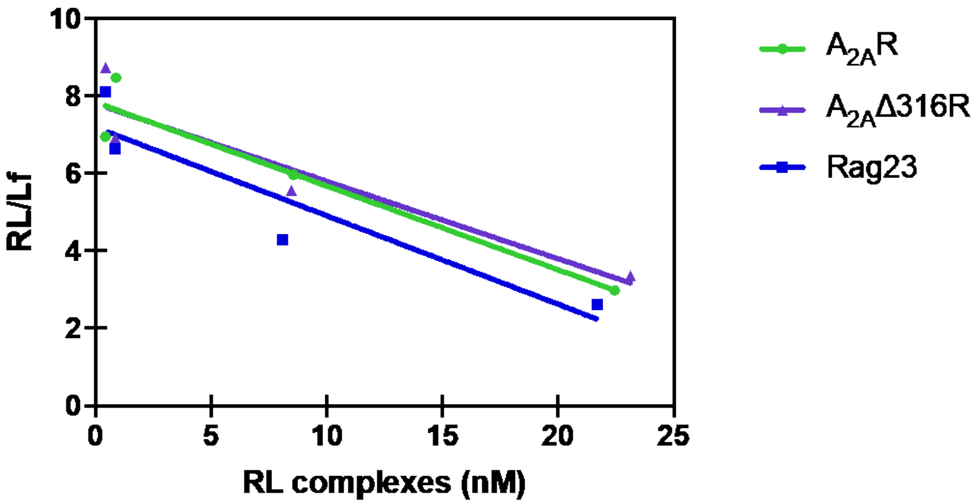

Figure 2.2 Conversion of the results shown in **Figure 2.1** to RL complexes (nM), graphed vs RL/Lf. Data points from FITC-APEC concentrations 0.5-30 nM (at or below the expected K_D) were linear and represented here. From this plot, the K_D can be determined from -1/slope, and the B_{max} is the x-axis intercept. n≥6.

	K_D (nM±SE)	**B_{max} (nM±SE)**
$A_{2A}R$	4.6 (±1.3)	36.3 (±2.6)
$A_{2A}\Delta 316R$	5.0 (±1.8)	39.0 (±3.2)
Rag23	4.4 (±1.7)	31.5 (±3.3)

Table 2.1 Equilibrium dissociation constant, K_D, and maximum potential binding capacity, B_{max}, were determined from the Scatchard plot in **Figure 2.2**.

2.3.2. IC_{50} values were affected by mutations to $A_{2A}R$

Inhibitor dissociation constants (IC_{50}) were determined for unlabeled ligands--adenosine, CGS 21680, NECA, and ZM 241685. Adenosine, CGS 21680, and NECA are $A_{2A}R$ agonists, while ZM 241685 is an antagonist. All four ligands are expected to have a greater affinity than FITC-APEC for receptor (McNeely 2017), and, therefore, should out-compete FITC-APEC for a common ligand binding site. Increasing amounts of an unlabeled ligand was incubated with 800 nM of receptor and 30 nM FITC-APEC for two hours before collecting polarized light intensities. Anisotropy was determined and then transformed into RL (**Figure 2.3**). For agonist (adenosine, CGS 21680, and NECA) IC_{50} values (**Table 2.2**) were highly significant for $A_{2A}R$ as compared to Rag23. The IC_{50} values were determined to be 2-3 fold greater for $A_{2A}R$, indicating that Rag23 has a greater affinity for these agonists, as expected when considering the five point mutations of Rag23 were chosen to increase the receptor affinity for agonist. The IC_{50} results for antagonist ZM 241385 are also significant. Here, the IC_{50} of Rag23 is three-fold greater than $A_{2A}R$, suggesting that $A_{2A}R$ has a greater affinity for this antagonist. These results indicate that the point mutations designed to favor agonist binding in Rag23 appear to increase affinity for agonist and decrease affinity for antagonist.

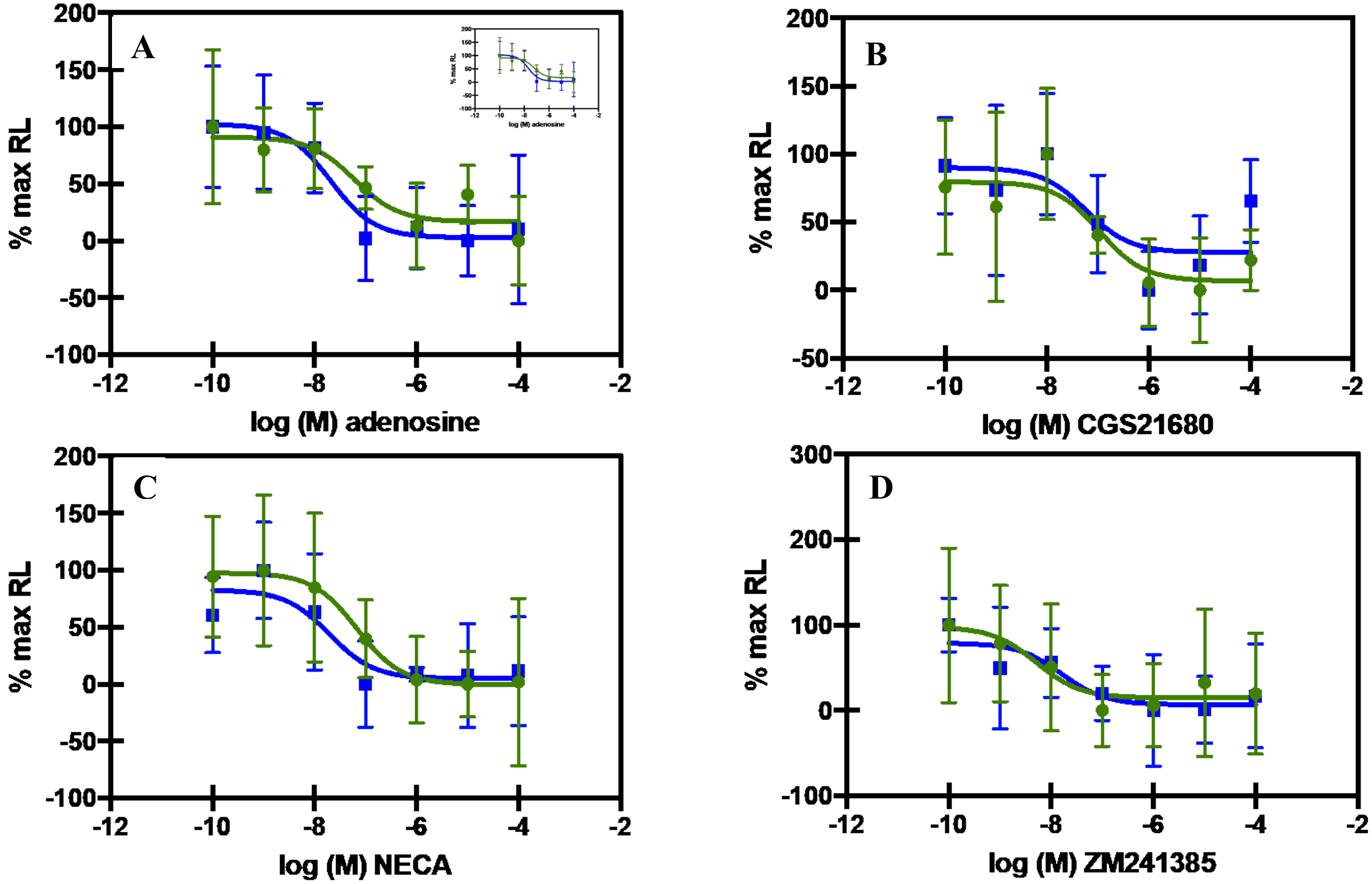

Figure 2.3 Equilibrium ligand binding of unlabeled agonist and antagonist in competition with 30 nM FITC-APEC. RL complexes decrease as concentration of competitor increases. Competition of FITC-APEC with increasing concentrations of adenosine (A), CGS 21680 (B), NECA (C), and ZM 241385 (D). Curves represent a fit for IC50 binding model from Prism. n=6.

IC$_{50}$ (nM±95% CI)		**A$_{2A}$R**	**Rag23**
Agonist	**Adenosine****	60.7 (±2.8)	20.7 (±2.4)
	CGS21680**	108.6 (±3.0)	58.4 (±3.9)
	NECA**	68.0 (±2.7)	20.0 (±2.8)
Antagonist	**ZM241385**	5.1 (±5.3)	16.1 (±3.9)

Table 2.2 IC$_{50}$ values for unlabeled ligand to A$_{2A}$R and Rag23. Agonist was found to have highly significantly different IC$_{50}$ values between receptors (** indicates $p<0.0001$), while antagonist, ZM 241385, showed no significant difference.

2.3.3. Kinetic rates were affected by mutations to A$_{2A}$R

Kinetic binding rates can be difficult to obtain, but by quantifying fluorescent ligand binding with anisotropy, we can determine association and dissociation rates of labeled agonist, FITC-APEC, followed by rate constants of unlabeled agonist, CGS 21680, and unlabeled antagonist, ZM 241685. We began by monitoring fluorescence anisotropy of 30 nM FITC-APEC binding to receptor for two hours (**Figure 2.4 A**). Next, 1 µM of unlabeled competitor was added and fluorescence anisotropy data collected for another two hours (**Figure 2.4 B**).

After calculating anisotropy and RL complexes, data were fit as described in Materials and Methods to determine k_{on} and k_{off} of FITC-APEC (**Table 2.3**). From these fits, A$_{2A}$R has a significantly greater B_{max} for FITC-APEC than does Rag23. However, Rag23 has a significantly faster association rate and significantly slower dissociation rate, and therefore a smaller K_D than A$_{2A}$R.

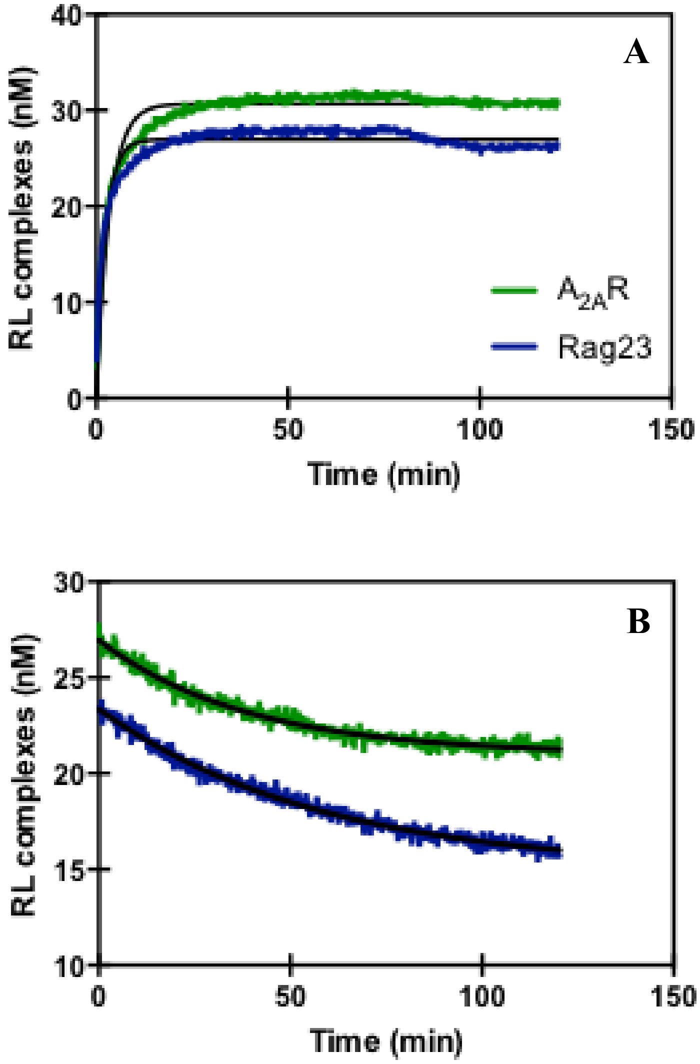

Figure 2.4 (A) 30 nM FITC-APEC associating to A_{2A}R and Rag 23, and (B) addition of 1 µM CGS 21680 to cause dissociation of FITC-APEC. Data were fit to association kinetics and dissociation decay, respectively, in Prism. Data were collected from two purifications of receptor, collected in duplicate, n=4.

	k_{on} ±SE (nM^{-1} min^{-1})	**k_{off} ±SE (min^{-1})**	**K_D (nM)**	**B_{max} ±SE (nM)**
$A_{2A}R$	0.0088 ±0.0003**	0.02577 ±0.0026*	2.9	33.7 ±0.14**
Rag23	0.0133 ±0.0002	0.01724 ±0.0014	1.3	28.1 ±0.05

Table 2.3 k_{on}, k_{off}, and B_{max} values, as well as calculated K_D, for FITC-APEC binding to receptor. (*) indicates values between receptors are statistically significant ($p=0.0277$), while (**) indicates values between receptors are highly significantly different ($p<0.0001$). Data were from two purifications collected in duplicate, n=4. Constants represent average ± standard error.

Upon characterization of kinetic rates for FITC-APEC, experiments were conducted to determine kinetic rates for unlabeled competitors CGS 21680 and ZM 241385 (**Figure 2.5** and **Table 2.4**). 30 nM FITC-APEC and 1 or 50 nM unlabeled competitor was added to receptor simultaneously. Association was collected for 2 hours, and k_{on} and k_{off} for competitors were determined by restricting the kinetic rates for fluorescent ligand to the rates previously determined. Addition of agonist to receptor had significantly faster on rate and significantly slower off rate for Rag23 than wild-type protein. Taken together, this change in kinetic rates also suggests Rag23 has a higher affinity for CGS 21680 than does $A_{2A}R$. Addition of antagonist to receptor shows significantly faster association of ZM 241385 to Rag23, but no significant difference in dissociation rates between the two receptors.

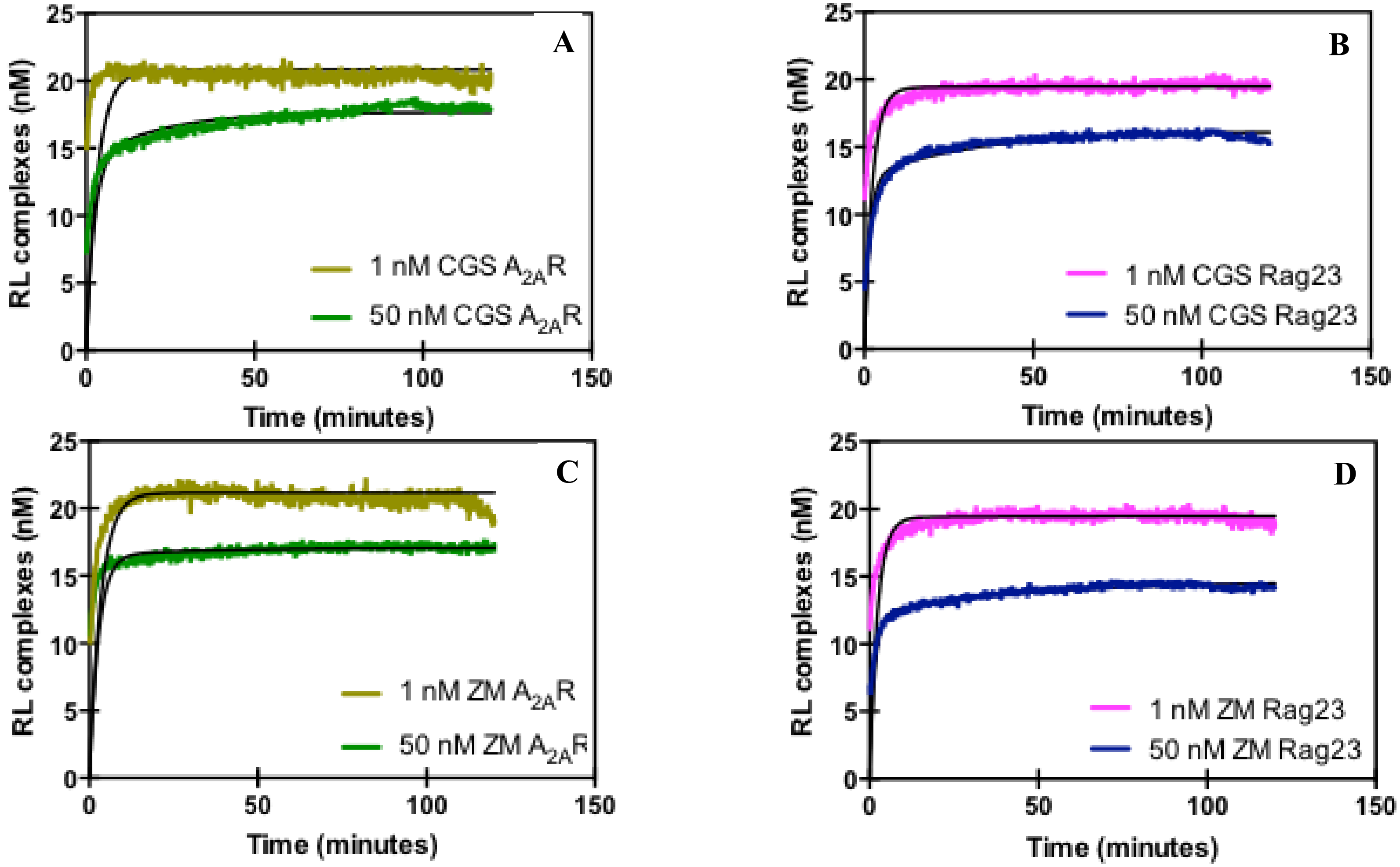

Figure 2.5 Association curves of 30 nM FITC-APEC and 1 or 50 nM competitor to 800 nM purified $A_{2A}R$ or Rag23. CGS 21680 was chosen as an unlabeled agonist and binding was observed to $A_{2A}R$ (A) and Rag23 (B). ZM 241385, an antagonist, was competitively bound to $A_{2A}R$ (C) and Rag23 (D). 50 nM concentrations are n=6, and 1 nM concentrations are n=2.

	k_{on} ±SE (nM^{-1} min^{-1})	k_{off} ±SE (min^{-1})	K_D (nM)
A_{2A}R CGS 21680	0.0024 ±0.00007*	0.0591 ±0.0020*	24.6
Rag23 CGS 21680	0.0042 ±0.00008	0.0409 ±0.0009	9.7
A_{2A}R ZM 241385	0.0016 ±0.00004**	0.0300 ±0.0008	18.8
Rag23 ZM 241385	0.0050 ±0.00006	0.0298 ±0.0005	6.0

Table 2.4 Association and dissociation rates were fit in Prism to kinetics of competitive binding model using k_1 and k_2 values that were restricted to previously determined k_{on} and k_{off} values, respectively, for FITC-APEC. (*) represents values where receptors are significantly different, and (**) represents values were receptors are highly significantly different ($p<0.0001$).

2.3.4. Thermostability was affected by mutations

Unfolding temperature (T_{unf}) was determined to compare the thermostabilizing effects of the A_{2A}R C-terminus and stabilizing point mutations. Here, CPM, a thiol reactive dye, was used to determine unfolding. CPM fluoresces upon binding to exposed cysteines; thus, as a receptor unfolds and exposes internal cysteines, fluorescence due to CPM binding increases. Receptor at equilibrium with CPM was incubated at increasing temperature and fluorescence was measured at each temperature (**Figure 2.6**). Using an [agonist] vs response variable slope binding model the relative unfolding was determined (**Table 2.5**). Note that A_{2A}R binds more CPM in the folded state as one cysteine (C394) is removed in the Δ316 truncation. There was a small but stastically significant difference between T_{unf} for $A_{2A}Δ316R$ and Rag23. $A_{2A}Δ316R$ was found to have T_{unf} decreased by 3°C, while Rag23 had T_{unf} increased by 3°C as compared to A_{2A}R. This is consistent with the results from the Tate lab, who saw a difference of 9°C between $A_{2A}\Delta316R$ and Rag23. The Tate lab used a different method of determining unfolding temperature. They incubated purified receptor with ligands at the specified temperature for 30 minutes, placed the samples on ice with radioligand for an additional hour, and then separated the bound and free radioligand before determining the counts per minute. By testing thermostability with a different method, we show that the difference in T_{unf} between our receptors is comparable to the Tate lab. These results suggest that removal of the C-terminus causes a destabilizing effect on the receptor, but that addition of thermostabilizing point mutations can provide additional stability.

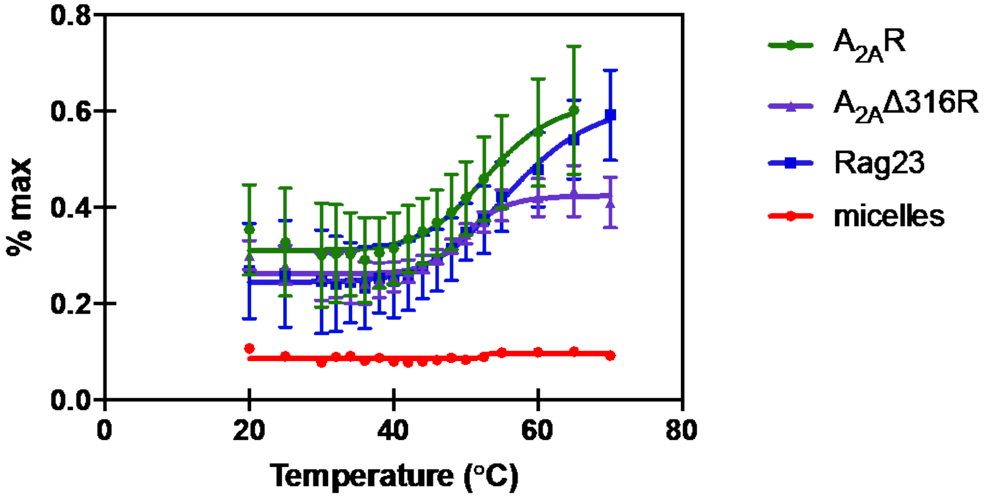

Figure 2.6 Incubation of receptor with a thiol reactive dye, CPM, which binds to exposed cysteines, allows for monitoring of protein unfolding due to increasing temperatures. 800 nM of receptors were incubated with CPM at increasing temperature and fluorescence was determined on the plate reader every 2-10 °C. Points represent the average of 3 purifications with experiments performed in duplicate, n=6. Error bars are standard deviation from the mean.

	T_{unf} (°C) (SE)
$A_{2A}R$	53.1 (±2.9)
$A_{2A}\Delta 316R$	49.8 (±0.8)
Rag23	56.3 (±2.9)

Table 2.5 Unfolding temperature (T_{unf}) is determined for each receptor. No comparisons were statistically significant, although values for $A_{2A}\Delta 316R$ and Rag23 were similar to those seen by the Tate lab (Magnani 2008). n=6.

2.4. Discussion and Conclusions

Ligand binding data from this chapter suggests that the mutations made to create Rag23 alter ligand binding characteristics of $A_{2A}R$. It appears that Rag23 has highly significantly decreased IC_{50} value for agonists, but no significant change in IC_{50} for ZM 241385, an antagonist. These findings follow the motivation behind designing Rag23—to have an increased affinity for agonist so the receptor could be crystallized while agonist bound. Additionally, during characterization of FITC-APEC kinetic on and off rates to receptor, these data suggested that Rag23 had a highly significantly faster k_{on}, and a significantly slower k_{off} than $A_{2A}R$. However, $A_{2A}R$ had a highly significantly greater B_{max} for FITC-APEC. These results are interesting because they indicate that Rag23 binds to FITC-APEC quickly and dissociates slowly, which suggests a higher affinity for the agonist, as is expected due to the point mutations in Rag23. However, $A_{2A}R$ has a greater maximum potential binding capacity for FITC-APEC, although it takes a higher concentration of ligand to reach that potential. Similar to the FITC-APEC results, CGS 21680 binds significantly faster to Rag23 and dissociates significantly more slowly as compared to $A_{2A}R$. This again follows the design of Rag23—to have a greater affinity for agonist. Interestingly from the unlabeled competitor association and dissociation rates, Rag23 also has highly significantly faster association rate to antagonist ZM 241385, although the dissociation rate for either receptor is not significantly different. It is possible that the nature of the point mutations given to Rag23 allow the receptor to associate with ligand more quickly, as well as bind agonist more tightly.

Thermostability experiments were performed to examine the effects of truncating the $A_{2A}R$ C-terminus and addition of point mutations to stability of the receptor. Although not statistically significant, these results suggest that truncation of the C-terminus, as with $A_{2A}\Delta316R$, somewhat destabilizes the receptor, or decreases the T_{unf}. Interestingly, addition of the five agonist favoring point mutations, as with Rag23, stabilize the receptor to the same or possibly greater than the T_{unf} determined for WT $A_{2A}R$.

Taken together, truncation of the $A_{2A}R$ C-terminus appears to affect receptor thermostability in terms of maintaining proper folding; however, removal of the C-terminus is presently the only method of trapping the receptor in a specific conformation for crystallization, as the last 96 amino acids are likely somewhat free-form. It seems that one solution to regaining some thermostability is addition of thermostabilizing point mutations that double as agonist favoring mutations. Rag23 is no doubt a useful construct, as it has been crystallized in its agonist bound conformation. Yet, we should be cautious about relying too heavily on the crystal structure of a mutated receptor that, as indicated in this chapter, may behave differently from wild-type.

Chapter 3

EFFECTS OF THE $A_{2A}R$ C-TERMINUS ON G PROTEIN ASSOCIATION

3.1. Introduction

All GPCRs are known to interact with intracellular G proteins as part of a cell's downstream signaling cascade (**Figure 1.2**) (Watts 2014). Interactions are typically characterized by FRET, crystallization of receptor with G protein, or observation of a downstream product of the signaling cascade (e.g. cAMP) (Hoffmann 2005; Palczewski 2000; Rasmussen 2011; Hebert 2006; Sun 2017; Mcgraw 2019; Uddin 2018). Although interactions between receptor and G protein can be shown directly or indirectly via these methods, it has been difficult to characterize kinetic binding rates and affinities of the proteins to one another.

Surface plasmon resonance (SPR) is a label free method used to characterize interactions between one target immobilized to a chip and another target flowing across the first. Polarized light is used to observe a change in molecular weight on the chip surface by measuring the change in refractive index caused due to interactions. SPR allows for observation of real time binding events, and therefore determination of kinetic rates and affinity (Watts 2014; Chu 2014; Segala 2015).

Upon activation by agonist, $A_{2A}R$ couples with $G\alpha_s$, which activates adenylyl cyclase, and increases cyclic-AMP (cAMP) formation. Previous work in the Robinson lab (Jain, in review; McGraw 2018) showed that truncation of the adenosine A_{2A} receptor

($A_{2A}R$) at amino acid 316 ablates intracellular downstream signaling cascades (**Figure 1.4**). Wild-type $A_{2A}R$ led to constitutive cAMP formation, and increased cAMP activity approximately 50% upon addition of agonist. In contrast, $A_{2A}\Delta316R$ showed no constitutive or agonist-induced cAMP formation (Jain, in review; McGraw 2018). Comparison of cAMP formation by wild-type $A_{2A}R$ to $A_{2A}\Delta316R$ suggests that truncation of the C-terminus could have an effect on receptor coupling to $G\alpha_s$, preventing downstream cAMP activation.

In this chapter, I explore the effects of truncating the $A_{2A}R$ C-terminus on the receptor affinity for $G\alpha_s$. SPR was used to characterize kinetic on and off rates, as well as affinity of purified $A_{2A}R$ and $A_{2A}\Delta316R$ to purified $G\alpha_s$. These experiments can be used to determine if the change in downstream signaling activation stems from the coupling of G protein to receptor.

3.2. Materials and Methods

3.2.1. Cell Growth and Expression of G protein

DNA containing pET15b- $G\alpha_s$ ($G\alpha_s$ constructs were generously donated from the Linder lab at Cornell University and subcloned into pET15b by Dr. Claire McGraw) was freshly transformed into Rosetta (DE3) *E. coli* cells before growing cells. Rosetta (DE3) cells were chosen due to their inducible *lacUV5* promoter which when combined with a pET vector, such as pET15b, facilitates IPTG-inducible protein expression as well as contain humanized codon preferences. The pET15b vector was chosen because it contains ampicillin resistance, and a 6xHis tag was included on the N-terminus of the expressed protein so that the G protein could be purified via NTA affinity. Rosetta-pET15b- Gα_s colonies were inoculated into two 10mL cultures of LB media containing 100 μg/mL ampicillin and 25 μg/mL chloramphenicol (LB-AMP-CAM) and grown at 37°C and 250 RPM for approximately 12 hours. After reaching an optical density (O.D.) of 10, all 20 mL of culture were added to 1 L of LB-AMP-CAM media and grown at 30°C until reaching an O.D. of 0.6. Once the flasks reached an O.D. of 0.6, Gα_s protein expression was induced with 100 μM IPTG, and grown at 30°C for an additional 12-15 hours. The entire 1 L of culture was pelleted by centrifugation at 10,000g, the supernatant removed, and the cell pellet stored at -80°C until purification. Note that the flasks were grown at 30°C to help solubilize the Gα_s.

3.2.2. Cell Growth and Expression of Membrane Protein

Receptors were expressed in yeast strain BJ5464 (*MATa ura3-52 trp1 leu2Δ1 hisΔ200 pep4::HIS3 prb1Δ1.6R can1* GAL) using the multi-integrating vector, pITy4. pITy4 contains a Gal1-10 promoter, allowing for galactose induction, and a C-terminal His10 tag, allowing for efficient purification of the receptors, as described previously (O'Malley 2007). However, for this experiment we chose to insert a rho1d4 tag and stop codon before the His10 tag to ensure expression of the rho1d4 tag for purification and no expression of the His10 tag, which would interact with the NTA chip in the SPR experiments. $A_{2A}R$ and $A_{2A}\Delta 316R$ with 1d4 tags (created by Dr. Claire McGraw) were grown overnight at 30ºC and 275 rpm in glucose-containing media (YPD consisting of 1% yeast extract, 2% peptone, and 2% glucose) to an O.D. of 13 or more. Protein expression was induced by transfer into galactose-containing media (YPG consisting of 1% yeast extract, 2% peptone, and 2% galactose) to an O.D. of 1 and grown for an additional 30 hours before pelleting by centrifugation at 3000 g in a tabletop centrifuge. Cell pellets contained 1250 ODs of yeast cells and were stored at -80°C prior to purification up to 3 months.

3.2.3. Purification of G protein

Frozen cell pellets were thawed on wet ice and resuspended in 100 mL lysis buffer consisting of 50 mM Tris-HCl, pH 8, 20 mM β-mercaptoethanol, 0.1 mM phenylmethane sulfonyl fluoride (PMSF), and one cOmplete™, EDTA-free Protease Inhibitor tablet (Sigma Aldrich). Cells were sonicated while on ice for 30 pulses, then left to rest on ice for 1 minute. This was repeated for a total of three times. After sonication, lysed cells were centrifuged at 10,000 g for 30 minutes at 4°C in a Sorvall supercentrifuge to pellet out the cell membranes and cell debris. The $G\alpha_s$ is present in the supernatant as a soluble protein.

Next, approximately 10 mL of Ni-NTA agarose resin (Qiagen cat#30210) was equilibrated in a 50 mL column with 100 mL equilibration buffer containing 50 mM Tris-HCl, pH 8, 20 mM β-mercaptoethanol, 0.1 mM PMSF, 100 mM NaCl, and 10 mM imidazole to prevent non-specific binding. After equilibration, over the Ni-NTA resin was contacted with the supernatant by gravity flow through the column, followed by three column wash steps to elute non-specifically bound proteins from the Ni-NTA resin. The three column wash buffers were 100 mL each consisting of 50 mM Tris-HCl, pH 8, 20 mM β-mercaptoethanol, 0.1 mM PMSF, 100 mM NaCl, and 20, 40, or 50 mM imidazole, respectively. Finally, 30-50 mL of elution buffer (50 mM Tris-HCl, pH 8, 20 mM β-mercaptoethanol, 150 mM imidazole, 10% glycerol) was flowed over the Ni-NTA resin to elute the protein. Elution buffer was collected in 2 mL fractions, and A_{280} readings were obtained for each fraction to determine the protein concentration. Once the A_{280} readings began to drop, typically after 30 mL of elution buffer had flowed through, collection ceased. Protein-containing fractions were combined and concentrated to 1-2 mL via Amicon ultra centrifugal filters (Millipore Sigma cat#UFC901024). Once concentrated, buffer exchange was performed by adding 25 mL of dilution buffer (50 mM Tris-HCl, pH 8, 1 mM DTT, 10% glycerol) and the sample reconcentrated until the final volume was 2 mL. A_{280} readings were taken to determine final protein concentration, and samples were aliquoted in 200 µL aliquots and stored at -80°C. Typical protein concentrations were 8-16 µM.

Ni-NTA resin was regenerated by flowing 5-10 mL of 1M imidazole over the resin, followed by 50 mL ddH_2O. Regenerated resin was stored in 20% ethanol at 4°C.

3.2.4. Purification of Membrane Protein

Receptors were purified as previously described (Naranjo 2016). Briefly, cell pellets were resuspended with 22 mL lysis buffer (phosphate buffer, pH 8, 10% glycerol, 300 mM NaCl), 220 µL 100 mM PMSF, and one cOmplete™, EDTA-free Protease Inhibitor tablet (Sigma Aldrich) before lysis with 10 mL 0.5 mm zirconia silica beads (BioSpec). Cells were vortexed for 1 minute, then left to rest on ice for 1 minute. This was repeated for a total of six cycles. Lysed cells were then sonicated at 50% pulses for 20 seconds, placed on ice for 20 seconds, and sonicated a second time. The sonicated samples were centrifuged at 3200 g on a tabletop centrifuge for 30 minutes to pellet any remaining cell debris. The supernatant was then centrifuged at 100,000 g in an Optima

XE ultracentrifuge (Beckman Coulter) for 1 hour to pellet the cell membranes. Membranes were resuspended in 0.1% n-Dodecyl-β-D-Maltopyranoside (DDM)/0.1% 3-[(3-Cholamidopropyl)-Dimethylammonio]-1-Propane Sulfonate (CHAPS)/0.02% cholesterol hemisuccinate (CHS) (Anatrace, Maumee, OH) and left to equilibrate overnight at 4°C. The next day, the solution was centrifuged at 70,000 g for 1 hour to remove any insoluble material. Supernatant was incubated overnight with 0.5 mL Rho-1d4 resin (Cube Biotech) previously equilibrated with lysis buffer and detergents. The next day, the resin was washed three times with 15 mL of wash buffer (lysis buffer containing 0.1% DDM, 0.1% CHAPS, 0.02% CHS, 10 μM PMSF). Protein was eluted by incubation at 4°C for two hours in 2.7 mL of elution buffer (lysis buffer containing 200 μM Rho-1d4 peptide (Cube Biotech), 0.1% DDM, 0.1% CHAPS, 0.02% CHS, 10 μM PMSF, and cOmplete PI tablet. The elution was applied to a PD-10 desalting column (GE Healthcare), previously equilibrated with lysis buffer and 0.1% DDM/0.1% CHAPS/0.02% CHS, to remove any remaining salts, and receptor concentrations were determined by A_{280} measurements. Purified receptors were stored at 4°C and used within one week of purification.

3.2.5. Mant-GTP assay

Mant-GTP (N-Methylanthraniloyl) is a fluorescent GTP analog that fluoresces upon binding to most proteins. Here, Mant-GTPγs was used to determine activity of purified $G\alpha_s$, as the GTP both fluoresces upon binding to G protein, and also does not hydrolyze to GDP. All experiments were performed in 96 well half-area black Corning plates (catalog #3875, Corning Incorporated) on a Synergy H1 plate reader (BioTek, Winooski, VT) using an excitation of 260 nm and an emission of 440 nm. Mant-GTP has a second excitation maximum of 360 nm, but in these experiments, excitation at 360 nm produced less fluorescence intensity than excitation at 260 nm, so 260 nm was chosen to quantify fluorescence intensity. Buffer was prepared as previously described (McEwen 2002). Briefly, 90 µL of buffer (50 mM HEPES, 1 mM EDTA, 0.1 M NaCl, 10 mM $MgCl_2$, 1 mM DTT, pH 8.0) containing 500 nM Mant-GTPγs was added to each well. 0 or 400 µM purified $G\alpha_s$ was then added, and samples were incubated on a plate shaker at room temperature for 20-30 minutes before determining fluorescence intensity via plate reader.

3.2.6. Fluorescent ligand binding

Fluorescence anisotropy was used to observe effects of purified $G\alpha_s$ on fluorescent ligand, FITC-APEC, binding to purified $A_{2A}R$, as described in Chapter 2. 800 nM purified receptor in 0.1% DDM, 0.1% CHAPS, 0.02% CHS was combined with 0 or 800 nM $G_{\alpha s}$ and 0, 1, 10, 30, or 100 nM FITC-APEC. Samples were incubated at room temperature for two hours before being read on a Synergy H1 plate reader using a polarized filter cube with an excitation wavelength of 480-485 nm and an emission wavelength of 520-528 nm. Parallel and perpendicular intensities were recorded, and anisotropy was calculated as previously described (Swonger 2018).

3.2.7. Surface Plasmon Resonance

Interactions between purified receptor and purified $G\alpha_s$ were observed by SPR using a Biacore T200 (GE Healthcare). All experiments were performed with a running buffer consisting of phosphate buffer, pH 8, 0.1% DDM, 0.1% CHAPS, and 0.02% CHS to maintain the concentration of detergents well above the critical micelle concentration (CMC), which is necessary for formation of micelles and maintaining proper folding of the purified membrane proteins. All SPR data was collected at 20°C. Before beginning the experiment, some of the purified $G\alpha_s$ was denatured for 10 minutes at 65°C to act as a negative control. An NTA series S sensor chip was used for experiments, and conditioned before each set of experiments. Conditioning cycle consisted of injecting 350 μM EDTA for 180 seconds at 30 μL/min over all flow paths (1-4). After conditioning, kinetics cycles were run. Each kinetic cycle began with a general injection of $NiCl_2$ for 60 seconds at 10 μL/min over all flow paths, followed by an extra wash of 3 mM EDTA in DCC buffer to prevent nonspecific binding. Next, G protein was captured on flow paths 1-4 by injecting sample for 60 seconds at 10 μL/min over a specified flow path. Negative control, denatured $G_{\alpha s}$, was added to flow path 1. After attachment of $G\alpha_s$, sample injections occurred over all flow paths to ensure consistency in observed interactions. Purified protein was injected for 120 seconds at 20 μL/min. After sample injection, all protein was removed from the chip by regeneration with 350 μM EDTA for 180 seconds at 30 μL/min (**Figure 3.1**). Kinetics were then repeated, beginning with a $NiCl_2$ injection, with varying receptor concentrations and additives (e.g. ligand).

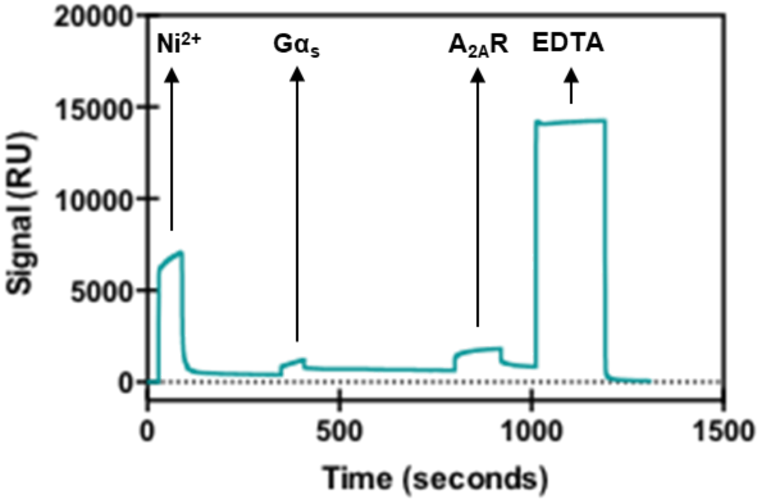

Figure 3.1 Representative sensorgram of SPR injections. Here, nickel is used to regenerate NTA chip, then Gα_s is attached by 6xHis tag to Ni-NTA chip. Once the baseline with Gα_s stabilizes, $A_{2A}R$ is injected. Finally, anything bound to the chip is removed by EDTA injection before beginning the cycle again.

3.3. Results

3.3.1. Expression and Purification of Active G protein

Gα_s was expressed and purified successfully, as seen by Coomassie total protein stain and Western blot prepared by Dr. Claire McGraw (**Figure 3.2** and **Figure 3.3**). This Western blot indicates that Gα_s is present in eluted fractions 3-5 (lanes 7-10); thus, eluant from these fractions was combined and used as purified Gα_s. Comparison of the Coomassie total protein staining to His-tag specific bands from the Western blot, we believe the purity of full-length protein to be >60%. Gα_s production requires IPTG to induce expression; however, too much IPTG leads to insolubility of Gα_s. To help keep as much Gα_s as possible soluble, flasks were grown at a lower temperature (30ºC), and a low concentration of IPTG was used for induction (100 µM). Note that a small amount of Gα_s degraded protein is present in the purified sample – the identity is tentative but is based on its detection by Western assay.

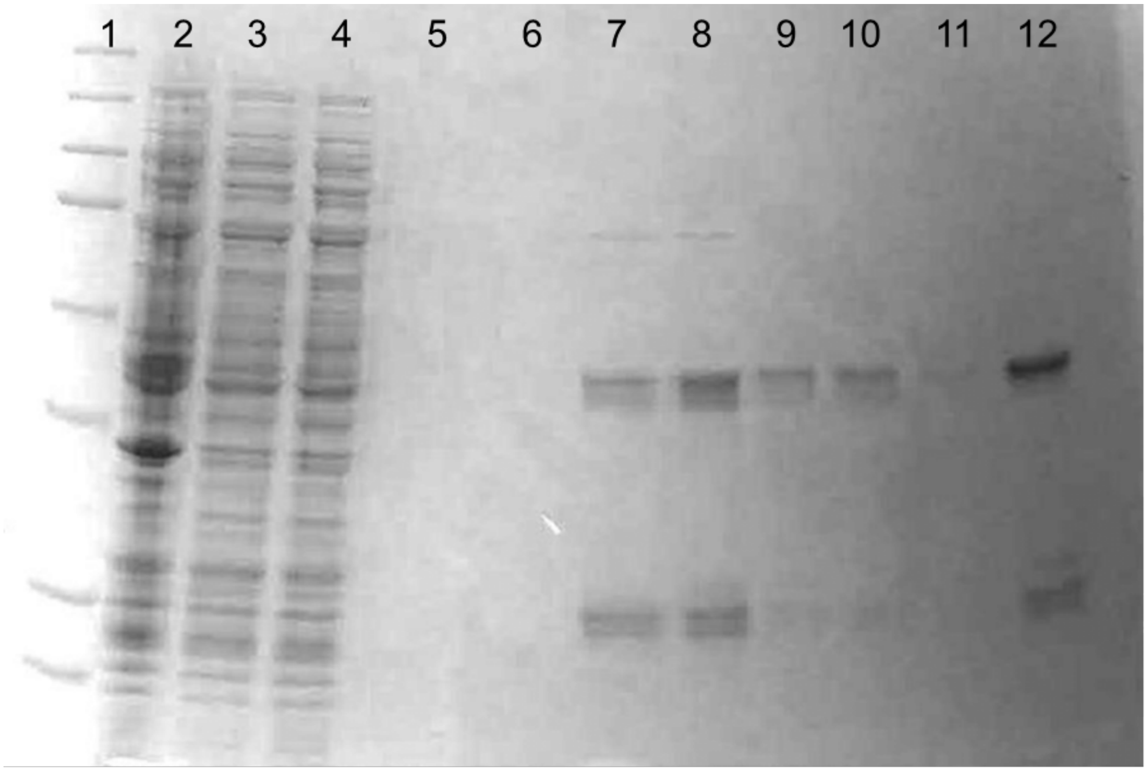

Figure 3.2 Coomassie stain to detect total protein present in various steps throughout Gα_s purification. (1) Western C ladder, (2) whole cell lysate, (3) soluble protein lysate (post centrifuge), (4) lysate from (3) after flowing over Ni-NTA resin, (5) flow through after wash 1, (6) flow through after wash 2, (7-10) eluant of fractions 1-4, (11) eluant of fraction 6, (12) combined fractions 3, 4, and 5. Coomassie stain courtesy of Dr. Claire McGraw.

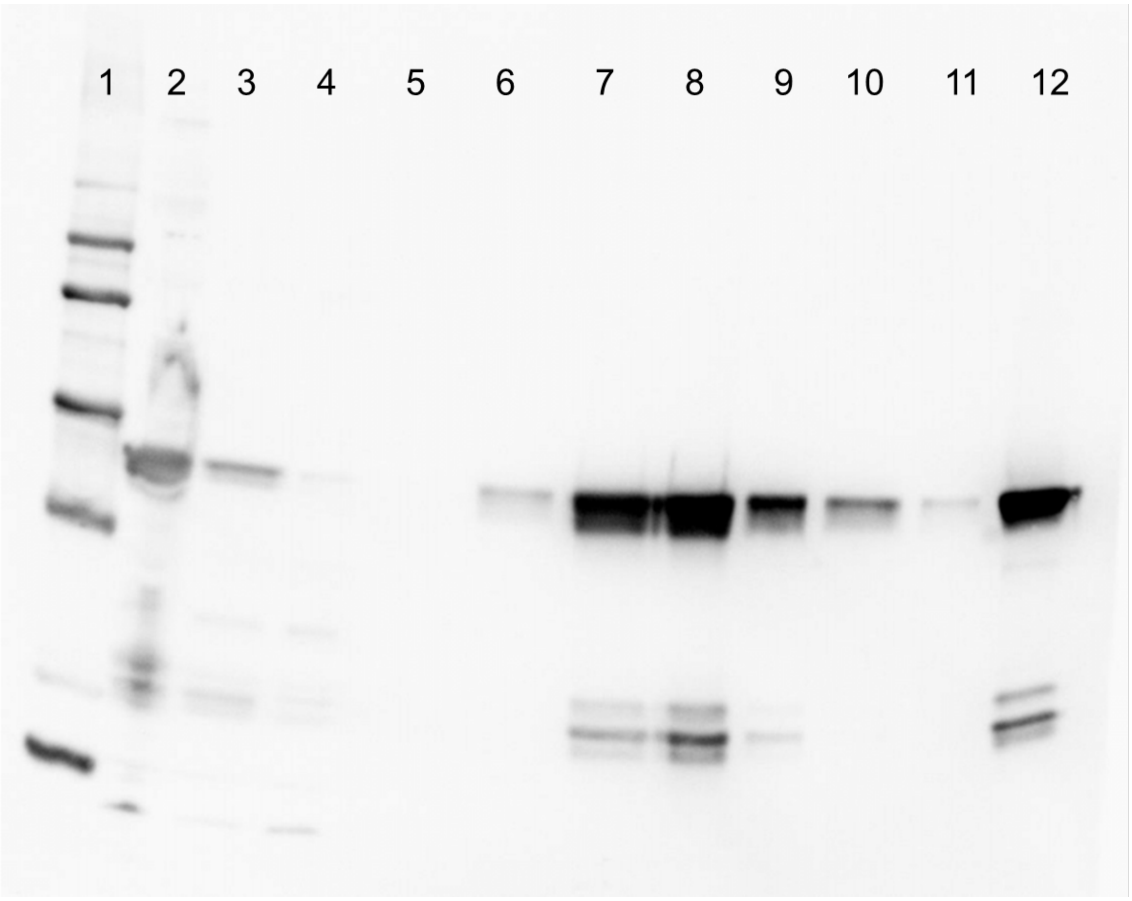

Figure 3.3 Western blot of Gα_s purification steps to examine whether Gα_s was present. His-tag primary antibody was used to bind to Gα_s. (1) Western C ladder, (2) whole cell lysate, (3) soluble protein lysate (post centrifuge), (4) lysate from (3) after flowing over Ni-NTA resin, (5) flow through after wash 1, (6) flow through after wash 2, (7-10) eluant of fractions 1-4, (11) eluant of fraction 6, (12) combined fractions 3, 4, and 5. Western blot courtesy of Dr. Claire McGraw.

To ensure purified Gα_s was active, Mant-GTP, a fluorescent nucleotide that binds Gα_s, was used to observe an interaction with G protein (**Figure 3.3**). When no Gα_s is present, there is a small fluorescence signal, which acts as a negative control. Upon addition of Gα_s, fluorescence intensity increases, indicating Mant-GTP is binding active G protein, as Mant-GTP increases in fluorescence intensity upon binding to G protein. These results suggest that Gα_s was successfully purified in an active state.

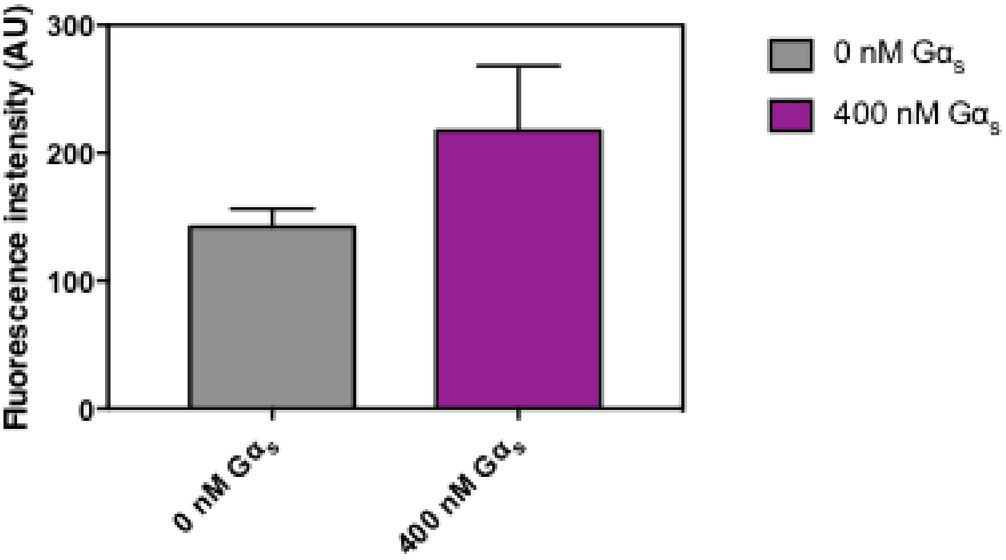

Figure 3.4 Fluorescence intensity of Mant-GTP in the absence or presence of 400 nM Gα_s. Addition of Gα_s increases the fluorescence intensity, indicating Mant-GTP is binding to G protein. Results are the average of 2 Gα_s purifications (n=3).

3.3.2. Fluorescent ligand binding is affected by addition of G protein

Equilibrium binding of FITC-APEC to 800 nM A_{2A}R and $A_{2A}\Delta 316$R was observed in the absence and presence of 800 nM Gα_s (**Figure 3.4**). The addition of Gα_s was followed by an overall decrease in anisotropy and, therefore, RL complex formation. For A_{2A}R, the K_D with or without Gα_s was not significantly different, but B_{max} was significantly decreased when Gα_s was present (**Table 3.1**). When A_{2A}R was truncated to $A_{2A}\Delta 316$R, the addition of Gα_s resulted in a significantly decreased K_D and B_{max} (**Table 3.1**), suggesting that perhaps the truncation causes the less stable receptor to be more susceptible to external changes.

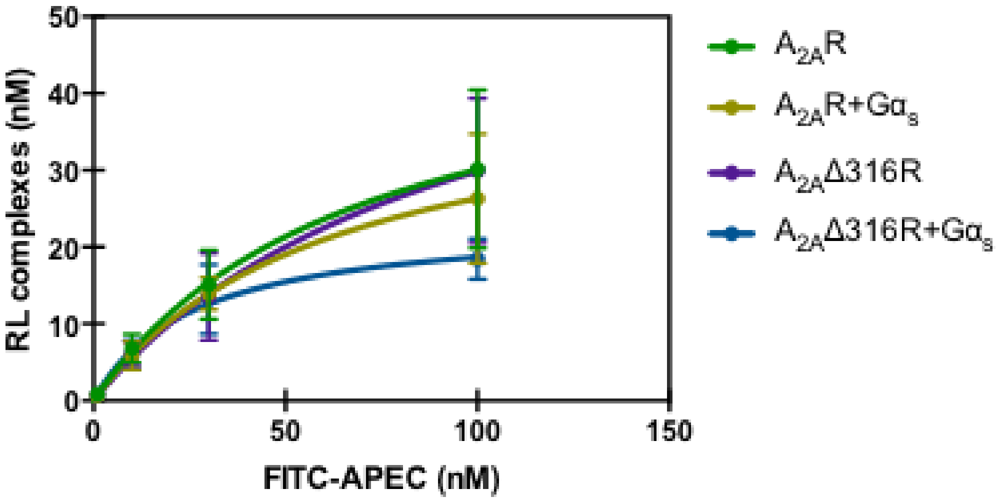

Figure 3.5 800 nM purified $A_{2A}R$ or $A_{2A}\Delta316R$ was incubated with 0, 1, 10, 30, or 100 nM FITC-APEC in the absence or presence of 800 nM $G\alpha_s$. Curves were fit to One site specific binding model in Prism, and K_D and B_{max} values are significantly decreased upon addition of $G\alpha_s$ except the K_D for $A_{2A}R$. Error bars represent SD. Results are from 3 separate receptor purifications, n=3.

	K_D ±SE (nM)	**B_{max} ±SE (nM)**
$A_{2A}R$	69.4 ±5.1	51.0 ±1.9*
$A_{2A}R + G\alpha_s$	62.3 ±0.8	42.7 ±0.3*
$A_{2A}\Delta316R$	97.6 ±12.7*	59.1 ±4.3^
$A_{2A}\Delta316R + G\alpha_s$	26.1 ±4.2*	23.5 ±1.4^

Table 3.1 Dissociation constants and maximum potential binding capacities of $A_{2A}R$ and $A_{2A}\Delta316R$ in the absence or presence of $G\alpha_s$. (*) and (^) represent values that are statistically significantly different from one another.

3.3.3. Attachment of G protein to NTA chip

Purified Gα_s was successfully attached to Ni-NTA chip via 6xHis tag, as is apparent by the change in response units (RU) that occurs after the injection of Gα_s begins at time = 0s, as well as the increased baseline after the end of the injection event at time = 60s (**Figure 3.5**). It should be noted that Gα_s was chosen at concentrations below 1 μM, as the K_D of His-tag for Ni-NTA is 1-20 μM (Soh 2008). Flowing any concentration above this value would result in a substantial loss of Gα_s during the experiment, as the protein would be more inclined to dissociate from the NTA chip. Gα_s was attached at various concentrations, but at 300 nM Gα_s, the protein showed good binding to the NTA chip and couple with receptor at a high enough concentration to have a good signal (RU) to noise ratio.

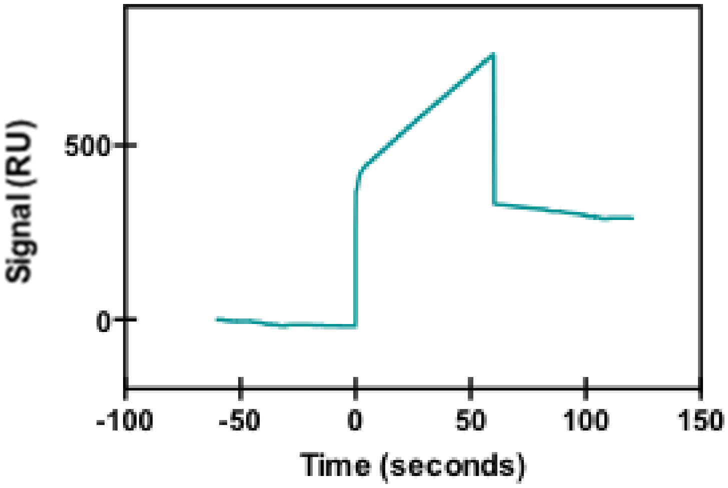

Figure 3.6 Injection of 300 nM purified Gα_s at time = 0 seconds. Injection lasts for 60 seconds, after which a new baseline is determined. Data are from one experiment as a representative indicator of Gα_s associating with Ni-NTA chip.

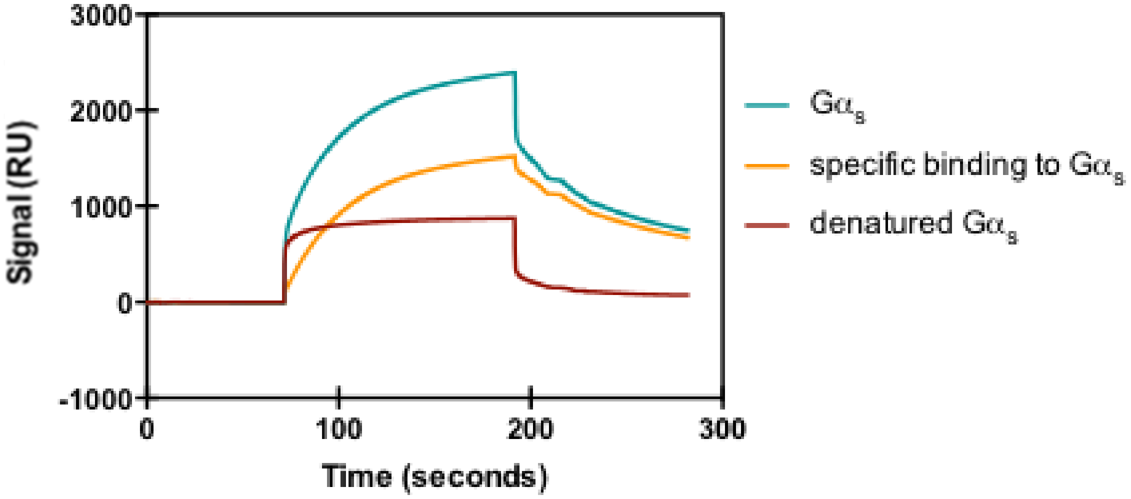

Figure 3.7 2000 nM purified $A_{2A}R$ is injected at time = 60 seconds at 10 µL/second across denatured Gα$_s$ (red) and active Gα$_s$ (green). Nonspecific binding of $A_{2A}R$ to denatured Gα$_s$ is subtracted from that of $A_{2A}R$ to the active Gα$_s$ curve to give a specific binding curve shown in orange. Data are representative of typical results from a single experiment and expressed in RU.

3.3.4. Choice of appropriate negative control (denatured G protein)

Denatured Gα$_s$ was chosen as a negative control and attached to the Ni-NTA chip at the same concentration as Gα$_s$. $A_{2A}R$ was injected onto the SPR chip containing bound Gα$_s$ (either denatured negative control on chip 1 or active protein on chips 2-4) to determine binding (**Figure 3.6**). By subtracting the denatured Gα$_s$ curve from the active protein curve, nonspecific binding was obtained to yield a curve representing the specific binding of receptor to Gα$_s$.

3.3.5. Removal of C-terminus effects association with G protein

To examine the effects of truncation of the $A_{2A}R$ C-terminus on receptor association with $G\alpha_s$, $A_{2A}R$ (**Figure 3.7**) and $A_{2A}\Delta316R$ (**Figure 3.8**) were injected over Ni-NTA chip bound $G\alpha_s$ at a variety of concentrations. Nonspecific binding was subtracted as described in Section 3.3.4, and B_{max}, k_{on}, and k_{off} were determined by fitting data to kinetic analysis using the Biacore T200 evaluation software (GE Healthcare). Ultimately, kinetic variables were determined using solely 1333 and 2000 nM concentrations of receptor, as these concentrations were close to or above the K_D in most experiments.

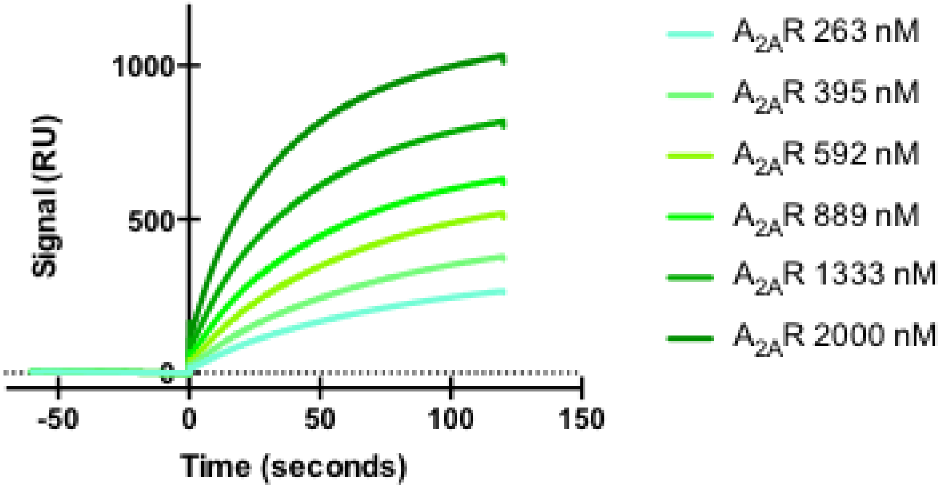

Figure 3.8 Average specific binding of purified $A_{2A}R$ at 263, 395, 592, 889, 1333, and 2000 nM associating with 300 nM $G\alpha_s$. Upon further analysis, only $A_{2A}R$ concentrations of 1333 and 2000 nM were used to determine k_{on} (8235 ±45.2), k_{off} (0.0110 ±0.00008), B_{max} (1554 ±10.1), n=6.

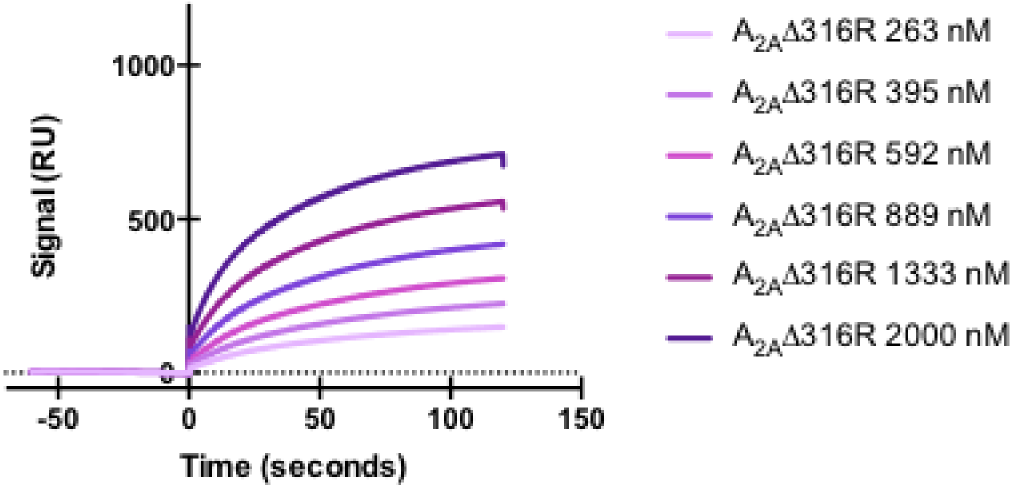

Figure 3.9 Average specific binding of purified $A_{2A}\Delta316R$ at 263, 395, 592, 889, 1333, and 2000 nM associating with 300 nM $G\alpha_s$. Upon further analysis, only receptor concentrations of 1333 and 2000 nM were used to determine k_{on} (7869 ±60.0), k_{off} (0.0125 ±0.00011), B_{max} (1078 ±10.3), n=6.

B_{max} was found to be 1554 RU for $A_{2A}R$ and 1078 RU for $A_{2A}\Delta316R$, and these values were significantly different ($p<0.0001$), with $A_{2A}R$ having a higher maximum binding capacity for $G\alpha_s$. k_{on} was 8235 $M^{-1}s^{-1}$ for $A_{2A}R$ and 7869 $M^{-1}s^{-1}$ for $A_{2A}\Delta316R$, and these values were significantly different ($p<0.0001$), with $A_{2A}R$ binding more quickly to $G\alpha_s$. k_{off} was 0.0110 s^{-1} for $A_{2A}R$ and 0.0125 s^{-1} for $A_{2A}\Delta316R$, and these values were highly significantly different, with $A_{2A}\Delta316R$ dissociating more quickly from $G\alpha_s$. K_D was calculated from k_{off}/k_{on} and determined to be 1503 nM for $A_{2A}R$ and 1894 nM for $A_{2A}\Delta316R$, with $G\alpha_s$ having a greater affinity for $A_{2A}R$ than $A_{2A}\Delta316R$ (**Table 3.2**). Although SPR is a sensitive, accurate method for measuring unlabeled protein-protein interactions, one downside is that from these data alone, we cannot extract a B_{max} value in molar units.

	k_{on} (M^{-1} s^{-1}) ±SE	k_{off} (s^{-1}) ±SE	RT (s)	K_D (nM)	B_{max} (RU) ±SE
$A_{2A}R$	8235 ±45.2*	0.0110 ±0.00008*	90.9	1503	1554 ±10.1*
$A_{2A}\Delta316R$	7869 ±60.0	0.0125 ±0.00011	80	1894	1078 ±10.3

Table 3.2 Association and dissociation rates of receptor and $G\alpha_s$ were determined by fitting kinetic SPR readings of 1333 and 2000 nM of receptor coupling to 300 nM $G_{\alpha s}$, n=6. The (*) indicates that upon comparison of the $A_{2A}R$ and $A_{2A}316R$ data, the values were found to be significantly different ($p>0.0001$).

3.4. Discussion and Conclusions

In this chapter, $G\alpha_s$ was successfully, actively expressed and purified from Rosetta (DE3) cells. The Mant-GTP assay gives little fluorescence in the absence of purified $G\alpha_s$, and increases in fluorescence upon addition of $G\alpha_s$, suggesting an interaction with folded G protein. Additionally, fluorescence anisotropy data indicates that the addition of $G\alpha_s$ may affect ligand binding to both $A_{2A}R$ and $A_{2A}\Delta316R$. This will be examined further in Chapter 4, but these fluorescence anisotropy results show that $G\alpha_s$ appears to be purified and active.

SPR proved to be a successful method of evaluating receptor coupling to G protein. By using denatured $G\alpha_s$ (heat shocked at 65°C for 10 minutes) as a negative control, active $G\alpha_s$ interactions with receptor could be determined by subtracting the denatured $G\alpha_s$ data to ensure kinetic responses represented specific binding. Data were collected at 300 nM $G\alpha_s$ (denatured and active concentration) and 263, 395, 592, 889, 1333, and 2000 nM (1:1.5 dilution) of receptor using 3 receptor purifications and 2 replicates per purification. After analysis of data, an approximate K_D of receptor to $G\alpha_s$ was determined to be on the order of 1-5 μM. Only receptor concentrations at or above the approximate K_D (1333 and 2000 nM) were used to fit k_{on}, k_{off}, and B_{max} values so as to determine the constants when receptor was in excess.

SPR kinetic fits of $A_{2A}R$ give a k_{on} rate (8235 ±45.2 M^{-1} s^{-1}) that is highly significantly faster than the k_{on} of $A_{2A}\Delta 316R$ (7869 ±60.0 M^{-1} s^{-1}). Additionally, $A_{2A}R$ has a k_{off} rate (0.0110 ±0.00008 s^{-1}) that is significantly slower than the k_{off} of $A_{2A}\Delta 316R$ (0.0125 ±0.00011 s^{-1}). From these rate constants, a dissociation constant, K_D, can be calculated by dividing k_{off} by k_{on}. The K_D of $A_{2A}R$ (1503 nM) is smaller than that of $A_{2A}\Delta 316R$ (1894 nM), indicating that $A_{2A}R$ has a greater affinity for $G\alpha_s$ than does $A_{2A}\Delta 316R$.

Additionally, these experiments indicate $A_{2A}R$ has a significantly greater maximum potential binding capacity (B_{max}) for $G\alpha_s$ than does $A_{2A}\Delta 316R$. The B_{max} of $A_{2A}R$ was determined to be 1554 ±10.1 RU, while for $A_{2A}\Delta 316R$ the maximum potential binding is 1078 ±10.3 RU. These data suggest that the truncation of the $A_{2A}R$ C-terminus has a significant effect on receptor activation of $G\alpha_s$ because if fewer receptors interact with $G\alpha_s$, there will be reduced activation of the downstream signaling pathway, as seen by Dr. Claire McGraw (McGraw 2018).

The affinities of receptor for $G\alpha_s$ determined here are lower than the affinity of the neurotensin receptor type 1 (NTS1), which has an affinity of 31 ±18 nM, k_{on} of 1.9 x 10^5 ±1900 M^{-1} s^{-1}, and k_{off} of 0.0024 ±0.000042 s^{-1} for $G\alpha_s$ (Watts 2014). From these data, it appears that NTS1 has a greater affinity for $G\alpha_s$, as the receptor has a faster rate of association and slower rate of dissociation than $A_{2A}R$. This discrepancy could be due to the NTS1 experiments occurring at pH 5.5, while the $A_{2A}R$ experiments were conducted at pH 7. pH 7 was chosen for the SPR experiments, as it is more representative of physiological pH. Additionally, the difference in affinities could be due to NTS1 being purified in nanodiscs, which have been shown keep the receptor more stable (Ashok 2016). Another reason for the difference could also be that the NTS1 receptor simply has a greater affinity for Gα_s. Nonetheless, very few experiments have examined the kinetic rates and affinity of receptor for G protein, as until SPR it was a difficult interaction to quantify. Interestingly, the NTS1 receptor also appears to associate with Gα_s in the presence of GTPγs. As will be discussed further in Chapter 4, GTPγs was observed to all but completely inactivate Gα_s, preventing Gα_s from associating with purified receptor.

Taken together, we can observe that A_{2A}R associates more quickly, dissociates more slowly, and couples to more Gα_s than does $A_{2A}\Delta$316R. This could explain why cAMP assay data from Dr. McGraw showed little cAMP formation by $A_{2A}\Delta$316R—because it associates at a lower capacity with Gα_s. Future experiments of interest include comparing the rates of association and dissociation of receptor purified in micelles (seen here) to receptor in nanodiscs binding to Gα_s. These experiments could help determine how much of a factor receptor stability is in regards to receptor association to Gα_s.

Chapter 4

EFFECTS OF PERTURBANCES ON G PROTEIN ASSOCIATION WITH $A_{2A}R$ AND $A_{2A}\Delta 316R$

4.1. Introduction

GPCRs are membrane proteins that bind to extracellular ligands in order to activate intracellular downstream signaling cascades. These signaling events begin with a conformational shift in the receptor structure that in turn activates the intracellular associated G protein (Watts 2014). In the case of the adenosine A_{2A} receptor, activation of the $G\alpha_s$ subunit leads to the already associated GDP being exchanged for GTP, and then $G\alpha_s$ dissociates from the receptor to continue the signaling pathway. The stimulatory downstream signaling pathway includes activation of adenylyl cyclase, which in turn upregulates cAMP production, as seen in our lab by Dr. McGraw (McGraw 2018).

Previously, our lab has shown that $A_{2A}R$ produces cAMP constitutively, and produces greater levels of cAMP upon activation by agonist (CGS 21680). However, we also saw that truncation of $A_{2A}R$ at amino acid 316, as is common for crystal structures, led to no constitutive or agonist induced cAMP activation (McGraw 2018). Although our lab sees a decrease in the downstream signaling pathway with $A_{2A}\Delta 316R$, it was unclear which step was causing the effect. Thus, through SPR, the affinity and kinetic rate constants of $A_{2A}R$ and $A_{2A}\Delta 316R$ for $G\alpha_s$ were determined, as seen in Chapter 3.

In this chapter, I examine the effects of ligand (both agonist and antagonist) on $A_{2A}R$ and $A_{2A}\Delta316R$ association with $G\alpha_s$, as well as how the addition of GDP or GTPγs (non-hydrolyzable GTP) effects the activity of $G\alpha_s$. These results will characterize the effects of each perturbance on full-length and truncated receptor association with G protein using SPR.

4.2. Materials and Methods

4.2.1. Cell Growth and Expression of G protein

DNA containing pET15b- $G\alpha_s$ ($G\alpha_s$ constructs were generously donated from the Linder lab at Cornell University and subcloned into pET15b by Dr. Claire McGraw) was freshly transformed into Rosetta (DE3) *E. coli* cells before growing cells. Rosetta (DE3) cells were chosen due to their inducible *lacUV5* promoter which when combined with a pET vector, such as pET15b, facilitates IPTG-inducible protein expression as well as contain humanized codon preferences. The pET15b vector was chosen because it contains ampicillin resistance, and a 6xHis tag was included on the N-terminus of the expressed protein so that the G protein could be purified via NTA affinity. Rosetta-pET15b- $G\alpha_s$ colonies were inoculated into two 10mL cultures of LB media containing 100 μg/mL ampicillin and 25 μg/mL chloramphenicol (LB-AMP-CAM) and grown at 37°C and 250 RPM for approximately 12 hours. After reaching an optical density (O.D.) of 10, all 20 mL of culture were added to 1 L of LB-AMP-CAM media and grown at 30°C until reaching an O.D. of 0.6. Once the flasks reached an O.D. of 0.6, $G\alpha_s$ protein expression was induced with 100 μM IPTG, and grown at 30°C for an additional 12-15 hours. The entire 1 L of culture was pelleted by centrifugation at 10,000g, the supernatant removed, and the cell pellet stored at -80°C until purification. Note that the flasks were grown at 30°C to help solubilize the Gα_s.

4.2.2. Cell Growth and Expression of Membrane Protein

Receptors were expressed in yeast strain BJ5464 (*MATa ura3-52 trp1 leu2Δ1 hisΔ200 pep4::HIS3 prb1Δ1.6R can1* GAL) using the multi-integrating vector, pITy4. pITy4 contains a Gal1-10 promoter, allowing for galactose induction, and a C-terminal His10 tag, allowing for efficient purification of the receptors, as described previously (O'Malley 2007). However, for this experiment we chose to insert a rho1d4 tag and stop codon before the His10 tag to ensure expression of the rho1d4 tag for purification and no expression of the His10 tag, which would interact with the NTA chip in the SPR experiments. $A_{2A}R$ and $A_{2A}\Delta 316R$ with 1d4 tags (created by Dr. Claire McGraw) were grown overnight at 30ºC and 275 rpm in glucose-containing media (YPD consisting of 1% yeast extract, 2% peptone, and 2% glucose) to an O.D. of 13 or more. Protein expression was induced by transfer into galactose-containing media (YPG consisting of 1% yeast extract, 2% peptone, and 2% galactose) to an O.D. of 1 and grown for an additional 30 hours before pelleting by centrifugation at 3000 g in a tabletop centrifuge. Cell pellets contained 1250 ODs of yeast cells and were stored at -80°C prior to purification for up to 3 months.

4.2.3. Purification of G protein

Frozen cell pellets were thawed on wet ice and resuspended in 100 mL lysis buffer consisting of 50 mM Tris-HCl, pH 8, 20 mM β-mercaptoethanol, 0.1 mM phenylmethane sulfonyl fluoride (PMSF), and one cOmplete™, EDTA-free Protease Inhibitor tablet (Sigma Aldrich). Cells were sonicated while on ice for 30 pulses, then left to rest on ice for 1 minute. This was repeated for a total of three times. After sonication, lysed cells were centrifuged at 10,000 g for 30 minutes at 4°C in a Sorvall supercentrifuge to pellet out the cell membranes and cell debris. The Gα_s is present in the supernatant as a soluble protein.

Next, approximately 10 mL of Ni-NTA agarose resin (Qiagen cat#30210) was equilibrated in a 50 mL column with 100 mL equilibration buffer containing 50 mM Tris-HCl, pH 8, 20 mM β-mercaptoethanol, 0.1 mM PMSF, 100 mM NaCl, and 10 mM imidazole to prevent non-specific binding. After equilibration, over the Ni-NTA resin was contacted with the supernatant by gravity flow through the column, followed by three column wash steps to elute non-specifically bound proteins from the Ni-NTA resin. The three column wash buffers were 100 mL each consisting of 50 mM Tris-HCl, pH 8, 20 mM β-mercaptoethanol, 0.1 mM PMSF, 100 mM NaCl, and 20, 40, or 50 mM imidazole, respectively. Finally, 30-50 mL of elution buffer (50 mM Tris-HCl, pH 8, 20 mM β-mercaptoethanol, 150 mM imidazole, 10% glycerol) was flowed over the Ni-NTA resin to elute the protein. Elution buffer was collected in 2 mL fractions, and A_{280} readings were obtained for each fraction to determine the protein concentration. Once the A_{280} readings began to drop, typically after 30 mL of elution buffer had flowed through, collection ceased. Protein-containing fractions were combined and concentrated to 1-2 mL via Amicon ultra centrifugal filters (Millipore Sigma cat#UFC901024). Once concentrated, buffer exchange was performed by adding 25 mL of dilution buffer (50 mM Tris-HCl, pH 8, 1 mM DTT, 10% glycerol) and the sample reconcentrated until the final volume was 2 mL. A_{280} readings were taken to determine final protein concentration, and samples were aliquoted in 200 µL aliquots and stored at -80°C. Typical protein concentrations were 8-16 µM.

Ni-NTA resin was regenerated by flowing 5-10 mL of 1M imidazole over the resin, followed by 50 mL ddH_2O. Regenerated resin was stored in 20% ethanol at 4°C.

4.2.4. Purification of Membrane Protein

Receptors were purified as previously described (Naranjo 2016). Briefly, cell pellets were resuspended with 22 mL lysis buffer (phosphate buffer, pH 8, 10% glycerol, 300 mM NaCl), 220 µL 100 mM PMSF, and one cOmplete™, EDTA-free Protease Inhibitor tablet (Sigma Aldrich) before lysis with 10 mL 0.5 mm zirconia silica beads (BioSpec). Cells were vortexed for 1 minute, then left to rest on ice for 1 minute. This was repeated for a total of six cycles. Lysed cells were then sonicated at 50% pulses for 20 seconds, placed on ice for 20 seconds, and sonicated a second time. The sonicated samples were centrifuged at 3200 g on a tabletop centrifuge for 30 minutes to pellet any remaining cell debris. The supernatant was then centrifuged at 100,000 g in an Optima XE ultracentrifuge (Beckman Coulter) for 1 hour to pellet the cell membranes. Membranes were resuspended in 0.1% n-Dodecyl-β-D-Maltopyranoside (DDM)/0.1% 3-[(3-Cholamidopropyl)-Dimethylammonio]-1-Propane Sulfonate (CHAPS)/0.02% cholesterol hemisuccinate (CHS) (Anatrace, Maumee, OH) and left to equilibrate overnight at 4°C. The next day, the solution was centrifuged at 70,000 g for 1 hour to remove any insoluble material. Supernatant was incubated overnight with 0.5 mL Rho-1d4 resin (Cube Biotech) previously equilibrated with lysis buffer and detergents. The next day, the resin was washed three times with 15 mL of wash buffer (lysis buffer containing 0.1% DDM, 0.1% CHAPS, 0.02% CHS, 10 μM PMSF). Protein was eluted by incubation at 4°C for two hours in 2.7 mL of elution buffer (lysis buffer containing 200 μM Rho-1d4 peptide (Cube Biotech), 0.1% DDM, 0.1% CHAPS, 0.02% CHS, 10 μM PMSF, and cOmplete PI tablet. The elution was applied to a PD-10 desalting column (GE Healthcare), previously equilibrated with lysis buffer and 0.1% DDM/0.1% CHAPS/0.02% CHS, to remove any remaining salts, and receptor concentrations were determined by A_{280} measurements. Purified receptors were stored at 4°C and used within one week of purification.

4.2.5. Surface Plasmon Resonance

Interactions between purified receptor and purified $G\alpha_s$ was observed by SPR using a Biacore T200 (GE Healthcare). All experiments were performed with a running buffer consisting of phosphate buffer, pH 8, 0.1% DDM, 0.1% CHAPS, and 0.02% CHS to maintain the concentration of detergents well above the critical micelle concentration (CMC), which is necessary for formation of micelles and maintaining proper folding of the purified membrane proteins. All SPR data was collected at 20°C. Before beginning the experiment, some of the purified $G\alpha_s$ was denatured for 10 minutes at 65°C to act as a negative control. Where applicable, GDP, GTP, or ligand was added to G protein or receptor and incubated for at least thirty minutes before data collection began. An NTA series S sensor chip was used for experiments and conditioned before each set of experiments. Conditioning cycle consisted of flowing 350 μM EDTA for 180 seconds at 30 μL/min over all flow paths (1-4). After conditioning, kinetics cycles were run. Each kinetic cycle began with a general injection of $NiCl_2$ for 60 seconds at 10 µL/min over all flow paths, followed by an extra wash of 3 mM EDTA in DCC buffer to prevent nonspecific binding. Next, G protein was captured on flow paths 1-4 by injecting sample for 60 seconds at 10 µL/min over a specified flow path. For experiments involving G protein activated or inactivated with GDP or GTP, respectively, all four flow paths were used. Negative control, denatured $G\alpha_s$, was added to flow path 1, and flow paths 2-4 were used for unaltered $G\alpha_s$, $G\alpha_s$ with GDP, or $G\alpha_s$ with GTPγs. After attachment of $G\alpha_s$, sample injections occurred over all flow paths to ensure consistency in observed interactions. Purified protein was injected for 120 seconds at 20 µL/min. After sample injection, all protein was removed from the chip by regeneration with 350 µM EDTA for 180 seconds at 30 µL/min. Kinetics were then repeated, beginning with a $NiCl_2$ injection, with varying receptor concentrations and additives (e.g. ligand). All ligands were purchased from Tocris, GDP and GTPγs were purchased from Sigma Aldrich.

Data analysis was performed using the Biacore T200 evaluation software. Kinetic rates were analyzed using surface bound kinetic 1:1 binding fits. Preliminary dissociation constants were approximated and only receptor concentrations at or above the K_D were used for kinetic analysis.

4.3. Results

4.3.1. Effects of ligand added to $A_{2A}R$ may affect association with $G\alpha_s$

To examine the effects of agonist and antagonist on $A_{2A}R$ association with $G\alpha_s$, 300 nM of $G\alpha_s$ was attached to a Ni-NTA chip and 1333 and 2000 nM of $A_{2A}R$ previously incubated with 25 nM agonist (CGS 21680) or antagonist (ZM 241385) (**Figure 4.1**) was injected onto SPR chip bound with $G\alpha_s$ protein (**Figure 4.2**). 25 nM of ligand was chosen because the concentration is approximately at or above the K_i for each ligand, and concentrations much greater than K_i tended to have ligand in such excess that nonspecific binding to the chip was observed.

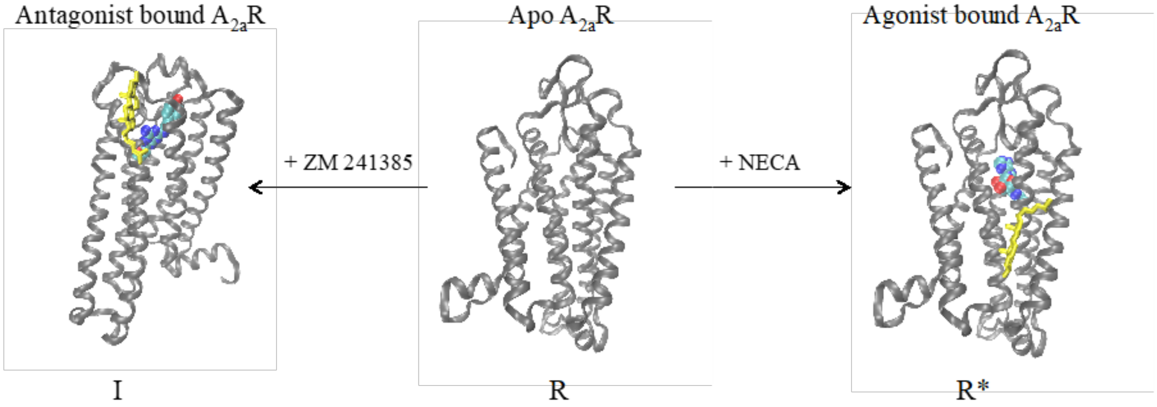

Figure 4.1 State dependent cholesterol binding sites on $A_{2A}R$. Snapshots taken from all atom simulations show cholesterol binding at different sites on $A_{2A}R$ depending on ligation state (cholesterol in yellow). Active receptor (R*) shows cholesterol bound at the CCM, in the intracellular leaflet between helices 2 and 4. Inactive receptor (I) shows cholesterol bound to helix 6 in the extracellular leaflet. $A_{2A}R$ is rotated to show the location of interaction. Figure reproduced with permission from Lyman, McGraw, and Robinson, unpublished work.

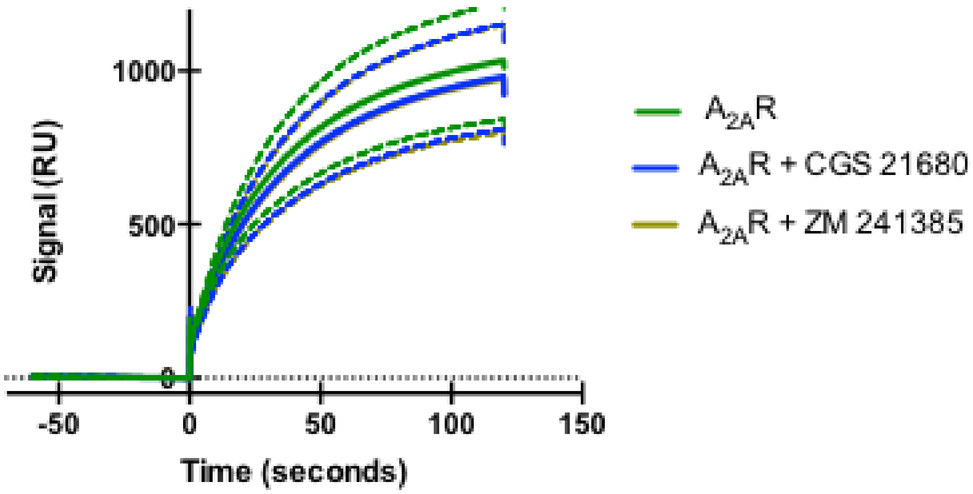

Figure 4.2 2000 nM $A_{2A}R$ without ligand (green) or preincubated with 25 nM agonist (CGS 21680) (blue) or antagonist (ZM 241385) (yellow) was injected at time zero onto $G\alpha_s$-bound SPR chips as described in section 3.2.7. In parallel, $A_{2A}R$ with and without ligand was injected onto denatured $G\alpha_s$-bound SPR chips to correct for non-specific binding (not shown). Kinetic fits were performed for specific binding of both 1333 and 2000 nM concentrations of $A_{2A}R$, but for clarity, only 2000 nM is shown in this figure. Dashed lines represent SEM, n=6.

B_{max} of receptor to G protein was determined as described in Section 3.3.5 to be 1554 ±10.1 RU for $A_{2A}R$ without ligand, 1460 ±8.1 RU for $A_{2A}R$ with CGS 21680, and 1090 ± 22.6 RU for $A_{2A}R$ with ZM 241385 (**Table 4.1**). A comparison of these values shows that all B_{max} values are significantly different ($p<0.0001$), except for $A_{2A}R$ with CGS 21680 compared to ZM 241385, which has a significant difference ($p=0.0017$) in B_{max} values. These data indicate that $A_{2A}R$ without ligand has a significantly greater maximum binding capacity to $G\alpha_s$ than receptor with ligand, while $A_{2A}R$ incubated with ZM 241385, an antagonist, has the lowest maximum binding capacity observed here.

Kinetic k_{on} and k_{off} rate constants for receptor binding to $G\alpha_s$ were also determined based on a single-site binding model (**Figure 4.3** and **Table 4.1**) with $A_{2A}R$ having k_{on} and k_{off} rate constants of 8235 ±45.2 M^{-1} s^{-1} and 0.0110 ±0.00008 s^{-1}, respectively. Association rates were not significantly different, except when comparing $A_{2A}R$ incubated with CGS 21680 to $A_{2A}R$ incubated with ZM 241385 (p=0.0326). The rate of association when receptor was incubated with antagonist was significantly faster than when incubated with agonist. Dissociation rate constants compared to the dissociation rate constant of ZM 241385 were significantly different (p=0.0357 for no ligand; p=0.0338 for CGS 21680), but comparison of no ligand to CGS 21680 showed no significant change. The rate of dissociation from $G\alpha_s$ when $A_{2A}R$ is incubated with ZM 241385 is significantly slower.

The dissociation constant, K_D, was determined by dividing k_{off} by k_{on}. $A_{2A}R$ in the absence of ligand was found to have a K_D for $G\alpha_s$ of 1338 nM, while addition of CGS 21680 or ZM 241385 yielded dissociation constants of 1359 and 1292 nM, respectively. These data suggest that $A_{2A}R$ + ZM 241385 has a higher affinity for $G\alpha_s$ as determined by a significantly faster k_{on} and significantly slower k_{off}.

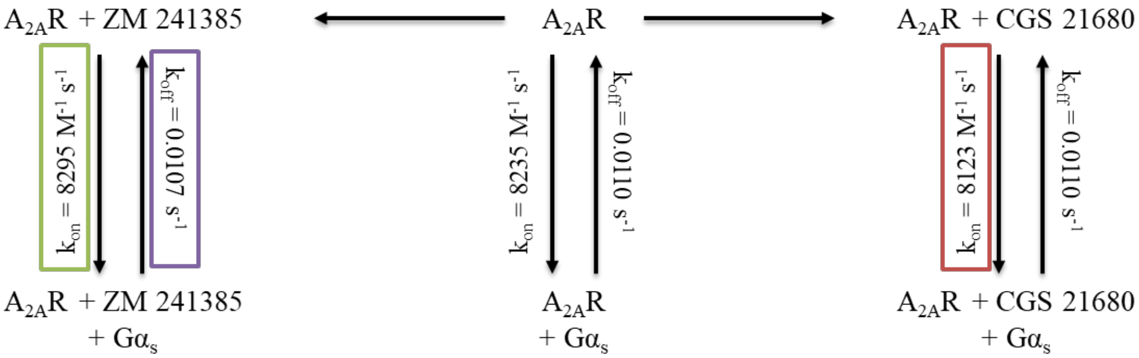
$A_{2A}R$ + ZM 241385
$A_{2A}R$
$A_{2A}R$ + CGS 21680
k_{on} = 8295 M^{-1} s^{-1}
k_{off} = 0.0107 s^{-1}
k_{on} = 8235 M^{-1} s^{-1}
k_{off} = 0.0110 s^{-1}
k_{on} = 8123 M^{-1} s^{-1}
k_{off} = 0.0110 s^{-1}
$A_{2A}R$ + ZM 241385 + $G\alpha_s$
$A_{2A}R$ + $G\alpha_s$
$A_{2A}R$ + CGS 21680 + $G\alpha_s$

Figure 4.3 Schematic of kinetic rate constants for $A_{2A}R$ associating with $G\alpha_s$ in the presence or absence of ligand. Rate of association was significantly faster when $A_{2A}R$ was bound to ZM 241385 (green) than bound to CGS 21680 (red). Additionally, when $A_{2A}R$ was bound to ZM 241385 the rate of dissociation was significantly slower (purple).

	k_{on} (M^{-1} s^{-1}) ±SE	k_{off} (s^{-1}) ±SE	RT (s)	K_D (nM)	B_{max} (RU) ±SE
$A_{2A}R$	8235 ±45.2	0.0110 ±0.00008*^	90.9	1338	1554 ±10.1$^{+\#}$
$A_{2A}R$ + CGS 21680	8123 ±51.7*	0.0110 ±0.00010^	90.9	1359	1460 ±8.1$^{+\wedge}$
$A_{2A}R$ + ZM 241385	8295 ±54.7*	0.0107 ±0.00010*	93.5	1293	1090 ± 22.6$^{\#\wedge}$

Table 4.1 Association and dissociation rates of purified receptor ± ligand binding to $G\alpha_s$ were determined by fitting time-dependent SPR data of 1333 and 2000 nM receptor ± 25 nM ligand, n=6. Data were collected from three separate membrane protein purifications tested in duplicate. (*) and (^) indicates that values with the same symbol are significantly different, while ($^+$) and ($^\#$) indicates values are highly significantly different ($p<0.0001$).

4.3.2. Effects of ligand added to $A_{2A}\Delta316R$ may affect association with $G\alpha_s$

Truncated $A_{2A}R$ ($A_{2A}\Delta316R$) was incubated in the absence of ligand or with 25 nM agonist (CGS 21690) or 25 nM antagonist (ZM 241385) before observing receptor coupling to 300 nM $G\alpha_s$ via SPR (**Figure 4.4**). Kinetic on and off rates, as well as B_{max}, were determined by fitting the data collected at receptor concentrations of 1333 and 2000 nM in the Biacore T200 Evaluation Software.

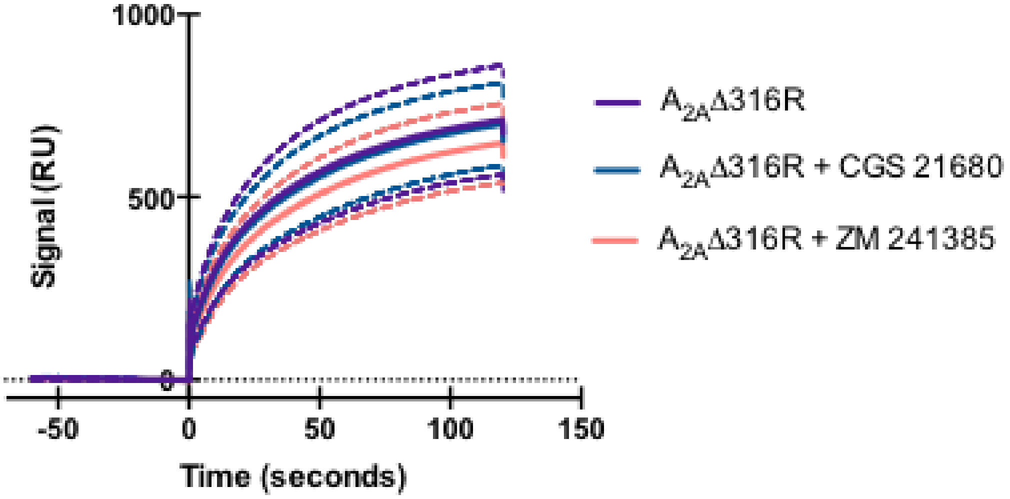

Figure 4.4 2000 nM $A_{2A}\Delta316R$ without ligand (purple) or preincubated with 25 nM agonist (CGS 21680) (blue) or antagonist (ZM 241385) (pink) was injected at time zero onto $G\alpha_s$-bound SPR chips as described in section 3.2.7. In parallel, $A_{2A}\Delta316R$ with and without ligand was injected onto denatured $G\alpha_s$-bound SPR chips to correct for non-specific binding (not shown). Kinetic fits were performed for specific binding of both 1333 and 2000 nM concentrations of $A_{2A}\Delta316R$, but for clarity, only 2000 nM is shown in this figure. Dashed lines represent SEM, n=6.

B_{max} was determined for $A_{2A}\Delta316R$ binding to $G\alpha_s$ in the absence and presence of ligand (**Table 4.2**). $A_{2A}\Delta316R$ without ligand was found to have a B_{max} of 1078 ±10.3 RU, while addition of CGS 21680 or ZM 241385 gave a B_{max} of 1020.8 ±10.7 RU and 1074.4 ±14.3 RU, respectively. Upon analysis, the difference in B_{max} without ligand compared to CGS 21680 was found to be highly significantly different ($p=0.0009$), and comparison of receptor with CGS 21680 to ZM 241385 indicated that the change in maximum binding capacity was significantly different ($p=0.0065$). However, the maximum binding capacity of receptor without ligand and receptor with ZM 241385 were found to be not significantly different. In sum, the addition of CGS 21680 to $A_{2A}\Delta316R$ appears to significantly decrease the maximum binding capacity of truncated receptor to $G\alpha_s$.

Kinetic association and dissociation rate constants, k_{on} and k_{off}, respectively, were determined in the same manner as B_{max} (**Figure 4.5** and **Table 4.2**). After examination of the k_{on} rates, all differences are highly significant ($p<0.0001$). The association rate constant for $A_{2A}\Delta316R$ binding to $G\alpha_s$ is fastest in the presence of CGS 21680, and slowest in the presence of ZM 241385. The dissociation rate constants were highly significantly different ($p<0.0001$), except for that of agonist to antagonist, which was significantly different ($p=0.0387$). The dissociation rate constants for binding of $A_{2A}\Delta316R$ to $G\alpha_s$ is fastest in the presence of ZM 241385, and slowest in the presence of CGS 21680.

K_D can be determined from association and dissociation rate constants, and was found to be 1587 nM for $A_{2A}\Delta316R$ without ligand and 1362 nM and 1919 nM for $A_{2A}\Delta316R$ with CGS 21680 and ZM 241385, respectively. Interestingly, the affinity of $A_{2A}\Delta316R$ for $G\alpha_s$ appears to be greatest in the presence of CGS 21680 and least when incubated with ZM 241385, which is different from results determined with full-length $A_{2A}R$.

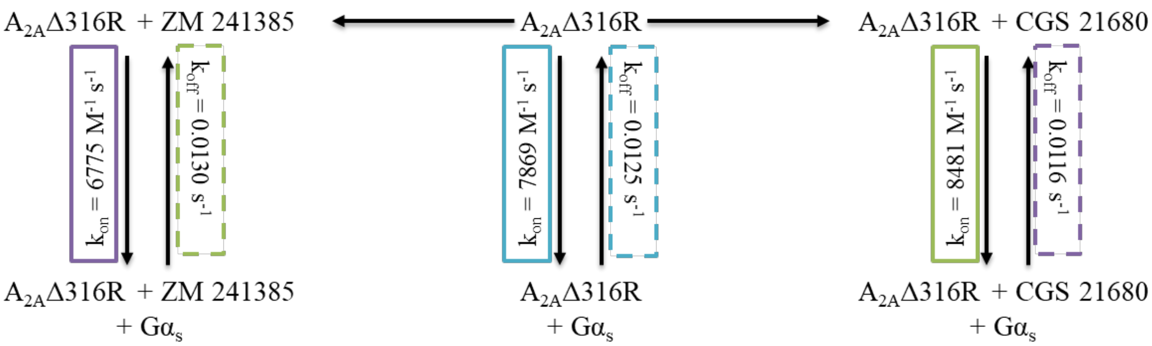
$A_{2A}\Delta316R$ + ZM 241385
$A_{2A}\Delta316R$
$A_{2A}\Delta316R$ + CGS 21680
k_{on} = 6775 M^{-1} s^{-1}
k_{off} = 0.0130 s^{-1}
k_{on} = 7869 M^{-1} s^{-1}
k_{off} = 0.0125 s^{-1}
k_{on} = 8481 M^{-1} s^{-1}
k_{off} = 0.0116 s^{-1}
$A_{2A}\Delta316R$ + ZM 241385 + $G\alpha_s$
$A_{2A}\Delta316R$ + $G\alpha_s$
$A_{2A}\Delta316R$ + CGS 21680 + $G\alpha_s$

Figure 4.5 Schematic of kinetic rate constants for $A_{2A}\Delta316R$ associating with $G\alpha_s$ in the presence or absence of ligand (blue). All k_{on} rates are significantly different. $A_{2A}\Delta316R$ with CGS 21680 has the fastest association to $G\alpha_s$ (green solid), while $A_{2A}\Delta316R$ with ZM 241385 has the slowest (purple solid). Dissociation rate constants were significantly different, with $A_{2A}\Delta316R$ bound to ZM 241385 having the fastest dissociation (green dashed) and $A_{2A}\Delta316R$ bound to CGS 21680 having the slowest dissociation (purple dashed).

	k_{on} (M^{-1} s^{-1}) ±SE	k_{off} (s^{-1}) ±SE	RT (s)	K_D (nM)	B_{max} (RU) ±SE
$A_{2A}\Delta316R$	$7869 \pm 60.0^{+}$	$0.0125 \pm 0.00011^{\#+}$	80	1587	$1078 \pm 10.3^{+}$
$A_{2A}\Delta316R$ + CGS 21680	$8481 \pm 72.1^{+}$	$0.0116 \pm 0.00014^{\#\wedge}$	86	1362	$1021 \pm 10.7^{+*}$
$A_{2A}\Delta316R$ + ZM 241385	$6775 \pm 107.9^{+}$	$0.0130 \pm 0.00021^{\wedge+}$	77	1919	$1074 \pm 14.3^{*}$

Table 4.2 Association and dissociation rate constants for of purified receptor ± ligand binding to $G_{\alpha s}$ were determined by fitting kinetic SPR data of 1333 and 2000 nM receptor ± 25 nM ligand, n=6. Data were collected from three separate membrane protein purifications tested in duplicate. (*) and (^) indicates that values with the same symbol are significantly different, while ($^{+}$) and ($^{\#}$) indicates values are highly significantly different ($p<0.0001$).

4.3.3. GDP affects receptor association

Here, the effects on receptor association to Gα$_s$ activated by GDP were examined by adding agonist or antagonist to receptor before injection over Gα$_s$-GDP. 300 nM Gα$_s$ was incubated with 600 nM GDP before being attached to Ni-NTA chip. Kinetic reads were collected for 1333 and 2000 nM A$_{2A}$R and A$_{2A}$Δ316R incubated with 0 or 25 nM CGS 21680 or ZM 241385 (**Figure 4.6** and **Figure 4.7**). Data were fit using the Biacore T200 Evaluation Software, and the effects of activating Gα$_s$ with GDP were observed.

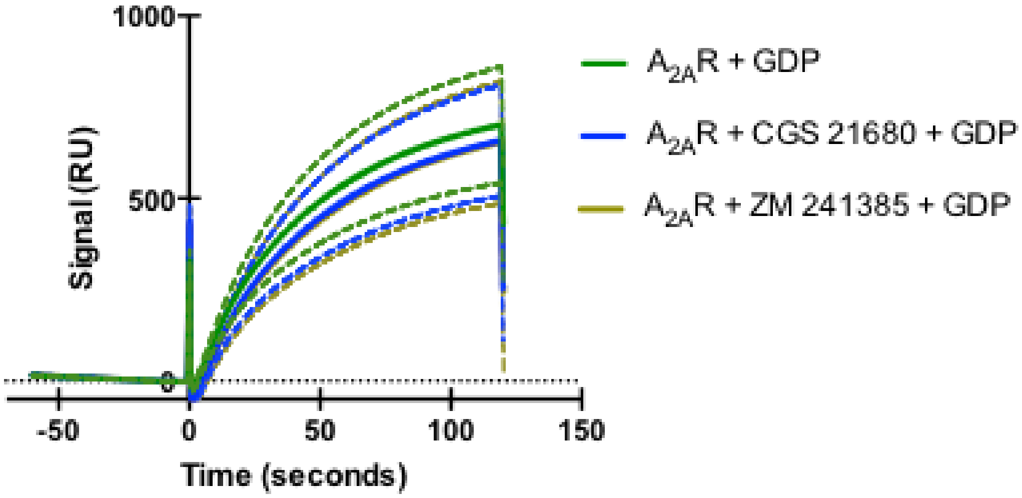

Figure 4.6 SPR data of 2000 nM A$_{2A}$R with or without ligand injected at time=0 onto 300 nM Gα$_s$ activated with 600 nM GDP. Data were fit using data from A$_{2A}$R at 1333 and 2000 nM, but for clarity only 2000 nM is shown. Dashed lines represent SEM. Experiments were performed using three separate receptor purifications collected in duplicate, n=6.

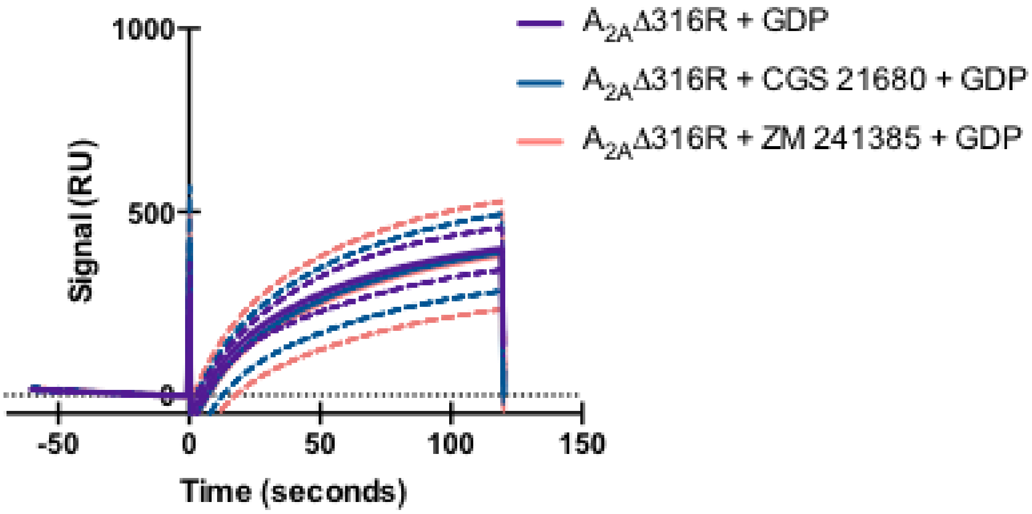

Figure 4.7 SPR data of 2000 nM $A_{2A}\Delta316R$ with or without ligand injected at time=0 onto 300 nM $G\alpha_s$ activated with 600 nM GDP. Data were fit using data from $A_{2A}\Delta316R$ at 1333 and 2000 nM, but for clarity only 2000 nM is shown. Dashed lines represent SEM. Experiments were performed using three separate receptor purifications collected in duplicate, n=6.

B_{max} values were determined for $A_{2A}R$ injected over GDP-activated $G\alpha_s$. Unliganded $A_{2A}R$ was 1162 ±19.7 RU, while addition of CGS 21680 or ZM 241385 gave B_{max} values of 1162 ±32.7 RU and 1090 ±22.6 RU, respectively (**Table 4.3**). These were not significantly different from one another, except when comparing no ligand to ZM 241385 ($p=0.0268$). All maximum binding capacities for $A_{2A}R$ in the presence of excess GDP were highly significantly lower ($p<0.0001$) than the B_{max} values shown previously in the absence of added GDP.

Maximum binding capacities for $A_{2A}\Delta316R$ with and without ligand were also determined. Without ligand, $A_{2A}\Delta316R$ had a B_{max} of 781 ±21.1 RU for binding to GDP-activated $G\alpha_s$. With the addition of CGS 21680 or ZM 241385 to truncated receptor, B_{max} was then observed to be 769 ±29.9 RU and 886 ±41.3 RU, respectively (**Table 4.3**). These data are highly significantly different from $A_{2A}R$ values in the presence of GDP, as it appears the truncation of the $A_{2A}R$ C-terminus significantly decreases the maximum binding capacity in the presence of excess GDP. Upon comparison to $A_{2A}\Delta316R$ B_{max} values with no added GDP, as seen in section 4.3.2, the maximum binding capacity is highly significantly different upon the addition of excess GDP. Additionally, comparison of the $A_{2A}\Delta316R$ maximum binding capacities to $G\alpha_s$ with additional GDP indicates that all are significantly different, except for no ligand compared with CGS 21680.

Association and dissociation rate constants were determined for $A_{2A}R$ with and without ligand in the presence of excess GDP. $A_{2A}R$ without ligand was found to have a k_{on} of 8618 ±247 M^{-1} s^{-1} and a k_{off} of 0.0088 ±0.00035 s^{-1}. Addition of CGS 21680 gave an association rate of 6905 ±326 M^{-1} s^{-1} and a dissociation rate of 0.0090 ±0.00056 s^{-1}, while ZM 241385 gave an association rate of 8396 ±332 M^{-1} s^{-1} and a dissociation rate of 0.0085 ±0.00049 s^{-1} (**Figure 4.8** and **Table 4.3**). Only the association rates were significantly different, except for comparison of no ligand to ZM 241385. Additionally, the k_{on} rate for CGS 21680 and all k_{off} rates were found to be significantly different from the same experiment performed with no added GDP. From these data, the addition of excess GDP to $G_{\alpha s}$ slows the dissociation rate constant compared to without GDP, but only slows the association rate constant in the presence of receptor bound to CGS 21680.

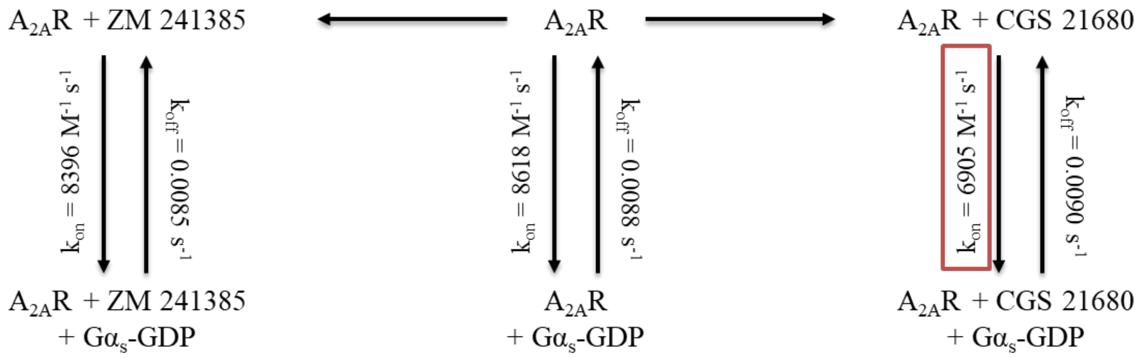
A2AR + ZM 241385
A2AR
A2AR + CGS 21680
kon = 8396 M-1 s-1
koff = 0.0085 s-1
kon = 8618 M-1 s-1
koff = 0.0088 s-1
kon = 6905 M-1 s-1
koff = 0.0090 s-1
A2AR + ZM 241385 + Gαs-GDP
A2AR + Gαs-GDP
A2AR + CGS 21680 + Gαs-GDP

Figure 4.8 Schematic of kinetic rate constants for $A_{2A}R$ associating with $G\alpha_s$-GDP in the presence or absence of ligand. Kinetic rate constants are not significantly different, except for $A_{2A}R$ bound to CGS 21680, which has a significantly slower on rate (red).

Association and dissociation rates were determined for $A_{2A}\Delta316R$ with and without ligand in the presence of excess GDP to activate $G\alpha_s$. $A_{2A}\Delta316R$ without ligand was found to have a k_{on} of 7171 ±159 M^{-1} s^{-1} and a k_{off} of 0.0094 ±0.00030 s^{-1}. Addition of CGS 21680 gave an association rate of 7896 ±255 M^{-1} s^{-1} and a dissociation rate of 0.0087 ±0.00037 s^{-1}, while ZM 241385 gave an association rate constant of 6283 ±229 M^{-1} s^{-1} and a dissociation rate constant of 0.0103 ±0.00646 s^{-1} (**Figure 4.9** and **Table 4.3**). All association rate constants were significantly different from one another, but none of the dissociation rate constants showed a significant difference. CGS 21680 bound to $A_{2A}\Delta316R$ showed the fastest association with $G\alpha_s$ with excess GDP, while ZM 241385 bound to $A_{2A}\Delta316R$ had the slowest association. All k_{on} and k_{off} rates were significantly different when compared to data from $G\alpha_s$ without added GDP, except for when ZM 241385 was present. These values indicate that added GDP decreases both association and dissociation rates for $A_{2A}\Delta316R$ without ligand or with CGS 21680. $A_{2A}\Delta316R$ association rate constants (with and without ligand) are additionally highly significantly different ($p<0.0001$) from full-length receptor association in the presence of GDP. For receptor incubated without ligand or with ZM 241385, the k_{on} decreases in the absence of the C-terminus. However, when CGS 21680 is bound to receptor, the k_{on} increases with the truncation of the C-terminus.

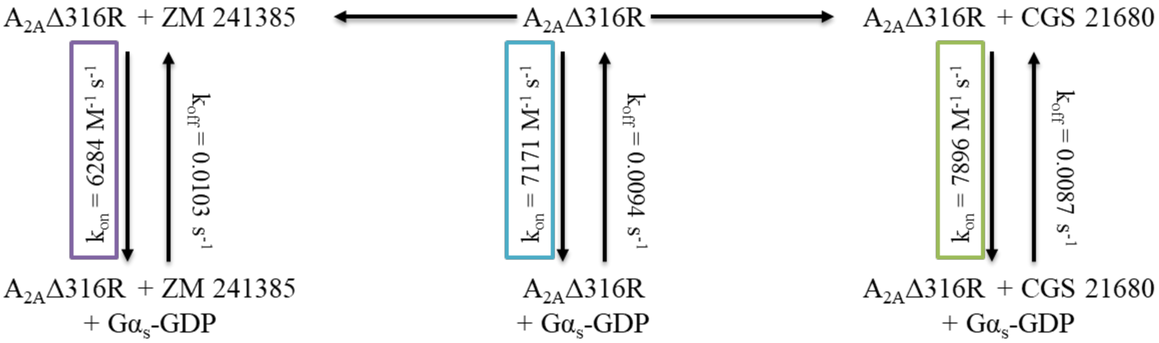
$A_{2A}\Delta316R$ + ZM 241385
$A_{2A}\Delta316R$
$A_{2A}\Delta316R$ + CGS 21680
$k_{on} = 6284\ M^{-1}\ s^{-1}$
$k_{off} = 0.0103\ s^{-1}$
$k_{on} = 7171\ M^{-1}\ s^{-1}$
$k_{off} = 0.0094\ s^{-1}$
$k_{on} = 7896\ M^{-1}\ s^{-1}$
$k_{off} = 0.0087\ s^{-1}$
$A_{2A}\Delta316R$ + ZM 241385 + $G\alpha_s$-GDP
$A_{2A}\Delta316R$ + $G\alpha_s$-GDP
$A_{2A}\Delta316R$ + CGS 21680 + $G\alpha_s$-GDP

Figure 4.9 Schematic of kinetic rate constants for $A_{2A}\Delta316R$ associating with $G\alpha_s$-GDP in the presence or absence of ligand (blue). All k_{on} rates are significantly different. $A_{2A}\Delta316R$ bound to CGS 21680 has the fastest association to $G\alpha_s$ (green), while $A_{2A}\Delta316R$ bound to ZM 241385 has the slowest (purple).

	k_{on} (M^{-1} s^{-1}) ±SE	k_{off} (s^{-1}) ±SE	RT (s)	K_D (nM)	B_{max} (RU) ±SE
$A_{2A}R$	$8618 \pm 247^{+}$	$\underline{0.0088 \pm 0.00035}$	114	1027	$\underline{1162 \pm 19.7^{*}}$
$A_{2A}R$ + CGS 21680	$\underline{6905 \pm 326^{+*}}$	$\underline{0.0090 \pm 0.00056}$	111	1296	$\underline{1162 \pm 32.7}$
$A_{2A}R$ + ZM 241385	$8396 \pm 332^{*}$	$\underline{0.0085 \pm 0.00049}$	118	1017	$\underline{1090 \pm 22.6^{*}}$
$A_{2A}\Delta316R$	$\underline{7171 \pm 159^{*\wedge}}$	$\underline{0.0094 \pm 0.00030}$	106	1307	$\underline{781 \pm 21.1^{\wedge}}$
$A_{2A}\Delta316R$ + CGS 21680	$\underline{7896 \pm 255^{*+}}$	$\underline{0.0087 \pm 0.00037}$	115	1108	$\underline{769 \pm 29.9^{*}}$
$A_{2A}\Delta316R$ + ZM 241385	$6283 \pm 229^{\wedge+}$	0.0103 ± 0.00646	97	1632	$\underline{886 \pm 41.3^{*\wedge}}$

Table 4.3 Association and dissociation rates of purified receptor ± ligand coupling to 300 nM $G\alpha_s$ with 600 nM GDP were determined by fitting kinetic SPR data of 1333 and 2000 nM receptor ± 25 nM ligand, n=6. Data were collected from three separate membrane protein purifications tested in duplicate. (*) and (^) indicates that values with the same symbol and receptor type are significantly different, while ($^{+}$) and ($^{\#}$) indicates values are highly significantly different ($p<0.0001$). Underlined values indicate that they are significantly different from the values determined by SPR without added GDP. All comparisons between experiments with full-length vs truncated receptor are significantly different, except for k_{off} values, of which none are significantly different. This significance is therefore not indicated in this table for clarity.

4.3.4. GTPγs inhibits receptor association

300 nM $G\alpha_s$ was incubated with 600 nM GTPγs, a non-hydrolyzable GTP analog that cannot be converted to GDP, and therefore locks the G protein in an inactive state. After incubation, $G\alpha_s$-GTPγs was attached via 6xHis tag to a Ni-NTA SPR chip, and 1333 or 2000 nM purified $A_{2A}R$ (**Figure 4.10**) or $A_{2A}\Delta316R$ (**Figure 4.11**) was injected. B_{max} was determined for each experiment after subtracting off the negative control of denatured $G\alpha_s$.

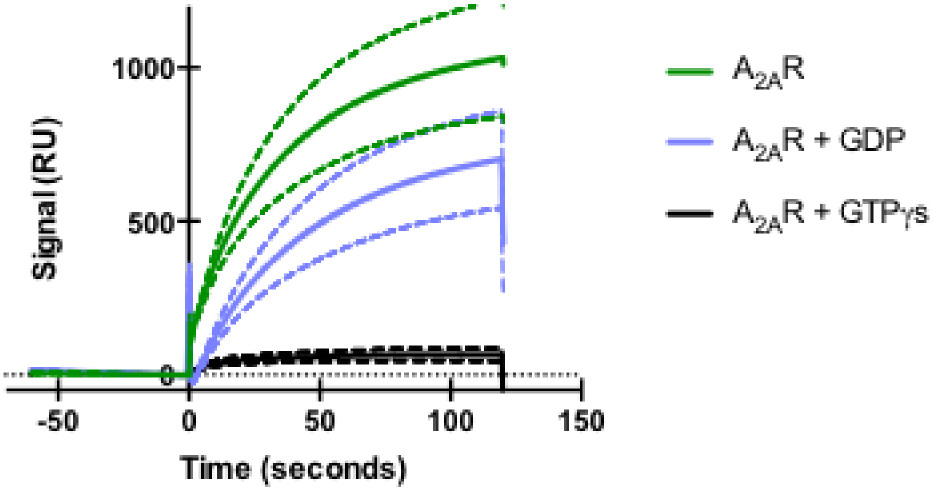

Figure 4.10 SPR of 2000 nM $A_{2A}R$ injected at time=0 over 300 nM $G\alpha_s$ in the absence of (green) or presence of either 600 nM GDP (blue) or 600 nM GTPγs (black). Data were fit using data from $A_{2A}R$ at 1333 and 2000 nM, but for clarity only 2000 nM is shown. Dashed lines represent SEM. Experiments were performed using three separate receptor purifications collected in duplicate, n=6.

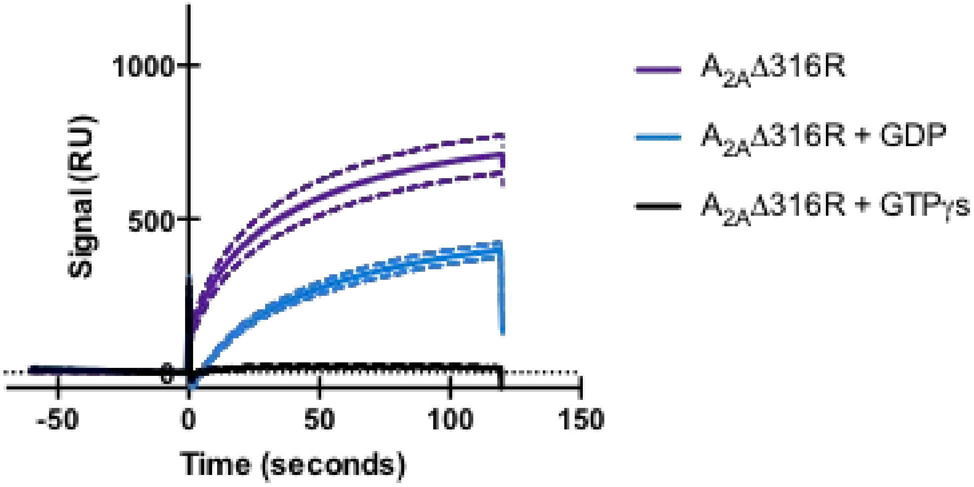

Figure 4.11 SPR of 2000 nM $A_{2A}\Delta316R$ injected at time=0 over 300 nM $G\alpha_s$ in the absence of (purple) or presence of either 600 nM GDP (blue) or 600 nM GTPγs (black). Data were fit using data from $A_{2A}\Delta316R$ at 1333 and 2000 nM, but for clarity only 2000 nM is shown. Dashed lines represent SEM. Experiments were performed using three separate receptor purifications collected in duplicate, n=6.

Maximum potential binding capacity was determined for $A_{2A}R$ and $A_{2A}\Delta316R$ associating with $G\alpha_s$-GTPγs (**Table 4.4**). $A_{2A}R$ was determined to have a B_{max} of 46.2 ±3.2 and $A_{2A}\Delta316R$ a B_{max} of 33 ±12. These B_{max} values were found to not be significantly different from one another. However, they are highly significantly different from the B_{max} values for receptor associating with $G\alpha_s$ in the absence of GTPγs. Addition of GTPγs saw a greater than 30 fold decrease in the maximum potential binding capacity of either receptor to $G\alpha_s$, indicating that exchange of GDP by GTPγs is successfully preventing the G protein from associating with adenosine receptor.

	$G\alpha_s$ B_{max} (RU) ±SE	$G\alpha_s$ + GDP B_{max} (RU) ±SE	$G\alpha_s$ + GTPγs B_{max} (RU) ±SE
$A_{2A}R$	1554 ±10.1	1162 ±19.7	46.2 ±3.2*
$A_{2A}\Delta316R$	1078 ±10.3	781 ±21.1	33 ±12*

Table 4.4 B_{max} values of 1333 and 2000 nM purified receptor associating with $G\alpha_s$ in the absence of or with 600 nM GDP or GTPγs, n=6. Data were collected from three separate membrane protein purifications tested in duplicate. All B_{max} values are highly significantly different ($p<0.0001$) except for comparison of $A_{2A}R$ to $A_{2A}\Delta316R$ when $G\alpha_s$ is inactivated with GTPγs, which is not statistically significant. (*) represents values that are not statistically different.

4.4. Discussion and Conclusions

In this chapter, the effects of additives (i.e. ligands, GDP, GTPγs) on the kinetic rates and affinity of $A_{2A}R$ and $A_{2A}\Delta316R$ for $G\alpha_s$ was determined using SPR. Data were collected at 263, 395, 592, 889, 1333, and 2000 nM of receptor, but as discussed in Chapter 3, only 1333 and 2000 nM concentrations were used to fit data. $G\alpha_s$ was attached at 300 nM, and GDP or GTPγs were added to 600 nM, where appropriate, to be present in excess.

$A_{2A}R$ association with $G\alpha_s$ was affected by pre-incubation of the receptor with agonist, CGS 21680, and antagonist, ZM 241385. A comparison of the B_{max} of $A_{2A}R$ with CGS 21680 (1460 ±8.1 RU) to $A_{2A}R$ with ZM 241385 (1090 ± 22.6 RU) indicated that receptor incubated with antagonist had the lowest maximum potential binding capacity to $G\alpha_s$. One explanation for this change in B_{max} is that as an antagonist, ZM 241385 keeps $A_{2A}R$ in a neutral state, preventing activation of downstream signaling. Part of preventing the downstream signaling could be decreasing the interaction of the receptor and G protein by a conformational change. Additionally, receptor without ligand bound may prefer to associate with G protein so that it is ready to initiate a downstream signaling cascade upon ligand binding. This could explain why the B_{max} for $A_{2A}R$ without ligand (1554 ±10.1 RU) is the highest of the three cases.

Kinetic k_{on} and k_{off} rate constants were also determined for $A_{2A}R$ binding to $G\alpha_s$ with and without pre-incubation with ligand. The only association rates that were significantly different were those of $A_{2A}R$ pre-incubated with agonist (CGS 21680) versus those of antagonist (ZM 241385), where the on rate for receptor incubated with ZM 241385 to G protein is significantly faster. However, the dissociation rate constant for $A_{2A}R$ when incubated with ZM 241385 is significantly slower when compared to receptor without ligand or receptor with agonist. Additionally, when calculating the dissociation constant, K_D from k_{off}/k_{on}, $A_{2A}R$ bound to ZM 241385 has the lowest dissociation constant (1293 nM), or highest affinity, for $G\alpha_s$ compared to $A_{2A}R$ without ligand or with CGS 21680 (1338 and 1359 nM, respectively). In an effort to neutralize the receptor and downstream signaling pathway, perhaps ZM 241385 puts the receptor in such a conformation so as to associate quickly with $G\alpha_s$, but then take a long time to dissociate, thus preventing downstream signaling activation. It is also worth noting that no significant differences were observed when comparing rate constants of $A_{2A}R$ without ligand or with CGS 21680. This suggests that the unbound receptor is already in an active state, and that binding to antagonist inactivates or neutralizes receptor activity. This is consistent with basal signaling levels observed in both yeast (Jain, in review) and mammalian systems (Klinger 2002).

The maximum potential binding capacity of a C-terminally truncated receptor, $A_{2A}\Delta316R$, with CGS 21680 to $G\alpha_s$ was significantly lower than $A_{2A}\Delta316R$ alone or with ZM 241385, while comparison of B_{max} of $A_{2A}\Delta316R$ without ligand to $A_{2A}\Delta316R$ with ZM 241385 showed no statistically significant difference. This is different from what was observed for $A_{2A}R$. It appears that the truncation of the $A_{2A}R$ C-terminus not only causes the receptor to couple at a decreased maximum potential with $G\alpha_s$, but also truncation of the C-terminus seems to alter in a complex way ligand-bound receptor interaction with G protein.

Association and dissociation rate constants, k_{on} and k_{off}, were determined for $A_{2A}\Delta316R$ with and without ligand associating to $G\alpha_s$ (**Table 4.2**). All association rates were highly significantly different from one another, and dissociation rates were all highly significantly or significantly different. This is in contrast to the effect of ligand on $A_{2A}R$ association to G protein, where ligand only sometimes had an effect on rate constants. Here, $A_{2A}\Delta316R$ bound to ZM 241385 had the slowest association rate and the fastest dissociation rate, while $A_{2A}\Delta316R$ bound to CGS 21680 had the fastest association rate and slowest dissociation rate. It then follows that $A_{2A}\Delta316R$ bound to ZM 241385 had the lowest affinity of the $A_{2A}\Delta316R$ experiments, and $A_{2A}\Delta316R$ bound to CGS 21680 had the greatest affinity for $G\alpha_s$. Recall that for full-length $A_{2A}R$, the presence of ZM 241385 had the opposite effect on receptor association with $G\alpha_s$; antagonist bound to $A_{2A}R$ allowed the receptor to associate more quickly and dissociate more slowly than receptor alone or with agonist. Thus, $A_{2A}R$ with ZM 241385 had the highest affinity for $G\alpha_s$, which is again in contrast to the truncation with ZM 241385, where the antagonist increases receptor affinity for G protein. These data suggest that truncation of the $A_{2A}R$ C-terminus not only affects the receptor affinity for $G\alpha_s$, but alters the characteristic effects of ligand binding to receptor to initiate or block downstream signaling.

Recall that activated $G\alpha_s$ exchanges GDP for GTP, indicating that a $G\alpha_s$-GTP complex has already dissociated from the receptor to further initiate downstream signaling (Alves 2004). This indicates that $G\alpha_s$-GTP should bind receptor at minimal levels. However, GTP can by hydrolyzed to GDP, which would allow for reassociation to the receptor. Here, GTPγs, a non-hydrolyzable GTP, was chosen is so it cannot be converted into GDP and restart the G protein cycle. These data show that the maximum potential binding capacity of $G\alpha_s$ is highly significantly decreased when incubated with GTPγs, to the point that it appears that GTPγs has nearly fully blocked the ability of G protein to associate with receptor. Injection of $A_{2A}R$ and $A_{2A}\Delta316R$ over $G\alpha_s$-GTPγs, B_{max} was determined to be 46.2 ±3.2 RU and 33 ±12 RU, respectively. These values are not significantly different between the two receptors, but they are highly significantly different from the B_{max} values determined when $G\alpha_s$ alone was attached to the chip (1554 ±10.1 RU and 1078 ±10.3 RU) or when $G\alpha_s$ was incubated with GDP (1162 ±19.7 RU and 781 ±21.1).

However, addition of 600 nM GDP to 300 nM $G\alpha_s$ had overall modest effects (**Table 4.3**). It appears that addition of GDP significantly decreased the B_{max} for both $A_{2A}R$ and $A_{2A}\Delta316R$, as well as increased the dissociation time (decreased k_{off}) for both receptors. Yet, only $A_{2A}\Delta316R$ showed a significant decrease in k_{on} in the presence of GDP. Additionally, the K_D of both receptors for $G\alpha_s$ decreased with addition of GDP. Likely, the dissociation time from $G\alpha_s$ is increased with GDP present because the conversion of GDP to GTP would normally take place to begin receptor dissociation and downstream signaling. As these experiments took place in a membrane-mimetic environment, conversion of GDP to GTP is unlikely, and therefore would decrease the rate of dissociation.

Taken together, these results suggest that addition of perturbances, be it ligand bound to receptor or a version of guanosine phosphate, affects the association of receptor and $G\alpha_s$. In summary, the truncation of the $A_{2A}R$ C-terminus not only affects the receptor association with $G\alpha_s$, but it also affects the way in which ligand binding promotes or inhibits association and dissociation with $G\alpha_s$. These results are consistent with our prior data (McGraw 2018) that show increased cAMP production by $A_{2A}R$ and insignificant cAMP production by $A_{2A}\Delta316R$, indicating that the truncation of the C-terminus affects the downstream signaling pathway via interaction, at least in part, directly with Gα_s. Future experiments could be performed using agonist and antagonist with different binding affinities for $A_{2A}R$ to determine if the affinity of a given ligand for receptor affects the affinity of ligand-bound receptor for Gα_s. Furthermore, examination of other adenosine receptors -- A_1R or A_3R -- in the presence and absence of ligand to Gα_i (inhibitory Gα) would help characterize the interaction of these receptors and Gα_i. These experiments would also provide insight into the effect of ligand on Gα_i as compared to Gα_s.

Chapter 5

CONCLUSIONS AND FUTURE DIRECTIONS

Characterizing the effect of the C-terminal truncation on ligand binding affinity and kinetics provides insight into the functionality of the $A_{2A}R$ C-terminus. Understanding how the C-terminus impacts ligand binding and stability highlight caveats in interpreting predictions from crystal structures used for novel drug design. Additionally, examination of downstream signaling events provides more information on the effects of not only the C-terminus, but also ligand, on receptor activation.

This work addresses how mutations made to the adenosine A_{2A} receptor affect ligand binding characteristics, stability, and downstream signaling. This was observed as described in Chapter 1:

- Fluorescent ligand binding to characterize equilibrium binding, competitive binding, and kinetic rate constants of $A_{2A}R$ and mutants (Chapter 2)
- Determination of thermostability of $A_{2A}R$ and mutants (Chapter 2)
- Observation and kinetic characterization of $A_{2A}R$ and mutants (Chapter 3)
- Effects of ligand on receptor association to $G\alpha_s$ via SPR (Chapter 4)

Fluorescent ligand binding was chosen as a means of characterizing ligand binding of $A_{2A}R$, $A_{2A}\Delta316R$, and Rag23, which is truncated at amino acid 316 and given five thermostabilizing, agonist-favoring point mutations. Parallel and perpendicular fluorescent intensities were converted to anisotropy and then to receptor-ligand complexes (RL) to determine ligand binding constants such as equilibrium dissociation constant, K_D, maximum potential binding capacity, B_{max}, inhibitor dissociation constant, IC_{50}, and kinetic association and dissociation rate constants, k_{on} and k_{off}, respectively (Chapter 2). Taken together, the ligand binding constants confirm that Rag23 has a greater affinity for agonist as compared to $A_{2A}R$.

Furthermore, the effects of the C-terminal truncation and mutants were observed relative to receptor thermostability (Chapter 2). CPM, a thiol reactive dye that binds to exposed cysteines, thus increasing fluorescence as receptor unfolds, was used to quantify the unfolding temperature, T_{unf}. Although none of the receptors had significantly different T_{unf}, the values seen in this work were similar to those described previously (Magnani 2008), which showed Rag23 with an unfolding temperature approximately 7°C higher than that of $A_{2A}\Delta316R$. Although $A_{2A}\Delta316R$ has a lower unfolding temperature than wild-type $A_{2A}R$, it appears that the addition of the five thermostabilizing point mutations more than recovers the receptor stability compared to that of wild-type.

Next, the downstream signaling pathway was examined using SPR to characterize the association kinetics of $A_{2A}R$ and $A_{2A}\Delta316R$ to $G\alpha_s$. From these data, truncation of the $A_{2A}R$ C-terminus was found to have a profound impact on receptor association with $G\alpha_s$. Not only did wild-type $A_{2A}R$ have a faster k_{on} compared to $A_{2A}\Delta316R$, but $A_{2A}R$ also had a slower k_{off}, indicating that $A_{2A}R$ has a greater affinity for $G\alpha_s$. Additionally, $A_{2A}R$ was determined to have a significantly greater B_{max} than the truncated receptor, which further confirms the results from Dr. McGraw's cAMP assay—that truncation of the C-terminus affects receptor association to Gα_s, thereby reducing activation of the downstream signaling pathway. These SPR results taken together attest that the C-terminus is necessary for association to Gα_s, not only in binding capacity, but also in regards to receptor affinity and the rate at which it associates to Gα_s.

Following quantification of kinetic rate constants of A_{2A}R and $A_{2A}\Delta$316R associating to Gα_s, perturbances, such as agonist, antagonist, GDP, or GTP, were added to examine the effect on the association of receptor to Gα_s. Addition of ligand to A_{2A}R decreased the B_{max} of receptor association to Gα_s, regardless of ligand type. However, only addition of antagonist, ZM 241385, decreased the dissociation rate constant, which follows the model that antagonist bound to receptor neutralizes the receptor such that it would not need to dissociate from Gα_s. Unliganded receptor and receptor bound to agonist likely had faster dissociation rates because these receptors are in conformations such that they can activate downstream signaling cascades by dissociating from Gα_s.

Next, addition of ligand to $A_{2A}\Delta$316R was found to affect all kinetic rate constants, as well as B_{max}. This work could be further explored to determine why $A_{2A}\Delta$316R association to Gα_s was affected differently by addition of ligands than the association of wild-type A_{2A}R. From these data, truncation of the C-terminus has an effect not only on unliganded $A_{2A}\Delta$316R association with Gα_s, but also the way in which ligand binding affects $A_{2A}\Delta$316R downstream signaling.

Finally, the effects of GDP and GTP on Gα_s association were observed. Pre-incubation of Gα_s with GDP was found to decrease B_{max} for both A_{2A}R and $A_{2A}\Delta$316R, as well as slow the dissociation rate constant, k_{off}. This could be because experiments are performed in the absence of GTP, which would be exchanged for GDP before Gα_s

dissociates from the receptor. When $G\alpha_s$ is unable to exchange GDP for GTP, it follows that the rate of $G\alpha_s$ dissociation from receptor should be slower. Additionally, when $G\alpha_s$ is pre-incubated with GTPγs, a non-hydrolyzable GTP analog that cannot be converted to GDP, little to no receptor association was observed. B_{max} values for either $A_{2A}R$ or $A_{2A}\Delta 316R$ associating to $G\alpha_s$-GTPγs indicate up to a 33-fold decrease in receptor association. This is expected, as $G\alpha_s$-GTP occurs after $G\alpha_s$ dissociates from receptor to initiate downstream signaling. If GTP is not hydrolysable into GDP, the $G\alpha_s$ is held in a conformation such that it is unable to associate with receptor (Alves 2004).

Determination of association kinetics between $A_{2A}R$ and $G\alpha_s$ elucidates the interaction between the proteins that comprise some of the first steps in the downstream signaling pathway. However, these experiments revealed the truncation of the C-terminus affects receptor association to $G\alpha_s$, which is one more piece of evidence to confirm that the truncation negatively affects downstream signaling. Additionally, the effects of perturbations on receptor behavior caused $A_{2A}R$ and $A_{2A}\Delta 316R$ to behave in different ways. The change in $A_{2A}R$ association to $G\alpha_s$ upon ligand addition can be explained by the expected effects of agonist or antagonist on the downstream signaling pathway (e.g. antagonist neutralizes the receptor); however, $A_{2A}\Delta 316R$ does not behave in the same manner after ligand addition. Future experiments could be performed to elucidate the effects of C-terminal truncation and addition of ligand to the downstream signaling pathway. This characterization could be useful when examining the crystal structures of $A_{2A}\Delta 316R$ to better improve drug design for the receptor.

Furthermore, the SPR experimental design described here presents a meaningful method of characterizing more GPCR interactions with G proteins. SPR with other receptors and types of G proteins would provide a useful method of examining the kinetic rates of association that has been previously difficult to characterize. These results would present a meaningful way to determine downstream signaling in terms important to drug efficacy. Additionally, experiments as described could be compared to receptor purified in nanodiscs to examine the effect of the type of membrane-mimetic environment on the receptor association with G protein (Dijkman 2015). This would be useful to determine if there is a significant change in receptor activity between environments.

Appendix A

CHARACTERIZATION OF $A_{2B}R$ CHIMERA BY FLUORESCENCE ANISOTROPY AND RADIOLIGAND BINDING

A.1. Introduction

The adenosine A_{2A} receptor ($A_{2A}R$) is the most well-characterized of the four adenosine receptors, A_1R, $A_{2A}R$, $A_{2B}R$, and A_3R, in part due to the increased level of expression seen by $A_{2A}R$. Higher levels of expression often leads to more ligand binding and/or downstream signaling in recombinant hosts, so there is a better signal to noise ratio when characterizing the receptor. Previously, the C-terminus of the $A_{2A}R$ receptor was found to affect receptor trafficking (Jain in review, Britton 2012), and upon addition of the C-terminus to other adenosine receptors, an increase in expression was noted (Moriyama 2010). This led to creation of adenosine receptor chimeras, all with the $A_{2A}R$ C-terminus that could be expressed at higher levels than wild-type, and therefore better characterized. Seeing as the intracellular loops are not mutated, it is possible that the chimeras could retain ligand binding properties similar to that of the wild-type receptor.

Here, the $A_{2A}R$ C-terminus is added to $A_{2B}R$ (BA) at the RIR homologous region (Britton 2012) to overexpress the low-expressing $A_{2B}R$ so that the receptor may be purified at high enough concentrations to be characterized. Characterization of $A_{2B}R$ would prove especially useful considering the receptor has lower affinity for many adenosine receptor agonists, which makes it more difficult to determine affinity of receptor for ligand (Trincavelli 2014). Additionally, a thermostable variant of BA (B*A) was created previously in our lab. The Rant21 variant created by the Tate group has 5 point mutations designed to favor antagonist binding in $A_{2A}R$ (Magnani 2008). These point mutations were translated by homology into $A_{2B}R$ and used to create a thermostable, antagonist favoring variant, $A_{2B}*R$. Using the same subcloning theory as when creating BA, the thermostable variant had the $A_{2A}R$ C-terminus added for overexpression to create B*A. This appendix examines the expression, purification, and characterization of BA and B*A.

A.2. Materials and Methods

A.2.1. Cell Growth and Expression

As described in Chapter 2, receptors were expressed in BJ5464 yeast cells using a multi-integrating vector, pITy, that contains a C-terminal His10 tag for purification of receptors. BA and B*A were grown overnight at 30ºC in YPD, then induced by transfer to YPG at an O.D. of 1 and grown for 24-30 hours. 1250 O.D. of cells were pelleted and stored at -80ºC until needed for purification.

A.2.2. Membrane Protein Purification

Receptors were purified as detailed in Chapter 2. Briefly, cell pellets were resuspended in lysis buffer and protease-inhibitors and lysed with 0.5 mm zirconia silica beads. Lysed cells were then sonicated for 20 seconds, placed on ice to cool, and sonicated a second time. Samples were centrifuged at 3200 g for 30 min to remove cell debris, and supernatant was ultracentrifuged at 100,000 g for 1 hour to pellet cell membranes. Membranes were resuspended in 0.1% DDM/0.1% CHAPS/0.02% CHS and left to rotate overnight at 4ºC. Next, samples were centrifuged at 70,000 g to remove any insoluble material, and supernatant was incubated overnight at 4ºC with Ni-NTA resin. The following day, resin was washed with increasing concentrations of imidazole (20-50 mM), and protein was eluted with 50 mM imidazole and 10 mM EDTA. The final elution was desalted using PD010 desalting columns, and purified receptors were stored for up to 7 days at 4ºC.

A.2.3 Fluorescence Anisotropy Assay

FITC-APEC was used to observe ligand binding, as detailed in Chapter 2. Briefly, samples were read in 96 well half-area black Corning plates (catalog #3875, Corning Incorporated-OR-FisherSci cat#07-200-735) on a Synergy H1 plate reader (BioTek, Winooski, VT) using a polarized filter cube with an excitation wavelength of 480-485 nm and an emission wavelength of 520-528 nm. Scatter measurements were subtracted and anisotropy was calculated as previously described (Swonger 2018).

A.2.4 Equilibrium Ligand Binding

1-1.6 µM of purified BA in DCC buffer was incubated with 0, 0.01, 0.1, 0.25, 0.5, 0.75, 1, 5, 7.5, or 10 nM FITC-APEC and protected from light at room temperature for 2 hours. Parallel and perpendicular light was read on a Synergy H1 plate reader using a polarized filter cube with an excitation wavelength of 480-485 nm and emission wavelength of 520-528 nm. As described in Chapter 2, anisotropy was determined, and RL complexes were calculated at each concentration of labeled ligand.

A.2.5 Kinetic Ligand Binding

To observe association of FITC-APEC to BA and B*A, 1 µM of purified receptor in DCC buffer was incubated with 0.5 nM FITC-APEC. Immediately after addition of fluorescent ligand, reads were taken every 7 seconds for 1 hour on the plate reader as described in Chapter 2. Anisotropy was calculated and converted to RL complexes.

A.2.6. Radioligand Binding

Purified membrane protein in DCC buffer (0.1% DDM/0.1% CHAPS/0.02% CHS) was left bound to Ni-NTA resin. As previously described (Naranjo 2016), receptor was diluted to 1 µM concentration in a final volume of 180 µL in ligand binding buffer (50 nM Tris-HCl, pH 7.4, 1 mM EDTA, 10 mM $MgCl_2$) and loaded onto poly(ethyleneimine) (0.1% v/v) treated 96-well glass fiber filter plates 49 (MultiScreen-FC filter type B, Millipore, Billerica, MA). Receptors were then incubated with 80 nM [^{3}H] NECA or 80 nM [^{3}H] MRE 2029-F20 with 0 or 5 µM of unlabeled competitor (BAY60-6583) and left shaking for 90 minutes at either 4°C or room temperature. After incubation, samples were washed 3 times with ice cold ligand binding buffer. After washes, 30 µL of scintillation fluid (ULTIMA Gold, PerkinElmer) was added to each well. Radioactivity was measured in counts per minute (CPM) by PerkinElmer 1450 Microbeta liquid scintillation counter at 2 and 24 hours (2 hours being right after addition of scintillation fluid). Future experiments should consider decreasing EDTA concentration when using purified membrane proteins bound to Ni-NTA resin, as EDTA chelates nickel, leading to elution of receptor from the resin.

A.3. Results

A.3.1 Overexpression of BA and B*A

The adenosine A_{2B} receptor, $A_{2B}R$, is the least well characterized of the four adenosine receptors. The addition of the $A_{2A}R$ C-terminus, BA, allows for overexpression of the low expressing $A_{2B}R$, and provides an opportunity to purify and characterize the receptor and the thermostable variant, B*A. Here, a Western blot of lysed cells with different induction durations (induction by galactose) indicates that cells are successfully overexpressing BA and B*A at different time points (**Figure A.1**).

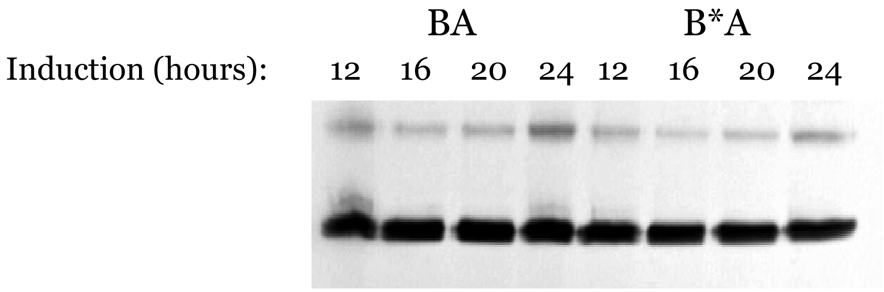

Figure A.1 Western blot of lysed cells expressing BA and B*A induced by galactose for 12-24 hours. The lower band at 40 kDa represents the expressed receptor.

A.3.2. Equilibrium binding of FITC-APEC to BA

Receptor was purified in a membrane-mimetic environment, as first described in Chapter 2. Typically, purification of BA yielded 1-2 μM of receptor. To determine if the purified receptor was active, anisotropy was calculated using 0-10 nM FITC-APEC (a nonspecific adenosine receptor agonist) incubated with BA. Results suggest that BA is active and associating with FITC-APEC, as there was an increase in RL complexes at higher concentrations of fluorescent ligand (**Figure A.2**). The anisotropy values for BA are greater than that of micelles (negative control), although an equilibrium binding curve was difficult to obtain. Likely, the affinity of BA for FITC-APEC is high, or the activity of the purified receptor is low. This makes it somewhat straightforward to obtain a binding plateau (beginning at approximately 1 nM FITC-APEC), but more difficult to obtain anisotropy values at lower concentrations to characterize the equilibrium binding curve. One strategy was to increase the receptor concentration (from 800 nM to 1000 nM), and another to collect more ligand binding at lower FITC-APEC concentrations. One downside to lowering the FITC-APEC concentration is the loss of fluorescence intensity can cause scatter due to the micelle environment to be a greater percentage of the anisotropy reading. Here, conversion of anisotropy to RL complexes (**Figure A.3**) was fit to a one site-specific binding model in Prism. These results indicated that BA has a B_{max} of 7.4 ±4.5 and a K_D of 24.2 ±19.7.

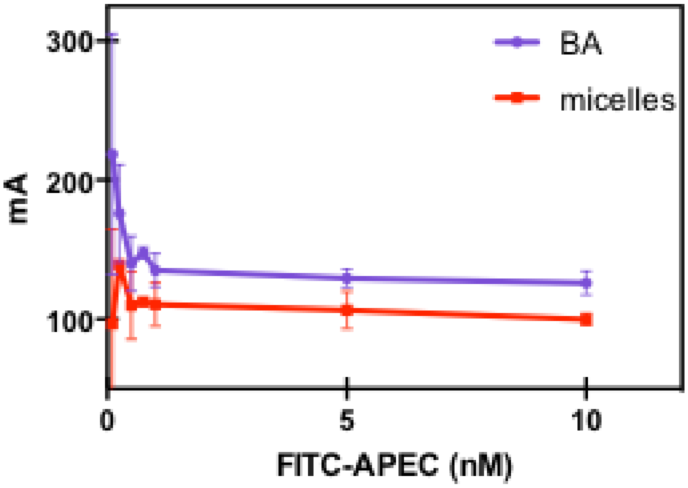

Figure A.2 Raw anisotropy data (scatter subtracted) of 1 μM BA and empty detergent micelles incubated with 0-10 nM FITC-APEC. Data suggests that BA is active and binding to FITC-APEC, as the anisotropy curve is greater than the micelle anisotropy. All points have at least 4 replicates, but most have n≥6. Error bars represent standard deviation from the mean.

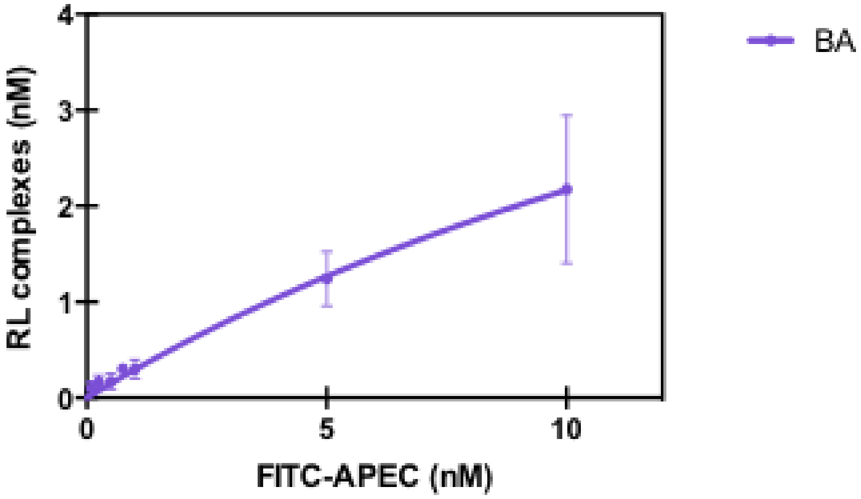

Figure A.3 RL complexes of FITC-APEC and BA. Anisotropy from Figure A.1. was converted into RL complexes as described in Chapter 2. Curve was fit to a One site-Specific binding model in Prism. Data represent n≥4. Error bars represent standard deviation from the mean.

A.3.3. Kinetic association of FITC-APEC to BA and B*A

Kinetic rates were observed to characterize ligand binding of FITC-APEC to purified BA and B*A (**Figure A.4**). Kinetic association suggests that BA and B*A are active and associating with FITC-APEC. 0.5 nM FITC-APEC was chosen, as it was possibly in the depleted ligand regime which is important for anisotropy studies (McNeely 2017). Kinetic rates were difficult to determine, and could be re-collected at higher FITC-APEC concentrations, as described in the kinetics section of Chapter 2, to obtain better association and dissociation rate constants.

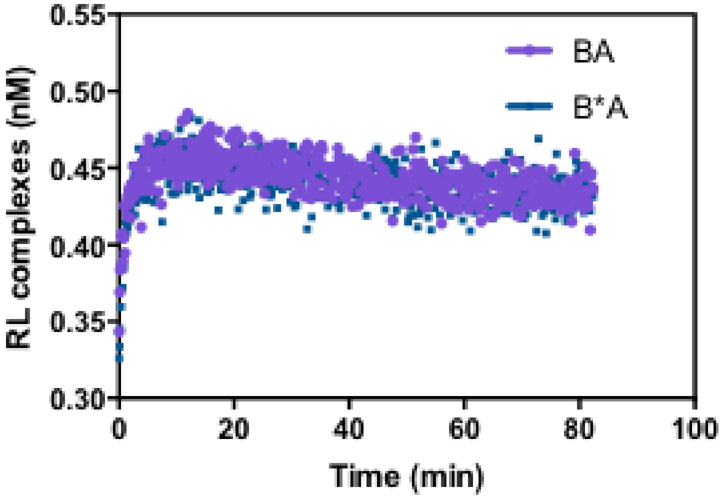

Figure A.4 RL complexes of 0.5 nM FITC-APEC associating to BA and B*A over 80 minutes. Raw anisotropy data (not shown) was converted to RL complexes to obtain ligand association curve. Data represent n=3.

A.3.4. Radioligand binding to BA and B*A

Radioligand binding experiments were performed with receptor still bound to Ni-NTA resin, as receptor eluted from resin would be small enough to pass through the pores on the filter on the 96 well plate used here. After receptor and hot ligand ([^{3}H] NECA or [^{3}H] MRE 2029-F20) were incubated for 2 hours shaking at room temperature, excess ligand was washed away and radioactive counts were read at 2 and 24 hours. Additional experiments with [^{3}H] MRE 2029-F20 were performed at 4ºC to determine whether temperature affected activity.

These experiments suggest that [^{3}H] NECA did not have strong affinity for BA, as addition of 5 µM BAY60-6583 (potent competitor) saw little decrease in counts per minute (CPM) (**Figure A.5**). Upon this observation, binding of [^{3}H] MRE 2029-F20 to BA and B*A was quantified (**Figure A.6**). CPM increased 3-4 fold after 24 hours.

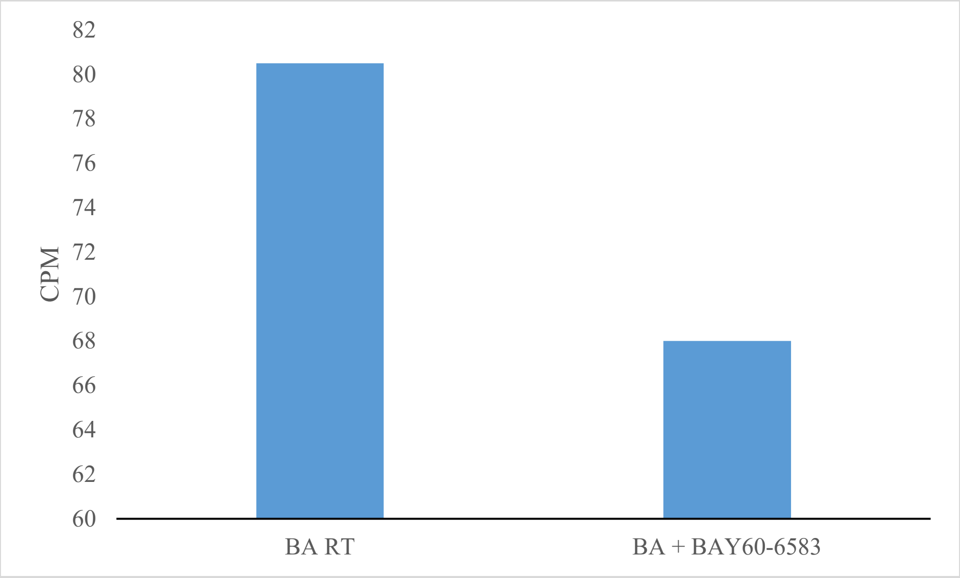

Figure A.5 Incubation of purified BA with 80 nM [^{3}H] NECA ± 5000 nM BAY60-6583. Addition of competitor appears to decrease radioligand binding by 15%, although perhaps with a hot ligand that binds more BA, the addition of BAY60-6583 would further improve the signal to noise ratio. Results were from one purification with experiment performed in duplicate.

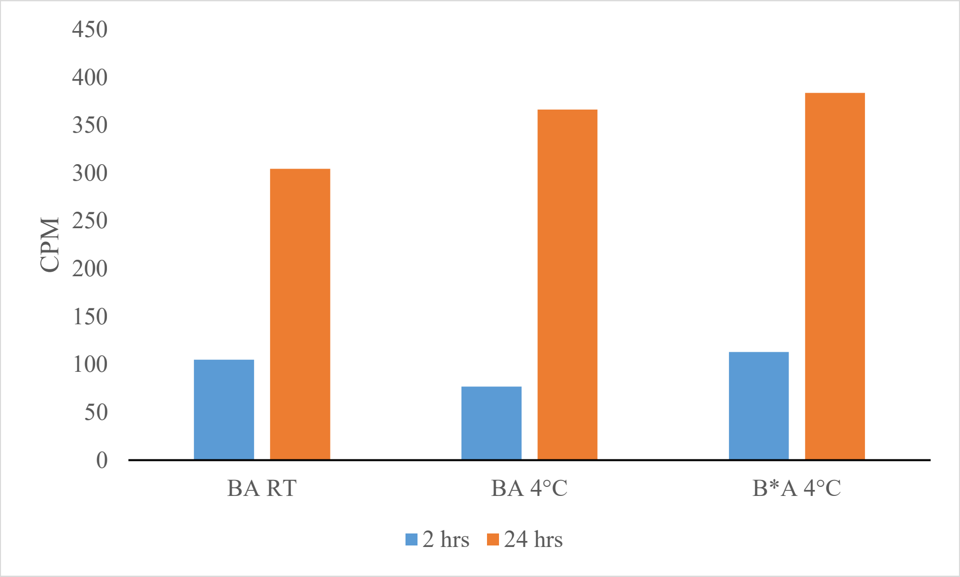

Figure A.6 CPM of purified BA and B*A at room temperature or 4°C incubated with 5 nM [^{3}H] MRE 2029-F20. Results were read after 2 hours of incubation with ligand (2 hrs shown in blue) and again after 24 hours without ligand (shown in orange). An increase in CPM was observed by reading the samples at 24 hours, although the amount of radioligand in each sample was the same at the 2 and 24 hour time points. Data are from one purification with each experiment performed in duplicate.

A.4. Discussion and Conclusions

Here, BA and B*A were successfully overexpressed by galactose induction in pITy. Receptors appear to have been active after purification, as the fluorescent ligand binding suggests the receptors associate with FITC-APEC. Additionally, purified receptors appear to bind [^{3}H] MRE 2029-F20, although they have little affinity for [^{3}H] NECA. This is somewhat expected as NECA is not specific for A_{2B}R, which tends to have a lower affinity for common adenosine receptor ligands than the other adenosine receptors. However, MRE 2029-F20 is a selective radioligand antagonist for A_{2B}R. For this reason, future experiments should be conducted using [^{3}H] MRE 2029-F20 to characterize purified BA. Additionally, as is described in Appendix B, BA and B*A chimera could be further characterized by SPR. There are few A_{2B}R specific labeled ligands (either fluorescent or radioactive) on the market, and SPR would enable using unlabeled ligand to determine the relationship to A_{2B}R.

Appendix B

CHARACTERIZATION OF A_1R CHIMERA BY FLUORESCENCE ANISOTROPY AND SURFACE PLASMON RESONANCE

B.1. Introduction

As discussed in Appendix A, the adenosine A_{2A} receptor, $A_{2A}R$ is the highest expressing of the four adenosine receptors, A_1R, $A_{2A}R$, $A_{2B}R$, and A_3R. Previously, the C-terminus of the $A_{2A}R$ receptor was found to affect receptor trafficking (Britton 2012). Here, the $A_{2A}R$ C-terminus was added to A_1R, creating an $A_{1\text{-}2A}R$ chimera that was expressed at higher levels than wild-type A_1R (Jain, in review). This increased level of expression enables purification of the receptor at higher concentrations so that it can be characterized by fluorescence anisotropy and surface plasmon resonance.

B.2. Materials and Methods

B.2.1. Cell Growth and Expression

As described in Chapter 2, receptors were expressed in BJ5464 yeast cells using a multi-integrating vector, pITy, that contains a C-terminal His10 tag for purification of receptors. BA and B*A were grown overnight at 30ºC in YPD, then induced by transfer to YPG at an O.D. of 1 and grown for 24-30 hours. 1250 O.D. of cells were pelleted and stored at -80ºC until needed for purification.

B.2.2. Membrane Protein Purification

Receptors were purified as detailed in Chapter 2. Briefly, cell pellets were resuspended in lysis buffer and protease-inhibitors and lysed with 0.5 mm zirconia silica beads. Lysed cells were then sonicated for 20 seconds, placed on ice to cool, and sonicated a second time. Samples were centrifuged at 3200 g for 30 min to remove cell debris, and supernatant was ultracentrifuged at 100,000 g for 1 hour to pellet cell membranes. Membranes were resuspended in 0.1% DDM/0.1% CHAPS/0.02% CHS and left to rotate overnight at 4ºC. Next, samples were centrifuged at 70,000 g to remove any insoluble material, and supernatant was incubated overnight at 4ºC with Ni-NTA resin. The following day, resin was washed with increasing concentrations of imidazole (20-50 mM), and protein was eluted with 50 mM imidazole and 10 mM EDTA. The final elution was desalted using PD010 desalting columns, and purified receptors were stored for up to 7 days at 4ºC.

B.2.3. Fluorescence Anisotropy Assay

FITC-APEC was used to observe ligand binding, as detailed in Chapter 2. Briefly, samples were read in 96 well half-area black Corning plates (catalog #3875, Corning Incorporated-OR-FisherSci cat#07-200-735) on a Synergy H1 plate reader (BioTek, Winooski, VT) using a polarized filter cube with an excitation wavelength of 480-485 nm and an emission wavelength of 520-528 nm. Scatter measurements were subtracted and anisotropy was calculated as previously described (Swonger 2018).

B.2.4. Equilibrium Ligand Binding

800 nM of purified $A_{1\text{-}2A}R$ and $A_{2A}R$ (as a positive control) in DCC buffer was incubated with 0, 1, 10, 30, 60, or 100 nM FITC-APEC and protected from light at room temperature for 2 hours. Parallel and perpendicular light was read on a Synergy H1 plate reader using a polarized filter cube with an excitation wavelength of 480-485 nm and emission wavelength of 520-528 nm. As described in Chapter 2, anisotropy was determined, and RL complexes were calculated at each concentration of labeled ligand.

B.2.5. Surface Plasmon Resonance

Ligand binding to receptor was characterized by SPR using a Biacore T200 (GE Healthcare). All experiments were performed with DCC running buffer at 20°C, as described in Chapter 3. NTA series S sensor chip was used and conditioned before each set of experiments by injecting 350 mM EDTA for 180 seconds at 30 μL/min. After conditioning, kinetic cycles were begun by injecting $NiCl_2$ for 60 seconds at 10 μL/min to regenerate the NTA chip with nickel. An extra wash of 3 mM EDTA diluted in DCC buffer was then included to help prevent nonspecific binding. Next, 1 μM of purified receptor was injected for 60 seconds at 10 μL/min to associate with Ni-NTA chip via 10xHis tag. After receptor bound to chip, ligand was injected for 120 seconds at 20 μL/min, and binding data was collected. After determining a post-injection baseline, chip was regenerated by injecting 350 mM EDTA for 180 seconds at 30 µL/min, as in the conditioning step. Kinetics were repeated for varying ligand concentrations.

B.3. Results

B.3.1. Equilibrium ligand binding anisotropy

Anisotropy was calculated as previously described in Chapter 2. Equilibrium ligand binding to FITC-APEC was used to test for receptor activity before performing SPR experiments (**Figure B.1**). Here, $A_{2A}R$ is also included as a positive control. Anisotropy was converted into receptor-ligand complexes (RL), as described in Chapter 2 (**Figure B.2**). It appears that $A_{1\text{-}2A}R$ binds FITC-APEC, although with a lower affinity than $A_{2A}R$. Additionally, there is a decrease in anisotropy as fluorescent ligand concentration increases, indicating that the sample is binding ligand and likely active.

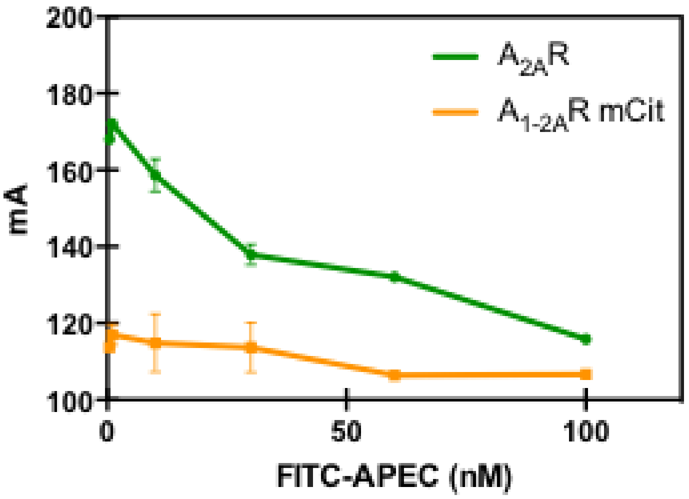

Figure B.1 Equilibrium ligand binding of 1-100 nM FITC-APEC to purified $A_{2A}R$ and $A_{1\text{-}2A}R$. Points represent FITC-APEC concentrations of 1, 10, 30, 60, and 100 nM, and each point represents 2 separate purifications tested to check for receptor activity.

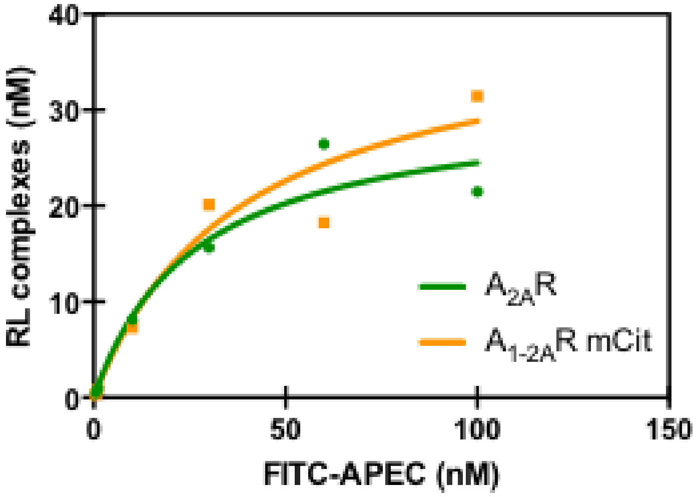

Figure B.2 Conversion of the data points from Figure B.1 to RL complexes (nM) as described in Section 2.2.4 Equilibrium Ligand Binding. Points represent FITC-APEC concentrations of 1, 10, 20, 60, and 100 nM binding to 800 nM of purified $A_{2A}R$ or $A_{1\text{-}2A}R$. Each point represents two separate purifications.

B.3.2. SPR binding

1 µM of purified $A_{1\text{-}2A}R$ or $A_{2A}R$ was attached to Ni-NTA chip via 10xHis tag. After capture of receptor, varying concentrations of NECA, an adenosine receptor agonist that associates with both A_1R and $A_{2A}R$, were injected to observe association of ligand to receptor (**Figure B.3**, **Figure B.4**, and **Figure B.5**). Additionally, DPCPX, a potent A_1R antagonist, was injected over $A_{1\text{-}2A}R$ in an effort to characterize binding of the antagonist to receptor (**Figure B.6**). From these results, the DPCPX appears to bind with greater affinity than NECA to $A_{1\text{-}2A}R$.

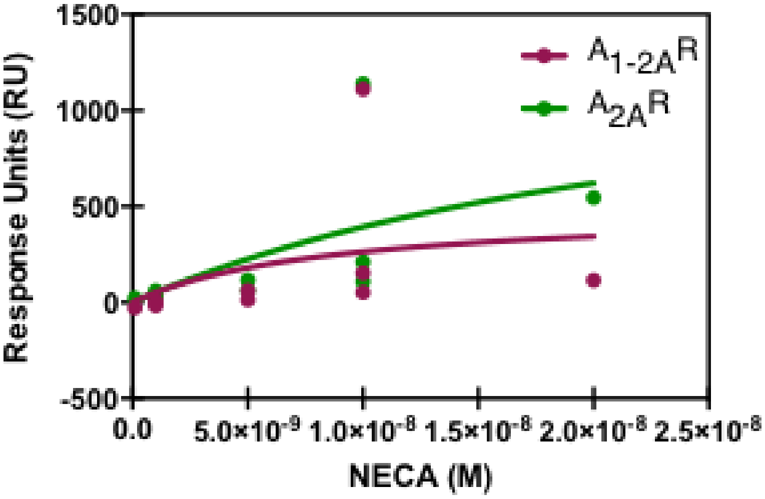

Figure B.3 Affinity curve of 1, 5, 10, and 20 nM NECA with 1 µM purified $A_{1\text{-}2A}R$ and $A_{2A}R$. $A_{2A}R$ appears to have a greater affinity for NECA. Data are from 2 separate receptor purifications. N=1, 2, or 3 depending on the NECA concentration.

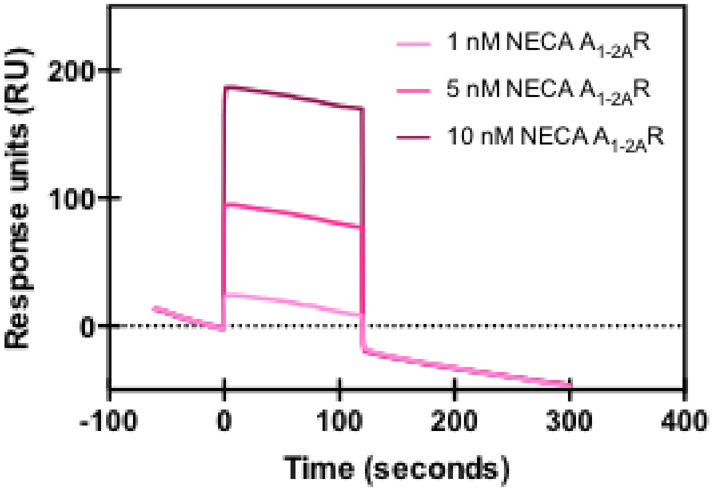

Figure B.4 Representative kinetic binding of 1, 5, or 10 nM NECA to 1 µM purified $A_{1\text{-}2A}R$. Data suggest a concentration dependent affinity of NECA for receptor.

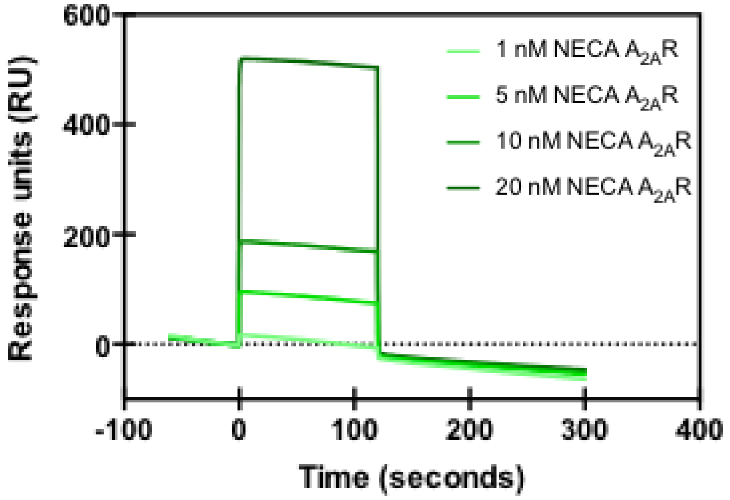

Figure B.5 Representative kinetic binding of 1, 5, 10, or 20 nM NECA to 1 µM purified $A_{2A}R$. Data suggest a concentration dependent affinity of NECA for receptor.

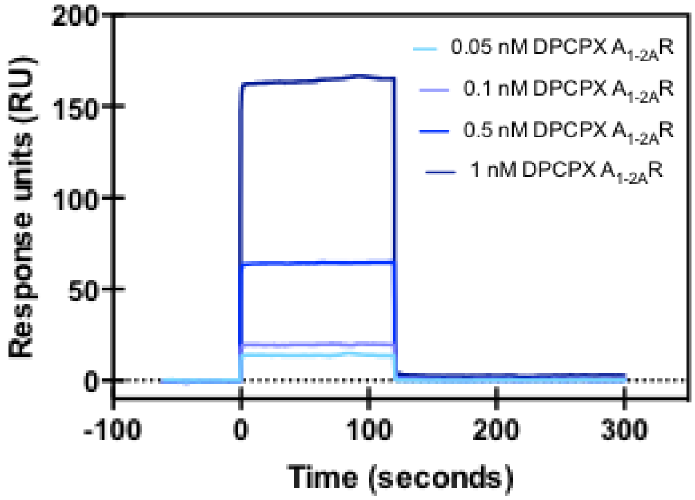

Figure B.6 Representative kinetic binding of 0.05, 0.1, 0.5, or 1 nM DPCPX to 1 µM purified $A_{1\text{-}2A}R$. Data suggest a concentration dependent affinity of antagonist for receptor.

B.4. Discussion and Conclusions

Fluorescent ligand binding results for $A_{1-2A}R$ suggests the purified receptor is active, although it has a lower affinity for FITC-APEC than $A_{2A}R$. Upon confirmation of activity, purified receptor was attached to Ni-NTA chip in a Biacore T200 SPR, while different concentrations of ligand were flowed across receptor. From the SPR results, $A_{2A}R$ seems to have a higher affinity for NECA than $A_{1-2A}R$, although more replicates would help better quantify the ligand binding characteristics of the receptors. Additionally, DPCPX, a potent A_1R antagonist, appears to have a higher affinity for $A_{1-2A}R$ than does NECA, as evidenced by the greater response at lower ligand concentrations. Future work includes collection of more ligand binding SPR data to characterize unlabeled ligand binding of $A_{1-2A}R$. This information can help determine if the chimera is a good representation of wild-type A_1R in regards to its affinity for different types of A_1R ligands.

Future experiments might also include observation and characterization of A_1R associating to G protein, as described for $A_{2A}R$ in Chapter 3.

REFERENCES

1. Hill, S. J. G-protein-coupled receptors : past, present, and future. *British Journal of Pharmacology* **147**, 27–37 (2006).

2. Rask-Andersen, M., Almen, M.S., & Schioth, H.B. Trends in the exploitation of novel drug targets. *Nature Reviews Drug Discovery* **10**, 579-590 (2011).

3. Sriram, K., & Insel, P. A. G Protein-Coupled Receptors as Targets for Approved Drugs: How Many Targets and How Many Drugs. *Mol Pharmacol* **93**, 251–258 (2018).

4. Devree, B. T. *et al*. Allosteric coupling from G protein to the agonist- binding pocket in GPCRs. *Nature* **535**, (2016).

5. Duc, N. M., Kim, H. R., & Chung, K. Y. Structural mechanism of G protein activation by G protein-coupled receptor. *European Journal of Pharmacology* **763**, 214-222 (2015).

6. Bokoch, M. P. *et al*. Ligand-specific regulation of the extracellular surface of a G-protein-coupled receptor. *Nature* **463**, 108–112 (2010).

7. Neves, S. R., Ram, P. T., & Iyengar, R. G Protein Pathways. *Science* **296**, 1636-1639 (2002).

8. Latorraca, N. R., Venkatakrishnan, A. J., & Dror, R. O. GPCR Dynamics: Structures in Motion. *Chemical Reviews* **117**, 139–155 (2016).

9. Tuteja, N. Signaling through G protein coupled receptors. *Plant Signaling & Behavior* **4**, 942–947 (2009).

10. Adamson, R. J., & Watts, A. Kinetics of the early events of GPCR signalling. *FEBS Letters* **588**, 4701–4707 (2014).

11. Fried, N. T., Elliott, M. B., Oshinsky, M. L., & Nahas, S. The Role of Adenosine Signaling in Headache: A Review. *Brain Sciences* **7**, 1–20 (2017).

12. Rivera-Oliver, M., & Díaz-Ríos, M. Using caffeine and other adenosine receptor antagonists and agonists as therapeutic tools against neurodegenerative diseases: A review. *Life Sciences* **101**, 1–9 (2014).

13. de Lera Ruiz, M., Lim, Y.-H., & Zheng, J. Adenosine A $_{2A}$ Receptor as a Drug Discovery Target. *Journal of Medicinal Chemistry* **57**, 3623–3650 (2014).

14. Jacobson, K. A., & Gao, Z. G. Adenosine receptors as therapeutic targets. *Nat Rev Drug Discov* **5**, 247–264 (2006).

15. Muller, C. E., & Jacobson, K. A. Recent Developments in Adenosine Receptor Ligands and Their Potential as Novel Drugs. *National Institute of Health* **1808**, 1290–1308 (2011).

16. Xu, F. *et al.* Structure of an Agonist-Bound Human A2A Adenosine Receptor. *Science* **332**, 322–327 (2011).

17. Jaakola, V.-P. *et al*. The 2.6 Angstrom Crystal Structure of a Human A2A Adenosine Receptor Bound to an Antagonist. *Science* **322**, 1211–1217 (2008).

18. Doré, A. S. *et al*. Structure of the Adenosine A(2A) Receptor in Complex with ZM241385 and the Xanthines XAC and Caffeine. *Structure* **19**, 1283–1293 (2011).

19. Hino, T. *et al*. G-protein-coupled receptor inactivation by an allosteric inverse-agonist antibody. *Nature* **482**, 237-240 (2012).

20. Carpenter, B., Nehmé, R., Warne, T., Leslie, A. G. W. & Tate, C. G. Structure of the adenosine A2A receptor bound to an engineered G protein. *Nature* **536**, 104-107 (2016).

21. Lebon, G. et al. Agonist-bound adenosine A 2A receptor structures reveal common features of GPCR activation. *Nature* **474**, 521–525 (2011).

22. McGraw, C. *Cholesterol Dependent Signaling of the Adenosine A2A Receptor*. PhD dissertation, Tulane University, 2018.

23. Kenakin, T. New concepts in pharmacological efficacy at 7TM receptors. *British Journal of Pharmacology* **168**, 554-575 (2012).

24. Tate, C. G. A crystal clear solution for determining G-protein-coupled receptor structures. *Trends in Biochemical Sciences* **37**, 343–352 (2012).

25. Strasser, A., Wittmann, H.-J., & Seifert, R. Binding Kinetics and Pathways of Ligands to GPCRs. *Trends in Pharmacological Sciences* **38**, 717-732 (2017).

26. Nederpelt, I. *et al*. From receptor binding kinetics to signal transduction; a missing link in predicting in vivo drug-action. *Nature Scientific Reports* **7**, (2017).

27. Guo, D., Hillger, J. M., Ijzerman, A. P., & Heitman, L. H. Drug-Target Residence Time-A Case for G Protein-Coupled Receptors. *Med. Res. Rev* **34**, 856–892 (2014).

28. Copeland, R. A., Pompliano, D. L., & Meek, T. D. Drug–target residence time and its implications for lead optimization. *Nature Reviews: Drug Discovery* **5**, 730–739 (2006).

29. Swonger, K. N., & Robinson, A. S. Using Fluorescence Anisotropy for Ligand Binding Kinetics of Membrane Proteins. *Current Protocols in Protein Science*, 1–15 (2018).

30. Stenlund, P., Babcock, G. J., Sodroski, J., & Myszka, D. G. Capture and reconstitution of G protein-coupled receptors on a biosensor surface. *Analytical Biochemistry* **316**, 243–250 (2003).

31. Surface plasmon resonance – GE Healthcare Life Sciences. *GE Healthcare* (2019). Available at: www.gelifesciences.com/en/us/solutions/protein-research/knowledge-center/surface-plasmon-resonance/surface-plasmon-resonance.

32. Piirainen, H., Ashok, Y., Nanekar, R. T., & Jaakola, V. P. Structural features of adenosine receptors: From crystal to function. *Biochimica et Biophysica Acta - Biomembranes* **1808**, 1233–1244 (2011).

33. Heydenreich, F. M., Vuckovic, Z., Matkovic, M., & Veprintsev, D. B. Stabilization of G protein-coupled receptors by point mutations. *Frontiers in Pharmacology* **6**, 1–15 (2015).

34. Carsten Hoffmann, Guido Gaietta, Moritz Bünemann, Stephen R Adams, Silke Oberdorff-Maass, Björn Behr, Jean-Pierre Vilardaga, Roger Y Tsien, Mark H Ellisman, M. J. L. A FlAsH-based FRET approach to determine G protein–coupled receptor activation in living cells. *Nature Methods* **2**, 171–176 (2005).

35. Palczewski, K. *et al*. Crystal Structure of Rhodopsin: A G Protein-Coupled Receptor. *Science* **289**, (2000).

36. Rasmussen, S. G. F. *et al*. Crystal structure of the b 2 adrenergic receptor–Gs protein complex. *Nature* **477**, (2011).

37. Hebert, T. E., Gales, C., & Rebois, R. V. Detecting and Imaging Protein–Protein Interactions During G Protein-Mediated Signal Transduction In Vivo and In Situ by Using Fluorescence-Based Techniques. *Cell Biochemistry and Biophysics* **45**, 85–109 (2006).

38. Sun, B. *et al*. Crystal structure of the adenosine A2A receptor bound to an antagonist reveals a potential allosteric pocket. *Proceedings of the National Academy of Sciences of the United States of America* **114**, (2017).

39. Magnani, F., Shibata, Y., Serrano-Vega, M. J., & Tate, C. G. Co-evolving stability and conformational homogeneity of the human adenosine A2a receptor. *Proceedings of the National Academy of Sciences* **105**, 10744–10749 (2008).

40. Bertheleme, N., Singh, S., Dowell, S. J., Hubbard, J., & Byrne, B. Loss of constitutive activity is correlated with increased thermostability of the human adenosine A2A receptor. *British Journal of Pharmacology* **169**, 988–998 (2013).

41. Jain, A., McGraw, C., Robinson, A.S. The Adenosine Receptor Carboxy-terminus is Necessary for Response but not Specificity of Downstream Signaling. *Molecular Pharmacology*, in review.

42. Naranjo, A. N. *Stability and Activity of a GPCR in vivo and in Membrane Mimetic Environments*, PhD dissertation, University of Delaware, 2014.

43. Naranjo, A. N., McNeely, P. M., Katsaras, J., & Robinson, A. S. Impact of purification conditions and history on A2A adenosine receptor activity: The role of CHAPS and lipids. *Protein Expression and Purification* **124**, 62–67 (2016).

44. Allen, M., J. Reeves, and G. Mellor, High throughput fluorescence polarization: A homogeneous alternative to radioligand binding for cell surface receptors. *Journal of Biomolecular Screening* **5**, 63-69 (2000).

45. McNeely, P. M., Naranjo, A. N., Forsten-Williams, K., & Robinson, A. S. A2AR Binding Kinetics in the Ligand Depletion Regime. *SLAS Discovery* **22**, 166–175 (2017).

46. Mcgraw, C., Yang, L., Levental, I., Lyman, E., & Robinson, A. S. Membrane cholesterol depletion reduces downstream signaling activity of the adenosine A 2A receptor. *BBA Biomembranes* **1861**, 760-767 (2019).

47. Uddin, R., Simms, J., & Poyner, D. Functional characterisation of G protein-coupled receptors. *Methods* **147**, 213-220 (2018).

48. Dijkman, P. M., & Watts, A. Lipid modulation of early G protein-coupled receptor signalling events. *BBA Biomembranes* **1848**, 2889–2897 (2015).

49. Chu, R., Reczek, D., & Brondyk, W. Capture-stabilize approach for membrane protein SPR assays. *Scientific Reports* **4**, (2014).

50. Segala, E., Errey, J. C., Fiez-Vandal, C., Zhukov, A., & Cooke, R. M. Biosensor-based affinities and binding kinetics of small molecule antagonists to the adenosine A2A receptor reconstituted in HDL like particles. *FEBS Letters* **589**, 1399–1405 (2015).

51. O'Malley, M. A., Lazarova, T., Britton, Z. T., & Robinson, A. S. High-level expression in Saccharomyces cerevisiae enables isolation and spectroscopic characterization of functional human adenosine A2a receptor. *Journal of Structural Biology* **159**, 166–178 (2007).

52. McEwen, D. P., Gee, K. R., Kang, H. C., & Neubig, R. R. Fluorescence Approaches to Study G Protein Mechanisms. *Methods in Enzymology* **344**, (2002).

53. Soh, N., Soh, & Nobuaki. Selective Chemical Labeling of Proteins with Small Fluorescent Molecules Based on Metal-Chelation Methodology. *Sensors* **8**, 1004–1024 (2008).

54. Ashok, Y., & Jaakola, V.-P. Nanodisc-T m : Rapid functional assessment of nanodisc reconstituted membrane proteins by CPM assay. *Methods* **3**, 212–218 (2016).

55. Klinger, M. *et al*. Removal of the carboxy terminus of the A2A adenosine receptor blunts constitutive activity: differential effect on cAMP accumulation and MAP kinase stimulation. *Naunyn-Schmiedeberg's Arch Pharmacol* **366**, 287-298 (2002).

56. Alves, I. D. *et al*. Selectivity, Cooperativity, and Reciprocity in the Interactions between the-Opioid Receptor, Its Ligands, and G-proteins. *The Journal of Biological Chemistry* **279**, 44673–44682 (2004).

57. Dijkman, P. M., & Watts, A. Lipid modulation of early G protein-coupled receptor signalling events. *BBA - Biomembranes* **1848**, 2889–2897 (2015).

58. Britton, Z. *Novel Approaches to the Expression and Purification of G Protein-coupled Receptors*. PhD dissertation, University of Delaware, 2012.

59. Moriyama, K., & Sitkovsky, M. V. Adenosine A2A receptor is involved in cell surface expression of A2B receptor. *Journal of Biological Chemistry* **285**, 39271–39288 (2010).

60. Trincavelli, M. L. *et al*. Allosteric modulators of human A 2B adenosine receptor-ketoindole derivatives A 2B adenosine receptor. *BBA - General Subjects* **1840**, 1194–1203 (2014).

BIOGRAPHY

Kirsten Swonger Koretz received her B.S. in Chemical Engineering from Northwestern Unviversity in 2012. During her time at Northwestern she studied gene silencing and ribosome engineering in Dr. Michael Jewett's synthetic biology laboratory. Following graduation, Kirsten researched quality of life improvements for persons with spinal cord injury at the Center of Excellence for the Medical Consequences of Spinal Cord Injury at the James J. Peters VA Medical Center in Bronx, NY. She left human subjects research to return to school and joined Dr. Anne Robinson's laboratory to study G protein-coupled receptors.